Deliverable 15.2: Updated State-of-the-art of WP ConCorD

Work Package 15

This project has received funding from the European Union's Horizon 2020 research and innovation programme 2014-2018 under grant agreement N°847593.

Document information

Project Acronym	**EURAD**
Project Title	**European Joint Programme on Radioactive Waste Management**
Project Type	**European Joint Programme (EJP)**
EC grant agreement No.	**847593**
Project starting / end date	**1st June 2019 – 30 May 2024**
Work Package No.	**15**
Work Package Title	**Container Corrosion under Disposal conditions**
Work Package Acronym	**ConCorD**
Deliverable No.	**15.2**
Deliverable Title	**Updated State-of-the-Art of WP ConCorD**
Lead Beneficiary	**GRS**
Contractual Delivery Date	**30/04/2024**
Actual Delivery Date	**31/05/2024**
Type	**Document**
Dissemination level	**Public**
Authors	**Abdesselam Abdelouas (SUBATECH), Ana María Fernández (CIEMAT), Andrea Cherkouk (HZDR), Andrés G. Muñoz (GRS), Andrés Idiart (AMPHOS21), Arnau Pont (AMPHOS21), Ashutosh R. Singh (KIT-INE), Cedric Bosch (EMSE), Cristiano Padovani (JACOBS), David Dobrev (UJV), James Hesketh (JACOBS), Katerina Černá (TUL), Kristel Mijnendonckx (SCK), Lola Sarrasin (SUBATECH), Michaela Matulová (SURAO), Mohamed Merroun (UGR), Nathalie Texier-Mandoki (Andra), Nicholas Smart (JACOBS), Nicolas Finck (KIT-INE), Olga Riba (AMPHOS21), Paul Wersin (University of Bern), Pauliina Rajala (VTT), Rizlan Bernier-Latmani (EPFL), Roberto Gaggiano (Ondraf/Niras), Šárka Šachlová (UJV), Sergey Sayenko (KIPT), Ursula Alonso (CIEMAT), Vaclava Havlová (UJV), Vanessa Montoya (UFZ).**

To be cited as:

A. Abdelouas, A.M. Fernández, A. Cherkouk, A.G. Muñoz, A. Idiart, A. Pont, A.R. Singh, C. Bosch, C. Padovani, D. Dobrev, J. Hesketh, K. Černá, K. Mijnendonckx, L. Sarrasin, M. Matulová, M. Merroun, N. Texier-Mandoki, N. Smart, N. Finck, O. Riba, P. Wersin, P. Rajala, R. Bernier-Latmani, R. Gaggiano, Š. Šachlová, S. Sayenko, U. Alonso, V. Havlová, V. Montoya: Updated State-of-the-Art of WP ConCorD. Final version as of 31.05.2024 of deliverable D15.2 of the HORIZON 2020 project EURAD. EC Grant agreement no: 847593.

Acknowledgement

This document is a deliverable of the European Joint Programme on Radioactive Waste Management (EURAD). EURAD has received funding from the European Union’s Horizon 2020 research and innovation programme under grant agreement No 847593.

Status of deliverable		
	By	Date
Delivered (Lead Beneficiary)	Andrés G. Muñoz (GRS)	14/03/2024
Verified (WP Leader)	N. Diomidis	31/05/2024
Reviewed (Reviewers)	F. King, G. Bracke, C. Lilja, M. Behazin, S. Suzuki	12/04/2024
Approved (PMO)		
Submitted to EC (Coordinator)	Andra (Coordinator)	31/05/2024

Executive Summary

A sealed container for the geological disposal of spent nuclear fuel and vitrified high-level waste is the primary component of the deep geological repository that provides complete containment of radionuclides. As such, attention is frequently focused on its lifetime. The lifetime of the container is influenced by materials degradation processes during disposal and is expected to attain a length of of the order of several millennia and, for some container materials, up to one million years. Designing, manufacturing, and predicting the performance of containers over such long periods requires an in-depth understanding of their materials properties, fabrication processes and degradation mechanisms. Scientific and technological progress can improve both the performance of containers as well as the robustness of lifetime predictions. For many national radioactive waste disposal programmes, optimisation of these aspects is of primary importance.

In this report the different aspects concerning the degradation of nuclear waste containers and the technological approaches for a better performance are summarized. The information is thematically organized in correlation with the organization of the activities pertaining to the different tasks. The discussion is based on a comprehensive review of the existing knowledge, actualized in view of new insights gained in project ConCorD. Beginning with a discussion on the complexity of the chemical environment created by irradiation, mainly γ-radiation at the container wall-bentonite interface, the discussion embraces the effects of temperature, saturation, oxygen content and pressure on the corrosion rate, emphasizing the evolution of the corroding interface during the first decades after the sealing. The discussion includes the microbial aspects of the corrosion emphasizing the effects of radiation, temperature, and saturation of bentonite on the survival and growth of microbes and their relevance for the corrosion process, considering copper and ferrous steels as reference materials. A chapter is dedicated to alternative materials and concepts including containers manufactured with ceramic materials, ceramic and metallic protecting coatings, and the evaluation of the use of commercially available metal alloys. The present report is rounded out with a comprehensive review of the existing tools allowing the prediction of long-term barrier integrity, discussing their reliability and limits.

Table of contents

List of Figures

List of Tables

Acronyms

CRH	Critical Relative Humidity
DSR	Dissimilatory Sulphate Reduction
Ecorr	Corrosion Potential
EDZ	Excavation Disturbed Zone
Eh	Redox Potential
FEBEX	Full-scale Engineered Barriers Experiment
GDF	Geological Disposal Facility
GDR	Geological Disposal Repository
HIC	Hydrogen Induced Cracking
HLW	High Level Waste
HotBENT	High Temperature Effects on Bentonite Buffers Experiment
HSR	High-strength Rock
IAEA	International Atomic Energy Agency
ILW	Intermediate Level Waste
LET	Linear Energy Transfer
LOT	Long Term Test of Buffer Material
MIC	Microbiologically Influenced Corrosion
RH	Relative Humidity
SCC	Stress Corrosion Cracking
SF	Spent Nuclear Fuel
SoTA	State-of-the-art
SRB	Sulphate Reducing Bacteria
THMC	Thermal, Hydraulic, Mechanical, and Chemical
TOC	Total Organic Carbon
URL	Underground Research Laboratory
WMO	Waste Management Organisation

1. Introduction

A sealed container (or canister) for the disposal of high-level radioactive waste (HLW) and spent fuel (SF) is a key component of all current deep geological repository programmes. The container constitutes the only barrier within the overall multi-barrier disposal system which can provide complete confinement of radionuclides within its lifetime. Therefore, attention is frequently focused on the performance of the canister, especially concerning the length of time during which the material stability and thus the barrier function can be guaranteed.

Pre-established lifetime requirements can vary significantly between the different national programmes. They are typically linked to the type of waste, the disposal concept, the geological environment, the characteristics of the nearfield and the selected canister material(s) . The failure of canisters is typically expected after the environmental induced degradation of the materials exceeds a permissible threshold, which typically depends on the mechanical stress. An especially critical case might arise in the case of localized corrosion, provided the conditions triggering the process are not arrested in a relative short time. The formation of small cavities at the container could be act as concentration points for stress forces favouring the growth of fissures, eventually in synergy with enhanced corrosion (stress corrosion cracking). In such a case, the possibility of the release of radionuclides in the nearfield can no longer be excluded.

The source of stress during disposal can be residual, lithostatic and hydrostatic pressures, the swelling of the bentonite buffer or rock displacements. The hydrostatic loads are essentially isotropic. The other types of canister loads, on the other hand, can be unevenly distributed, generating anisotropic stress fields and shear forces. The generated stresses in the canister wall, lid, and base, including the seal joint region, must remain under the failure limit for the expected lifetime of the canister by an adequate margin. This is typically demonstrated by structural assessments which consider the strength and fracture toughness of the canister material(s), the maximum conceivable size of manufacturing defects, and the evolving disposal environment.

The reduction of the wall thickness by environmentally induced corrosion is an important input to the structural analysis for some canister concepts. As the thickness reaches a critical value, stresses can lead to plastic collapse. The intrinsic materials properties can also be altered by hydrogen uptake, neutron embrittlement or preferential leaching/dissolution, which often leads to a reduction of the fracture toughness and to a larger risk of mechanical failure.

An overview of the currently planned container concepts and their expected exposure conditions is shown in Table 1. Copper (e.g., Sweden, Finland, Canada, Korea, Taiwan) and carbon steels (e.g., Belgium, France, Switzerland, Czech Republic, Japan, Slovakia, Hungary) are the container materials that have been traditionally considered for the disposal of SF/HLW in countries with advanced disposal programs. The feasibility of containers made from these materials has been demonstrated and the required manufacturing technology is available and mature.

The required prediction of the degradation rate needs an extensive knowledge of the corrosion mechanism under the environmental conditions created in the nearfield environment of the canister after the sealing of the disposal area. This includes the long-term change of the physicochemical properties of the environment caused by chemical-geological activity, radiolysis, and microbial activity.

While steels provide a strong solution for canisters, corrosion under anoxic conditions yields hydrogen gas. This will change the physiochemical environment, lead to gas transport and eventually overpressure. To provide alternative solutions to the use of steels for containers and thus limit the production of hydrogen in the long term, alternative materials to non-alloy steels have been studied in

recent years. One of the difficulties lies in achieving equivalent or better properties than steels to meet the requirements for the concerned components.

Alternative materials for nuclear waste containers should guarantee sufficient resistance to localised corrosion (e.g., stress corrosion cracking of welds). In this context the choice of the material and of the production route for the canister are very important. Chemical compatibility with all other components, including waste, must also be part of the formulation/manufacturing requirements. Recent developments (e.g., copper coatings) considered in Canada and investigated in Switzerland (Holdsworth et al. 2018), France and Japan have demonstrated that container optimisation is indeed possible. Further alternative and novel container materials are also under consideration (e.g., steels with more controlled composition, Cu-based alloys and composites, ceramics, Zr alloys) (Holdsworth 2013) (Baroux and Martin 2016).

This report summarises the state of the art on the research of corrosion of container materials in near real repository conditions presented with a structure defined by the targets of EURAD WP15 ConCorD, (based on a previous review of Padovani et al. 2017) and incorporates knowledge advances gained by the experimental and computational work carried out in this project. These are:

- to assess the corrosion mechanisms of traditional canister materials (i.e., carbon steel and copper) in complex disposal scenarios where the corroding environment is under the influence of irradiation (Section 2), temporal changes of the nearfield environment (Section 3), or microbial activity (Section 4)

- to assess the potential of novel materials for optimisation of the canister performance (Section 5), and

- to integrate experimental evidence on canister degradation into the prediction of container corrosion and lifetime assessment (Section 6).

Table 1: Canister concepts and illustrative environmental conditions for various WMO repository designs

WMO	Canister concept	Estimated or target lifetime (yr)	Nominal buffer dry density (g/cm^3)	Max canister temperature (°C)	Time to full nearfield saturation (yr)	Maximum surface absorbed dose rate (Gy/hr)	Expected mechanical loads (MPa)
SKB	Copper-cast iron	$>10^6$	1.6	95	Few tens to a few thousand	0.2	15 50 (glacial)
Posiva	Copper-cast iron	$>10^6$	1.55	95	Few tens to a few thousand	0.3	14 50 (glacial)
Andra	Carbon steel	>500	No buffer	90		10	
Ondraf-Niras	Carbon steel	Several thousand	Cementitious buffer	100	5-10 up to a few thousand	25	8
Nagra	Carbon steel	10,000	>1.45	~120	A few centuries	0.2	22-29 max
SURAO	Carbon Steel	10,000	1.4	95	100	0.3	20
NWMO	Copper coated steel	$>10^6$	1.6	85	50-5,000 depending on host rock type	0.8	15 45 (glacial)
NUMO	Carbon steel	>1,000	1.6	100	<1,000 Host-rock dependent	0.006-0.011	11 (hard rock)

2. Effects of irradiation

2.1 Effects of irradiation on the corrosion of carbon steel containers

The corrosion rate of carbon steel under disposal conditions depends on several factors, such as temperature, pH, the composition of solution and gas phases, and irradiation. The nature of the oxide phases formed on the surface can be influenced by changes of the corrosion potential (Ecorr) due to water radiolysis products. Most of the studies concerning corrosion under irradiation found in the literature report the formation of a passivating film constituted of magnetite and hematite. Some other phases such as lepidocrocite and goethite are also reported. The corrosion rate often increases under radiation, which is ascribed to the presence of water radiolysis products. However, quite high dose rates in the kGy h^{-1} range are necessary to show corrosion enhancement. Several studies report that the corrosion rate, after an initial increase, returns to the same value as measured in unirradiated experiments (Nelson et al. 1983) (Smart et al. 2008). This can be explained in terms of the formation of a protective passive film.

2.1.1 Effect of steel composition and microstructure

In their review of radiation effects on the corrosion of candidate container materials for the disposal of HLW, Shoesmith and King (1999) compared results of corrosion experiments of several types of steel. They concluded that, except for low chromium and low molybdenum steels, the composition and microstructure of the steel do not seem to affect the corrosion rate under irradiation. The presence of impurities or welding induce localized corrosion (Ahn and Soo 1995).

2.1.2 Effect of temperature

The temperature can play a major role by increasing the corrosion rate in aqueous media. An increase in temperature increases the rate of chemical and electrochemical reactions involved in the corrosion process. Moreover, it modifies the rate of diffusion processes and the solubility of the corrosion products (Konovalova 2021) (Kursten et al. 2003).

Gray (1987) observed an increase of the corrosion rate with temperature when studying the corrosion of mild steel in salt brines under gamma radiation at 75 and 150 °C. These results, however, do not distinguish between the contributions of temperature and irradiation.

Winsley et al. (2011) studied the corrosion of carbon steel in deaerated alkaline solution (pH ~13.4, $[O_2]$ < 10 ppm) under gamma radiation at a dose rate of 25 Gy h^{-1}. The initial corrosion rate at 80 °C is higher than at 25 °C but decreases more rapidly at 80 °C than at 25°C. The appearance of the oxide formed on the samples changes between 25 °C and 80 °C (magnetite). The irradiation, however, does not appear to modify the appearance or the composition of the corrosion products formed.

Daub et al. (2011, 2019) studied the effect of temperature (25 to 150 °C) on the corrosion of steel immersed in deaerated water with $pH_{25°C}$ ~7 or adjusted to 10.6 with LiOH ($[O_2]$ < 1000 ppm). They used a ^{60}Co gamma source with a dose rate of 6.2 kGy h^{-1} and samples were irradiated for 20 or 66 hours (~12 - 41 kGy). They showed that, in comparison to irradiation, temperature has little influence on the

corrosion potential and hence on the nature of the corrosion products formed. It may, however, determine the amount of corrosion products and the oxide layer thickness. These results are in line with the study by Čuba et al. (2011), who irradiated carbon steel plates immersed in deaerated deionized Millipore water or synthetic granitic water (pH of ~6.3 and ~6.9 respectively) at 25 °C, 50 °C and 70 °C. The dose rate was 0.22 kGy h^{-1} and total dose ranged from 0 to 120 kGy. They observed an increased quantity of dissolved iron in solution with increasing temperature, indicating a higher dissolution rate of iron.

2.1.3 Effect of the composition of test solution

Upon exposure to radiation, the vapour or aqueous phase decomposes into oxidizing and reducing species that can influence the corrosion processes. The nature and concentration of the radiolytically produced species (radicals or molecular products) depend on the environment. Beyond the iron ions, various inorganic ions present in groundwater such as carbonates, magnesium, calcium or chlorides can act as scavengers for radiolysis products. The solution composition might therefore impact the corrosion behaviour of steel under irradiation. Marsh and Taylor (1988) for instance measured higher corrosion rate in seawater than in granitic water.

Smart et al. (2008) studied the anaerobic corrosion of carbon steel in two synthetic waters (modified Allard groundwater and bentonite equilibrated groundwater) and observed in both cases an increase of the corrosion rate with radiation: 30 times higher for the Allard water and 10 to 20 times for the bentonite water compared to unirradiated controls. In contrast to the Allard groundwater with a pH 8.8, the bentonite groundwater (pH 10.4) has a simpler composition but has a high concentration of chloride and sodium and also contains carbonates. The lower enhancement in the corrosion rate for the bentonite groundwater was attributed to its a higher ionic strength and initial pH.

Daub et al. (2011) studied the effect of gamma radiation (6.2 kGy h^{-1}, total doses of ~12 - 41 kGy) on the corrosion of carbon steel as a function of the pH. They observed that when the carbon steel samples were irradiated at 150 °C in either LiOH ($pH_{25°C}$ 10.6) solution or distilled water ($pH_{25°C}$ ~7), pH has no impact on the nature of the formed oxides but does on their crystallinity. At mildly basic pH the layer formed is uniform and compact. This contrasts with that one formed at neutral pH which is non-uniform and porous. This is attributed by the authors to influence of pH on the iron solubility which can alter the rates of the reactions forming the oxide, thereby affecting its crystallinity and overall protective ability.

Among the radiolytic species produced by water radiolysis, H_2O_2 plays a key role in the control of carbon steel corrosion under radiation. Daub et al. (2010) also compared the gamma radiation effect on corrosion with that of the addition of H_2O_2. They demonstrated that the H_2O_2 concentration can change the nature of the corrosion products formed. While irradiation transforms maghemite into magnetite, the reaction is reversed towards maghemite with $[H_2O_2]<10^{-3}$ mol l^{-1}. At H_2O_2 concentrations higher than 10^{-3} mol l^{-1}, however, magnetite and maghemite transform to lepidocrocite. This study indicated that under the experimental conditions (i.e., room temperature and pH of 10.6), the corrosion rate of carbon steel in a γ-radiation environment can be predicted from the dependence of the corrosion potential on $[H_2O_2]$.

Vandenborre et al. (2013) also pointed out the role of hydrogen peroxide in the corrosion of carbon steel by showing similar results in the corrosion induced by the $^4He^{2+}$ water radiolysis (22 kGy) and by addition of H_2O_2 by comparable volumetric concentration (10^{-4} mol l^{-1}), among others the formation of lepidocrocite. An inhibition effect of H_2 in the corrosion process is also underlined, as well as a potential role of O_2 species.

2.1.4 Effect of relative humidity

Concerning the impact of the gas phase radiolysis on carbon steel, Brehm (1990) showed that, in an air/steam mixture, the irradiation effect on the corrosion rate of low-carbon steel at 150°C is very limited, but increases significantly (factor of ~10) at 250 °C.

Lapuerta et al. (2006, 2008) studied atmospheric iron corrosion under proton irradiation (3 MeV, 10 nA) as a function of the relative humidity (RH) and under several gas phases (N_2 with O_2 or H_2O or both). Their results indicate that, in their experimental conditions, the coupled action of H_2O and O_2 is necessary for the formation of an iron oxide layer since no iron oxidation was observed in the absence of one of the species. Moreover, corrosion starts at lower RH values (<20%) under irradiation than without (60%). A maximal corrosion rate was observed for a RH of 45% against 95% or higher without irradiation. A layer of water on the surface of the iron is necessary to induce atmospheric corrosion. It forms from RH of 40-60% on without radiation. Irradiation allows this layer to be formed at lower RH in particular via the formation of $H^+(H_2O)_n$ clusters.

2.1.5 Effect of the radiation source

The main effect of the type of ionizing particle for a particular form of radiation is to change the radiolysis products. The production of the primary products relies on the type of radiation while their concentration depends on the Linear Energy Transfer (LET). This concept corresponds to the loss of energy by unit length in the irradiated medium and depends on the energy and type of radiation particles. High LET radiation (heavy ion radiation) has a high production of molecules and a low production of radicals while low LET radiation (ionizing radiation) tends to produce more radicals (Mendoza, 2017).

2.1.6 Effect of the total dose and dose rate

There is some correlation between steel corrosion rates and the dose rate as shown in Table 2, which summarizes corrosion rates under irradiation found in the literature, although non-exhaustively. This effect is, however, limited in time, and corrosion rates often evolve toward those of unirradiated steel coupons after a few months.

Gray (1987) observed that at 75 °C the corrosion potential and corrosion rate of mild steel in salt brines increases at increasing dose rate. After three weeks of irradiation, the corrosion rate for a dose rate of 2.6 kGy h^{-1} is three times larger than that measured for a dose rate of 240 Gy h^{-1} (from 73 to 220 µm y^{-1}).

Marsh and Taylor (1988) observed a similar tendency on irradiating carbon steel in synthetic seawater at dose rates of 3, 35 and 1000-1500 Gy h^{-1} at 90 °C. The corrosion is accelerated when the radiation dose rate increases: at 35 Gy h^{-1} the measured corrosion rate is ~8 times higher than that for a non-irradiated sample and ~20 times greater for the highest dose rate applied. For a dose rate of 1000-1500 Gy h^{-1} and after a period of 100 days, a stabilization or even a decrease of the corrosion rate is observed. It is interesting to note that a negligible increase of the corrosion rate at a dose rate of 3 Gy h^{-1} was observed (Marsh and Taylor 1988). A similar effect was pointed out by Crusset et al. (2017) for 20 Gy h^{-1} dose rate irradiation in anoxic conditions.

Table 2: Corrosion rate (µm y^{-1}) of steel and iron under irradiation. Adapted from Shoesmith and King (1999).

Experimental conditions			**Corrosion rate (µm/y)**							**Reference**
			0 Gy/h	10^{-1} Gy/h	1 Gy/h	10 Gy/h	10^{2} Gy/h	10^{3} Gy/h	10^{4} Gy/h	
Granitic water	anoxic	90°C	0.1					3		Marsh and Taylor (1988)
Seawater	oxic	RT	6		~10	~50		~130		Marsh and Taylor (1988)
Brine A	oxic	RT	2–22			~2–22		60–175		Westerman et al. (1983)
Brine A	oxic	RT	20–50		20–50	20–50				Westerman et al. (1983)
Q-Brine	oxic	90°C	25–80		~20	~25–30		500–800		Smailos et al. (1991)
Basaltic water	oxic	250°C	1 – 8						8–30	Westerman et al. (1982)
Air/Steam	oxic	150°C	0.05–0.1		0.08–0.2	0.09–0.15				Brehm (1990)
Air/Steam	oxic	250°C	0.03–0.6		3–5	7–10	7–10			Brehm (1990)
Brine	anoxic	75°C	~12				73	220		Gray (1987)
Basaltic water	oxic	250°C	5					11		Nelson et al. (1983)
Allard water	anoxic	30°C	0.1			3	3			Smart et al. (2008)
Bentonite-equilibrated water	anoxic	50°C	0.05			0.05–0.2	0,8			Smart et al. (2008)
Cementous water	anoxic	25 or 80°C	~1	~1		~1				Winsley et al. (2011)
Concentrated groundwater	oxic	150°C	25–107						11–44	Ahn and Soo (1995)
Bentonite saturated with Beishan water	oxic	90°C	24					32		Liu et al. (2017)
Clay or clay/clay water	oxic	90°C	150					300		Debruyn (1988)

The variation of the corrosion rate under irradiation with time was also reported by Smart et al. (2008) who compared the corrosion of carbon steel at dose rates of 11 and 300 Gy h^{-1} in anoxic Allard water at 30 °C and bentonite-equilibrated water at 50°C. In both media, gamma radiation increases the anaerobic corrosion rate of steel. At 11 Gy h^{-1} the corrosion rate decreases after about 1000 h to finally reach the same value as for unirradiated conditions (roughly between 2000 and 4000 h, figure 1a). At 300 Gy h^{-1} the corrosion enhancement lasts longer and may even be continuous. Interestingly, the initial increase of corrosion rate seems to be less important at 300 Gy h^{-1} than at 11 Gy h^{-1}.

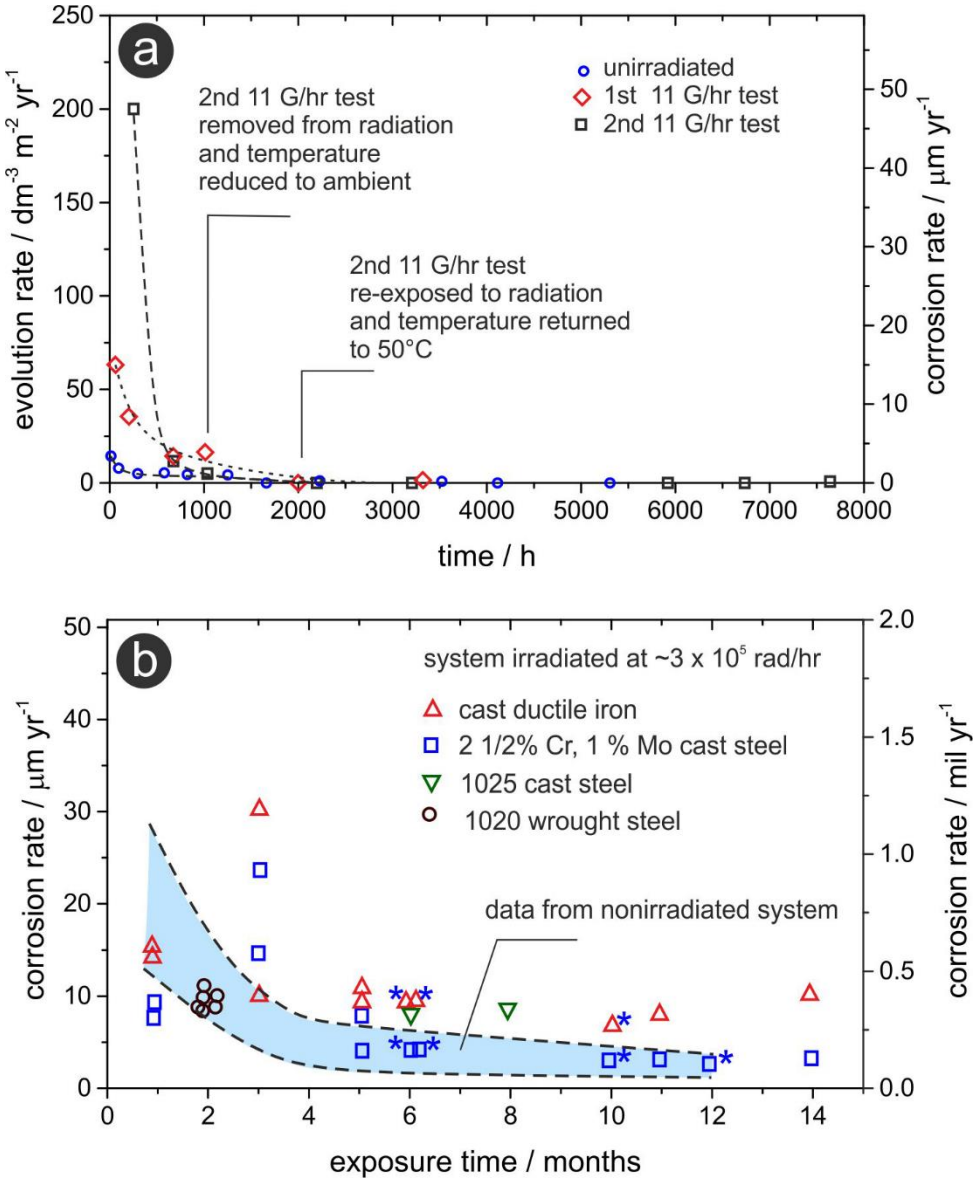

Figure 1: a) Hydrogen evolution and corrosion rates of carbon steel in anoxic bentonite-equilibrated water at 50°C at 0 and 11 Gy h^{-1} (adapted from Smart et al., 2008). b) Corrosion rates of iron-based alloys exposed to synthetic Hanford Grande Ronde basalt water at 250°C at 3×10^3 Gy h^{-1} (adapted from Nelson et al., 1983). Asterisks signify specimens stripped once prior to exposure shown.

Westerman et al. (1983) studied the corrosion of ferrous materials at 150 °C in anoxic brine. The corrosion rates observed at 1000 Gy h^{-1} were considerably higher than those obtained under non-irradiated conditions (by a factor of ~6). On the other hand, the corrosion rates determined at 150 ° C and 20 Gy h^{-1} showed an increase of the corrosion rate by factor of 1.5 - 2.0 after 1 month, but no significant increase over values measured under non-irradiated conditions was observed after 3 months of exposure. Similar results were observed at dose rates of 13000 Gy h^{-1} (Ahn and Soo, 1995) and 35000 Gy h^{-1} (Nelson et al., 1983) in basaltic water (figure 1(b)).

2.1.7 Buffer-container system

There are only a few reports on buffer-container systems under irradiation. Pusch et al. (1992) studied MX-80 bentonite in conditions close to those found in a repository. They enclosed bentonite saturated in Allard water (low salinity) in contact with carbon steel plates exposed to f a radiation (^{60}Co source) and elevated temperature gradient for 1 year. The temperature ranged from 130 °C in the clay area in contact with the carbon steel (strongest radiation: 3.97 kGy h^{-1}) to 90 °C at the opposite side in contact with stainless steel and where the irradiation dose was ten times lower (0.46 kGy h^{-1}). They replicated the experiment with no radiation source and extensively analysed the clay to determine if the bentonite properties were affected by the environmental conditions. The main conclusion is that the combined effect of gamma radiation and heating causes only insignificant modifications of the smectite properties. MX-80 bentonite is mainly composed of Na-montmorillonite and, as accessory minerals, quartz, feldspars and small amounts of calcite and opal. For the two experiments, the structure of the clay remained almost intact after one year. The major mineralogical alterations were the disappearance of feldspars, the formation of calcium and magnesium-bearing sulphates in the hotter part of the samples, and a slight dissolution and transformation of a 10 Å thick sheet of minerals. A slight cementation of the clay associated with the precipitation of silicious compounds was also reported. As a consequence, the clay significantly strengthened in the part of the sample heated at 130°C. Physical properties such as hydraulic conductivity and rheological behaviour underwent only small changes indicating that cementation effects were not very important, and that the swelling capacity did not decrease significantly.

Extensive pitting corrosion was observed in steel plates after experiments with and without radiation (Pusch et al. 1992). Irradiation enhanced the corrosion. An average corrosion depth of 80 µm was measured in the irradiated sample while 18 µm could be determined in the non-irradiated steel. The pitting depth was found to be 480 µm and 160 µm for the irradiated and non-irradiated systems, respectively. Iron was released from the steel and diffused into the clay to about 10 mm depth. This iron may have participated in the cementation of the clay and in the formation of new phases.

Radiation-enhanced corrosion has also been observed by Debruyn (1988) who summarized results obtained on the corrosion of several candidate container materials, including carbon steel and cast iron under clay repository conditions. In some of the tests, samples were in direct contact with the clay while others were in contact with interstitial clay water, a humid clay atmosphere (up to 170°C) or Antwerpian groundwater. Some tests were performed under gamma radiation (^{60}Co) with dose rates of 1 kGy h^{-1} in an inert or oxidizing atmosphere. Furthermore, they performed experiments on carbon steel in interstitial clay water and clay/clay water mixtures at 90°C for exposure times ranging from 50 to 1000 hours. After 40 days of irradiation the pH of the clay remained almost unchanged, but a slight acidification is observed in oxic conditions. The production of H_2 with a yield close to the one calculated for the radiolysis of water was measured. Concerning the steel corrosion mechanism, pitting was observed in both irradiated and non-irradiated samples with a similar penetration depth in both cases. A maximum corrosion rate of 150

µm y^{-1} was measured without radiation, whereas a value of 300 µm y^{-1} was determined under radiation in oxic conditions.

In more recent work, Liu et al. (2017) studied the corrosion of low carbon steel in bentonite containing 17 wt.% of Beishan groundwater (Na-Cl-SO_4 type) and irradiated with a ^{60}Co gamma source with a dose rate of 2.98 kGy h^{-1} for 1007 h (total dose 3 MGy). The same experiment was performed without radiation. Finally, samples were thermally aged at 90°C for 2880 hours. The corrosion products formed are mainly magnetite, hematite, and goethite with the formation of two new phases under irradiation: siderite and maghemite. The distribution of these corrosion products on the surface is not uniform and two corrosion layers were clearly observed on the samples, an inner and an outer layer, which is consistent with aerobic corrosion. Pitting was the main corrosion form observed in these experiments with deeper pits appearing in the irradiated sample. Irradiation was indeed shown to accelerate the corrosion rate of steel by ~33%, the corrosion rate being 24 µm y^{-1} in the non-irradiated samples and of 32 µm y^{-1} in the irradiated samples.

2.1.8 New insights about the effects of irradiation on carbon steel

Based on the results of a series of tests performed by four different organisations participating in WP ConCorD (JACOBS, UJV, CIEMAT and SUBATECH) it is clear that the effects of gamma radiation on the corrosion behaviour on carbon steel are complex and heavily influenced by the specific environmental conditions. The test duration, radiation dose rate and total dose, temperature, presence of bentonite and, for tests conducted in bentonite, both type of bentonite and the degree of saturation were found to have an impact. The four different sets of tests were not designed for systematic comparison. Thus, each of them will be commented on individually before attempting to draw findings from them as an ensemble. It is thought that these observations may offer new insights into the corrosion of carbon steel under repository conditions.

One set was performed by JACOBS in their Harwell-based corrosion laboratories. Corrosion testing of carbon steel was performed in a deaerated, artificial bentonite porewater solution containing 0.1 M NaCl + 0.2 M $NaCO_3$ of pH 8 at room temperature. Tests were performed over a range of dose rates (between 0.1 to 100 Gy h^{-1}), for durations between 1 to 10000 h (~13.6 months) to give total doses of radiation between 1 and 100 kGy (note that not every combination of dose rate and duration was investigated). The key observation from the JACOBS' tests was that an increase in corrosion rate due to radiation was observed at dose rates above 10 Gy h^{-1}, and the magnitude of the effect increased with increasing dose rate. At all dose rates, as well as in unirradiated tests, the biggest impact on corrosion rate was the test duration, with the decrease in corrosion rate with time approximating that of a power law decay. Therefore, the relative influence of both the radiation on the corrosion rate and the test duration on the corrosion rate can be evaluated by the so called 'enhancement factor' (King and Behazin, 2021). This was most clearly observed for tests that received dose rates higher than 10 Gy h^{-1}, where the relative magnitude of the corrosion in the presence of radiation compared to unirradiated control tests increased monotonically from ~1 (a value of 1 indicates little or no impact of radiation) to 1.4 for test durations between 100 to 10000 hours, respectively. For the test performed for 10000 hours at a dose rate of 10 Gy h^{-1}, the magnitude of the increase in the average corrosion rate due to radiation was ~0.9 µm y^{-1}. The largest impact of radiation was observed at the greatest dose rate tested (1000 Gy h^{-1}), which led to an increase in the average corrosion rate determined over 100 hours of ~20 µm y^{-1}. Due to the high corrosion rates observed at shorter durations, the increase in corrosion rate observed at 1000 Gy h^{-1} only translated to a doubling of the corrosion rate (i.e., an enhancement factor of 2) compared to that observed in an unirradiated control test over the same duration of exposure.

A series of long duration tests (6, 9, 12, and 18 months) was performed by UJV under a small range of exposure conditions in bentonite BCV[1] saturated with deaerated artificial granitic porewater supposed to represent typical waters of the Rožná mine formation layers (the Bohemian Massif) located 1000 to 1200 m under the surface (Červinka, 2018). Comparable tests were also performed in MX-80 bentonite but only for durations of 18 months. Tests were performed at elevated temperature (90 °C and 150 °C) at a single, constant dose rate (0.4 Gy h^{-1}). For both porewater simulant and real bentonite test results were compared to unirradiated control tests performed at ambient temperature, 90 °C and 150 °C. The main finding of these tests was that the presence of radiation resulted in a reduction of the corrosion rate for all tests using BCV bentonite, particularly at the shorter test duration of 6 months. A larger effect was observed at 150 °C compared to 90 °C. For tests using MX-80 bentonite, a slight reduction of the corrosion rate due to radiation was also observed at 150 °C, but no discernible impact of radiation was observed at 90 °C. The greatest impact of radiation was observed in BCV bentonite after testing for 6 months at 150 °C, where the corrosion rate in the absence of radiation was 24.3 µm y^{-1} compared to 12 µm y^{-1} in the presence of radiation. Considering the very small dose rates applied in the experiment and the different trend observed in the sets of samples heated at 90 °C compared to 150°C, it is thought that there is a dominating effect of saturation and temperature on the corrosion rate. CIEMAT performed a series of short-term tests on carbon steel including specimens exposed to FEBEX bentonite at either full saturation or 60% saturation, or to FEBEX porewater with no bentonite at ambient temperature. These tests were irradiated at dose rates of either 66 or 697 Gy h^{-1} for durations of roughly 201 to 212 hours (~8 days) to give total doses of 14 to 140 kGy. The main observations were that in the presence of bentonite the average corrosion loss was greater in the presence of radiation. However, the increase was small compared to variations associated with the statistical dispersion of the corrosion rate measured for different specimens in the same test, and there was no discernible influence of dose rate. Conversely, for the tests in which specimens were exposed to porewater in the absence of bentonite, there was a dose-dependent increase in corrosion rate associated with radiation, but the influence of radiation was also small compared to the variations associated with experimental deviations. It is assumed that the different results observed in porewater relate to the availability of water compared to that in hydrated bentonite, and the capacity of the bentonite to act as a buffer and also a sink for radiolytically produced oxidants.

Finally, SUBATECH performed tests on carbon steel under atmospheric exposure (i.e., without exposure to a bulk liquid phase) in the absence of bentonite and in unsaturated MX-80 bentonite. In both cases, the tests were performed at ambient temperature and at relative humidities of 66, 76 and 99% for between 125 (~ 5 days) and 1000 hours (~ 41 days) in an argon atmosphere. Tests were irradiated at dose rates of 400 Gy h^{-1} and were compared to unirradiated control tests. It was found that, in the absence of bentonite, the corrosion rate was much greater at 63% RH than at 76% or 99%, rising from ~10 to 20 µm yr^{-1} at the higher RH values to roughly 230 µm yr^{-1} at 66% RH, following nearly 1000 hours of radiation exposure. In bentonite, the corrosion rates were much lower, varying between ~1 to 56 µm yr^{-1} after 1000 hours of exposure, with no clear impact of relative humidity. In unirradiated conditions, at RH of 63% there was little or no corrosion (both in the presence and absence of bentonite), at 99% RH the corrosion rate in the absence of bentonite was 1 µm y^{-1}, whereas in bentonite it was of the order of 10's of µm y^{-1} and comparable to the rate observed under radiation for the same conditions. It should be noted that for these tests, there was a wide variation in results between nominally identical repeat specimens and trends of corrosion rate with time imply a high degree of measurement uncertainty (e.g., at 99% RH in bentonite in unirradiated conditions the corrosion rate was 63, 3 and 48 µm y^{-1} following exposure durations of 11, 26 and 42 days, respectively). These findings are consistent with those previously reported by Lapuerta et al., 2008 who demonstrated that radiation lowers the RH under which atmospheric corrosion initiates and lows the RH under which the maximum rate of corrosion is

[1] Černý vrch bentonite, dominated by montmorillonite, with prevailing divalent exchangeable cation, mainly magnesium.

observed. Based on the limited comparison that can be made from the different parallel testing programmes described in this work, it appears that, for tests performed at room temperature in solution (artificial bentonite porewater) there is a modest dose dependent increase in the average corrosion rate of carbon steel due to gamma radiation above 10 Gy h^{-1}. The influence of radiation on carbon steel corrosion, however, appears to prevail at dose rates higher than those expected at the surface of carbon steel canisters designed to be emplaced within a bentonite buffer i.e., 0.01 to 0.3 Gy h^{-1} (Table 2). Furthermore, the results of tests in which specimens were embedded within bentonite suggests that, at ambient temperature, the presence of bentonite inhibits the enhancement in corrosion rate caused by radiation, even at comparatively high dose rates, in both saturated and unsaturated conditions. At elevated temperatures there is evidence that when bentonite is present radiation may lead to an inhibition of the corrosion rate. These results support the approach taken by several WMOs to ignore the impact of radiation on the corrosion of carbon steel containers and is a key finding arising from this work package.

2.1.9 Advancement on performance assessments for carbon steel canisters

The results of the experiments on carbon steel performed in ConCorD provide evidence that the prediction of the extent of radiation-induced corrosion that may occur in a repository environment from tests performed in solution, as opposed to those performed in bentonite, will produce overly pessimistic predictions of the corrosion rate. For tests performed in bentonite, particularly at high temperatures, it was shown that radiation could even lead to reduced corrosion rates compared to unirradiated conditions (i.e., there was an inhibiting effect of radiation). However, it is important to consider the impact of test duration on the observed results. Inhibition of corrosion by the presence of bentonite was the greatest after 6 months exposure and was lower after 12 and 18 months. Hence, if the effect of radiation continued to diminish in the long term, the overall effect over the container lifetime could be quite small.

The corrosion rates obtained from experiments with compacted bentonite are explained in terms of various factors acting simultaneously, such as pore water and degree of saturation, Lower bentonite saturation leads to corrosion in water vapor environment, it being milder than in pore water. The effect of bentonite saturation on the corrosion rate prevails over that of irradiation in the compacted bentonite.

For tests performed in solution, which were more severe in terms of radiation induced corrosion than those performed in bentonite, the influence of radiation was modest compared to the corrosion rate that was observed in its absence, even at dose rates far exceeding those anticipated at the canister surface (0.01 to 0.3 Gy h^{-1} from Table 2). As with copper, there was not a linear relationship between the extent of radiation induced corrosion and the total dose or the dose rate. This implies that accelerated tests undertaken at different dose rates are expected to yield different results even if they performed to the same total radiation dose.

2.1.10 Complementary insights gained by modelling

The numerical model developed by AMPHOS 21 integrates the generation of water and chloride radiolysis species (Kelm and Bohnert, 2004; Pastina and LaVerne, 2001; Riba et al., 2021) by gamma radiation. The complexity of the water and chloride radiolysis models (Kelm and Bohnert, 2004; Morco et al., 2020), which required the implementation of tens of reactions for over 60 species in COMSOL, demanded a separate treatment to understand the evolution of the system. For this reason, several simulations considering different irradiation rates, durations, liquid saturation levels and chloride concentrations were carried out, excluding corrosion reactions.

First, the modeling results from AMPHOS 21 obtained considering at [Cl-] = 0.1 M, 5 Gy h^{-1} and up to 5-day irradiation (see figure 2a) underwent a validation benchmark exercise contrasting the simulation results with those obtained by Morco (2020) considering 5-day irradiation (at 5 Gy h^{-1}) of water with increasing chloride concentration up to 0.1M (see figure 2b and 2c). The comparison between the concentrations of the three main radiolytic species (O2, H2 and H2O2) obtained from the two models indicate similar profiles for these species. Both models predict [H2O2] of ~ $2 \cdot 10^{-7}$ M, at 5h of simulation. The concentrations of [O_2] (10^{-6} M) and [H_2] ($2.5 \cdot 10^{-6}$ M) obtained with AMPHOS 21 model at 5-day irradiation (at 5 Gy h^{-1}) which has not reached the steady state, are about one order of magnitude lower than those obtained by Marco (2020) for the same species at steady state.

Erreur ! Source du renvoi introuvable.

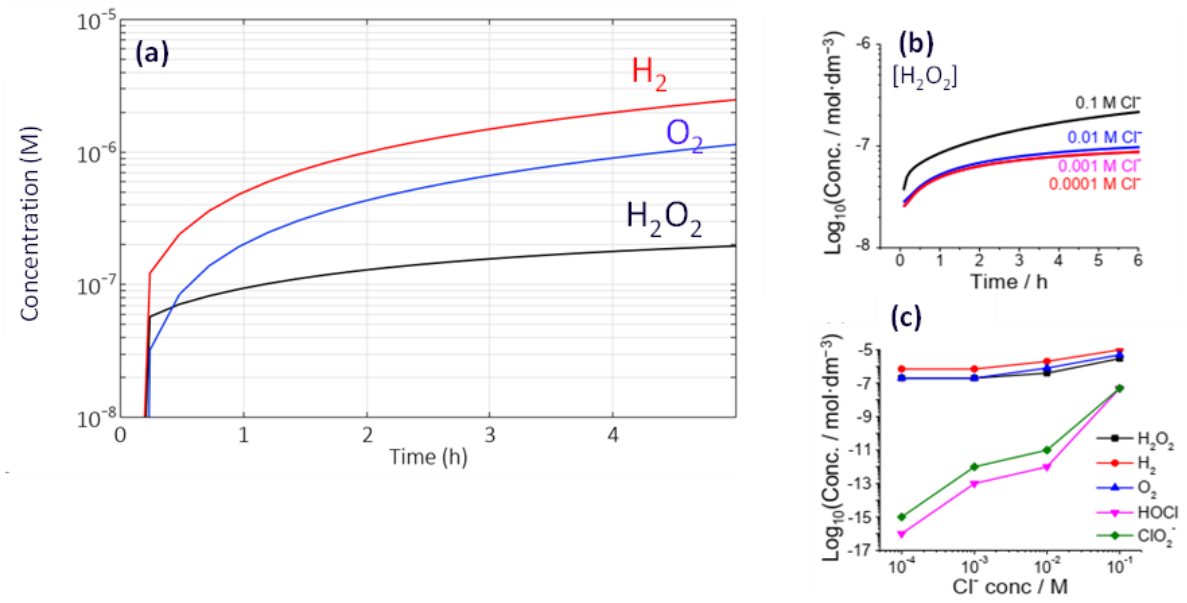

Figure 2: (a) Concentration of radiolysis products calculated using the model develop by AMPHOS 21 considering [Cl-] = 0.1M (a), and GWRM-simulated H2O2. (b) concentrations as a function of irradiation time in different low chloride solutions at pH 8.0, 25 ºC, deaerated conditions and a dose rate of 5 Gy·h−1. (c) Steady-state concentrations of major radiolysis products as a function of chloride concentration.

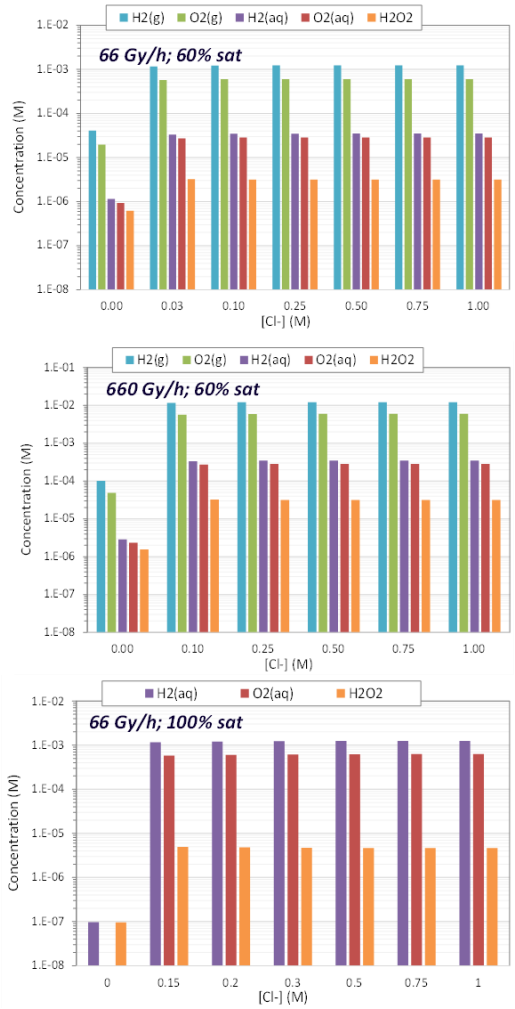

Figure 3: Concentration of radiolysis products calculated by the model developed in AMPHOS 21 considering several chloride concentrations, two different liquid saturation levels and irradiation rates of 66 and 660 Gy h^{-1}.

The next step was aimed to determine the relationship between the chloride concentration and the generation of radiolytic products shown in figure 2, as well as the effect of increasing the irradiation rate by one order of magnitude and considering saturated conditions. Figure 3 clearly shows that the presence of chloride (> 0.01M) in water induce an increase of about an order of magnitude in the concentration of the main radiolytic species under the conditions of 66 Gy h^{-1} and 60% saturation. On the other hand, a linear correlation with the irradiation rate was found, as going from 66 Gy h^{-1} to 660 Gy h^{-1} led exactly to 10-times higher concentrations.

Finally, figure 4 shows the evolution of the main radiolytic species from simulations with AMPHOS 21 model over 30 days when applying 66 Gy h^{-1} to a cell with 60% water saturation and a chloride concentration of 0.1 M. Whereas hydrogen peroxide reaches an equilibrium concentration, hydrogen and oxygen concentrations show a constant growth rate. Aqueous oxygen is expected to assist the corrosion of carbon steel unless a protective corrosion product layer is formed.

Erreur ! Source du renvoi introuvable.Erreur ! Source du renvoi introuvable.Erreur ! Source du renvoi introuvable.

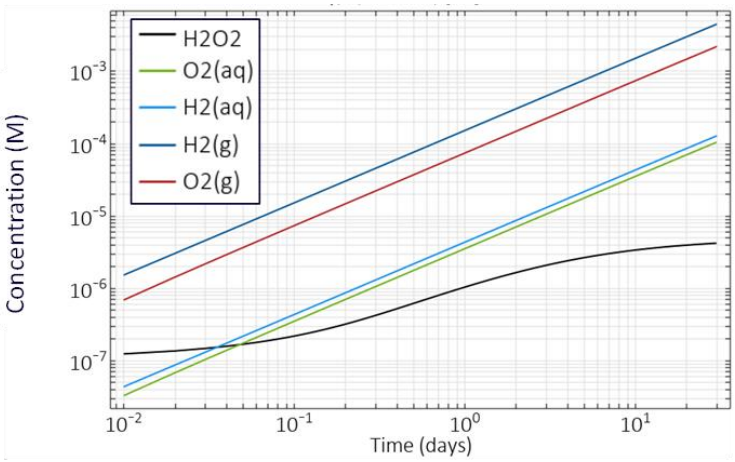

Figure 4: Evolution of the main radiolytic species for an irradiation rate of 66 Gy h^{-1}, 60% water saturation and $[Cl^-]$ = 0.1 M.

2.2 Effect of irradiation on the corrosion of copper containers

A comprehensive review of the effects of irradiation on the corrosion behaviour of copper was recently published in Posiva (2021a**).** In this report, we summarize the most relevant information.

2.2.1 Radiolysis effects on copper corrosion

The generation of oxidant species by radiolysis of aqueous solutions is the main factor influencing the corrosion of copper in a repository. In what extent the radiation does change the corrosion rate is represented by the enhancement factor. Figure 5 presents a compilation of values of this factor for the general corrosion of oxygen-free copper under diverse saturations and dose rates. The graphic points out that a perceptible corrosion enhancement is obtained for absorbed dose rates greater than 20 Gy h^{-1} (figure 5a). A decrease of the corrosion rate is observed, however, at lower dose rates. The initial aeration of the solutions and the exposure period do not seem to exert any significant influence on the corrosion enhancement Data plotted as a function of total dose (figure 5b) indicates that a corrosion enhancement appears only for absorbed doses >10 kGy. These tendencies, however, should be taken with caution, because the studies, from which these values were extracted, were not all conducted to the same total dose or for the same period of time. Also, the absence of an observable corrosion enhancement may simply be due to the low sensitivity of the corrosion rate measurements.

The mechanisms of radiation-induced corrosion of Cu-OFP (oxygen free – phosphorous doped) was investigated by Björkbacka et al in deaerated pure water (Björkbacka et al. 2012, 2013, 2015, 2016). The experiments were performed at dose rates of 80-770 Gy h^{-1} attaining total absorbed doses similar to those predicted for a KBS-3 style canister for about 100 years (~ 100 kGy). It was observed that (Björkbacka et al. 2012, 2013):

- the dissolved metal in the form of precipitated oxides or in solution was larger than that predicted by a homogeneous radiolysis/surface kinetic model,
- the concentrations of copper in solution exceeded the solubility of either Cu_2O or CuO,
- radiation induces localised attack characterized by circular pits of about 0.8 μm depth.

According to these studies, the maximum depth of penetration predicted for repository-relevant total absorbed doses was of the order of 1-2 μm.

These investigations pointed out a significant discrepancy between the experimental corrosion assessment and the corresponding predictions based on a radiolysis model. This was in principle attributed to the existence of an unknown process other than the radiolytic production of oxidants (Björkbacka et al. 2013, 2015, 2016). The modelling was based on a homogeneous radiolysis system considering H_2O_2 and hydroxyl radicals OH• as the primary oxidants (Björkbacka et al. 2016). This approach, which was successful in predicting the rate of oxidative dissolution of UO_2 (Ekeroth et al. 2006), failed in predicting the observed copper corrosion. that the formation of a semi-conducting oxide was supposed to enhance the extent of radiation-induced corrosion by the generation of electron-hole pairs (Björkbacka et al. 2016), thus increasing the potential difference between the (cathodic) oxide and (anodic) underlying copper. Also, it was presumed that the yield (G-value) of OH• was much higher in the presence of the oxide as it was assumed for the homogeneous radiolysis model. The higher yield of oxidants along with the large effective surface area of the oxide would bring about an enhancement of corrosion (Björkbacka et al. 2016).

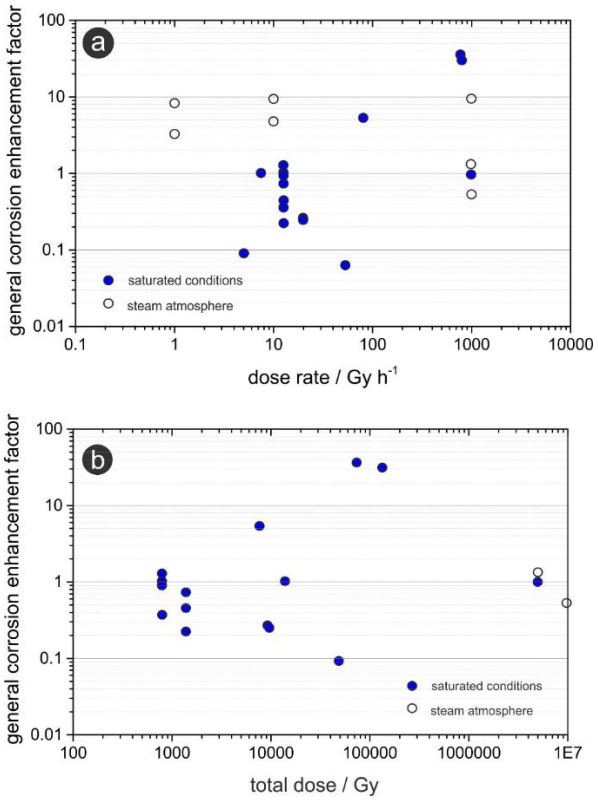

Figure 5: *Effect of gamma irradiation on the enhancement of the rate of uniform corrosion of oxygen-free copper as a function of (a) dose rate and (b) total dose (adapted from King and Behazin 2021). The enhancement factor is the ratio of the corrosion rate in the presence of radiation to that in the absence of radiation, as measured under similar environmental conditions and over a similar duration. An enhancement factor greater than one indicates that the corrosion rate is higher in the presence of irradiation.*

Soroka et al. (2021) have deepened this issue carrying out experiments where the thickness of the oxide film on copper coupons exposed to H_2O_2-containing anoxic water was monitored for different exposure

conditions and lengths. These experiments indicated that corrosion continues even after the complete consumption of H_2O_2 (either by the electrochemical reduction supporting corrosion or through heterogeneous decomposition to O_2 and H_2O). Thus, it was evident that O_2 rather than either H_2O_2 or OH• was the main oxidant species under radiation. Soroka et al. (2021) were able to calculate values of the oxide film thickness close to those reported by Björkbacka et al. (2013) by adding the H_2O_2 decomposition reaction:

$$2H_2O_2 \rightarrow O_2 + 2\ H_2O \qquad (1)$$

and the the reaction of Cu with O_2 treated as homogeneous reactions with rate constants characteristic of diffusion-controlled reactions.

Björkbacka et al. (2016) have found that copper nanoparticles of about 20 nm are released in the solution during corrosion. This should explain a measured copper concentration up to 30 times higher than the solubility of Cu_2O and three times higher than the solubility of CuO. The formation of colloids during the irradiation-induced corrosion of copper was also reported by Bessho et al. (2015).

The strongest radiation in a repository is expected for the early unsaturated phase. Therefore, irradiation studies have been carried out in humid air.

An extent of corrosion in humid air or humid argon (60% or 100% RH) in the presence of radiation (470-500 Gy h^{-1}, total absorbed dose 45-48 kGy) was found 7-9 times higher than in unirradiated systems (Björkbacka et al. 2017). Also, the similar enhancement factor measured in air and Ar lead the authors to conclude that, the HNO_3 radiolytically produced in air did not play a direct role in the increased corrosion. The extent of corrosion in irradiated unsaturated systems (as quantified by the mean film thickness) was higher than that in a similar experiment in anoxic water. This could be explained by the fact that in humid air the primary oxidant in irradiated systems is OH•. In bulk water systems, however, longer-lived H_2O_2 scavenges the HO• radical prior its reaction with the surface. This explanation, however, should be reconsidered if molecular O_2 rather than the HO• radical is considered to be the primary oxidant as suggested by Soroka et al. 2021. ,

The hypothesis of Björkbacka et al. (2017) the irradiation renders a more reactive surface toother species present in the repository does not seem to be supported by their own experimental results. Thus, no additional corrosion occurred if the irradiated sample was immerged in anoxic water after being irradiated in humid air (60% RH) for a period of 96 h at 500 Gyh^{-1} (total dose 48 kGy).

The radiation-induced corrosion of copper in humid air (70-85% RH, 75°C) was also studied by Ibrahim et al. (2018). Without radiation, a thin water layer and larger isolated droplets were formed. Under the thin water layer, a passive film constituted by a Cu_2O/CuO layer was formed. Thicker, porous and non-passivating deposits appeared under the droplets. Irradiation at a dose rate characteristic of the canister (0.35 Gy h^{-1}) had relatively little impact. No changes of the oxide thickness were observed under the thin water layer in comparison with the same experiment in the absence of radiation. Although irradiation brings about an increase the spreading of the condensed water droplets, corrosion did not extend any deeper. The rate of corrosion penetration was relatively low compared with the rate of lateral spreading of the droplets. Thus, irradiation induced a rather lateral than deeply extending corrosion.

Irradiation does not induce environmentally assisted cracking of copper. No evidence for the occurrence of stress corrosion cracking on various types of stressed samples exposed to irradiated environments at dose rates between 19 Gy h^{-1} and 4.9 kGy h^{-1}, total doses up to 10 MGy, and exposure periods up to 5 years, at temperatures up to 150°C (Johnson et al. 1996, Yunker 1990, Yunker and Glass 1987) was found.

An increase of the hydrogen content in 99.98 wt.% copper was reported by Lousada et al. (2016) after irradiation in anoxic pure water at a dose rate of 490 Gy h^{-1} and total doses between 35 and 70 kGy. Figure 6 shows the H content as a function of the total dose and the amount of adsorbed H_2O. The lack of correlation between the two data sets was presented as evidence for the absence of a dissociative adsorption of H_2O as a source of absorbed H (Lousada et al. 2016).

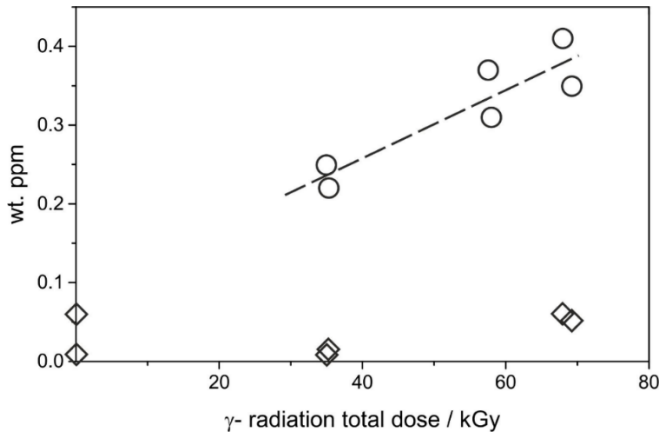

Figure 6: *Effect of absorbed dose on the hydrogen content of pure copper following irradiation in anoxic water at a dose rate of 490 Gy/h (adapted from Lousada et al. 2016). The circles indicate the H content, and the diamonds represent the amount of adsorbed H_2O.*

2.2.2 Effect of irradiation on material properties

Radiation damage of materials, including copper (Li and Zinkle 2012), is generally associated with in-reactor exposure and high neutron fluxes. Radiation damage can alter the mechanical properties of copper alloys, including an increase in yield strength (radiation hardening), a reduction of fracture toughness, and in-reactor creep (Li and Zinkle 2012). In contrast, typical neutron- and γ-dose rates in canisters are significantly lower and radiation damage of the copper has always been considered to be negligible (Guinan 2001, SKB 2010a).

Yang et al. (2019) confirmed earlier estimates of Guinan (2001) that the damage from neutron- and γ-irradiation over the lifetime of the canister will be between 10^{-7} displacements per atom (dpa) and 10^{-6} dpa. Thus, any effects of radiation hardening are immeasurable below 10^{-4} dpa (Li and Zinkle 2012). Recently experiments on γ-irradiation of 99.999% copper at a dose rate of 1 kGy h^{-1} to a total dose of 100 kGy did not show any microstructural changes or changes to the population or nature of defects. (Padovani et al. 2019, SKB 2019, Yang et al. 2019).

In the framework of ConCorD, JACOBS and CIEMAT performed separately sets of tests to ascertain the influence of radiation on the corrosion of copper. The impact of the radiation dose rate, the total dose and the presence of bentonite on copper corrosion was emphasized.

JACOBS evaluated the corrosion rate of copper upon exposure to a deaerated, artificial bentonite porewater containing 0.1 M NaCl + 0.2 M $NaCO_3$ of pH 8 at room temperature over a range of dose rates between 0.1 to 10 Gy h^{-1} (narrower than the range tested for carbon steel), and for durations of

10000 h (~13.6 months) to give total doses of radiation between 1 and 100 kGy. The results were compared to unirradiated control tests.

It was found that the copper corrosion rate exhibited a strong dose rate dependence over the full range of dose rates investigated by JACOBS. At the highest dose rate tested, 10 Gy h^{-1}, the increase of the average corrosion rate compared to unirradiated conditions was ~1.2 µm y^{-1}, which was similar to the 0.9 µm y^{-1} observed for carbon steel in the same conditions. However, for copper the increase in the average corrosion rate by 1.2 µm y^{-1} was an increase of roughly 60 times the rate observed in the absence of radiation, which was 0.02 µm y^{-1}. In contrast, for carbon steel, a radiation-induced increase in the average corrosion rate by 0.9 µm y^{-1} was only equivalent to a 40% increase compared to unirradiated conditions. A noteworthy observation was that there was a radiation-induced enhancement of the corrosion rate of copper even at the lowest dose rate tested (of 0.1 Gy h^{-1}). At 0.1 Gy h^{-1}, the average copper corrosion rate was 0.05 µm y^{-1} compared to just 0.02 µm y^{-1} without irradiation, thus reflecting an increase by 2.5 times. By comparison, for carbon steel at a dose rate of 1000 Gy h^{-1}, the radiation increased the corrosion rate by a factor of 2.

Tests performed by CIEMAT in deaerated FEBEX pore solution at ambient temperature under radiation at dose rates of 66 and 697 Gy h^{-1} has shown an increase in the average corrosion rate of copper. However, for the same exposure duration, the average corrosion rate did not increase with increasing dose / dose rate. The corrosion rate in unirradiated porewater was between 3.1 and 3.3 µm y^{-1}. After exposure times of roughly 201 to 212 hours, i.e., for total doses of 14 (66 Gy h^{-1}) and 140 kGy (697 Gy h^{-1}), the corrosion rate increased to 46 to 50 µm y^{-1} at and 20 to 30 µm y^{-1} respectively. In the case of tests performed in FEBEX bentonite, a different behaviour from that in artificial porewater was generally observed. Tests in irradiated bentonite showed lower corrosion rates compared with tests performed in its absence. At the higher radiation dose rate, the corrosion rate was lower for all conditions tested, i.e., at densities of 1.4 and 1.6 Mg m^{-3} and at 60% and 100% saturation. At the lower dose rate, the corrosion rate in bentonite at a density of 1.4 Mg m^{-3} was lower than that in unirradiated conditions. The opposite, however, was observed at a density of 1.6 Mg m^{3}.

In artificial porewater, copper exhibits a strong dose rate dependent increase of corrosion rate up to dose rates of 10 Gy h^{-1}, exceeding the maximum dose rates expected at the surface of some copper waste container designs within a GDF (0.2 to 0.8 Gy h^{-1} from Table 2). At 10 Gy h^{-1}, the absolute magnitude of the increase in corrosion rate induced by radiation is similar to that observed for carbon steel. However, due to the lower corrosion rate of copper in simulated repository environments, the relative increase of corrosion rate was considerably higher than observed for carbon steel, even at dose rates as low as 0.1 Gy h^{-1}.

As also pointed out for carbon steel for short-term tests, the presence of bentonite mitigates the influence of radiation on copper, and in some cases leads to a reversed effect, lowering the corrosion rates.

2.2.3 Advancement on performance assessments for copper canisters

The experimental results on radiation induced corrosion of copper gained in ConCorD indicate that the prediction of the extent of radiation induced copper corrosion in repository environments from tests performed in solution might generate overly pessimistic outputs. This is attributable to an apparent mitigation of the radiation-induced corrosion by bentonite. Furthermore, tests performed in solution have shown that the increase of corrosion rate assigned to radiation effects does not scale linearly with dose rate. This could imply that tests under radiation with different dose rates lead to different corrosion losses even if the total dose of radiation is the same and tests reach a steady corrosion rate. Hence, careful

consideration of an appropriate dose rate should be considered when performing tests to provide information on the likely behaviours in a repository in the long-term.

Furthermore, based on tests performed in test solutions (i.e., without bentonite), a significant influence of radiation was observed within the range of dose rates expected at the container surface under repository conditions. Although bentonite mitigated the influence of radiation at high dose rates, the extent to which the presence of bentonite could mitigate the corrosion of copper under representative dose rates was not determined and should be the focus of future work.

3. Corrosion under environmental transients

3.1 Nature of environmental transients

The understanding of the evolution of the environment surrounding the canister in the repository over long periods of time is essential for a reliable analysis of the corrosion of canister materials.

There are two important aspects of the disposal environment impacting the corrosion behaviour of the canister (King and Padovani, 2011): i) the changes of the corrosive nature of the environment in the geological disposal repository (GDR), and ii) the type of canister material.

The evolution of the chemistry of the environment after repository closure depends on the engineered barriers and the composition of groundwater. Other important factors include (King and Padovani, 2001):

(i) the maximum canister surface temperature: typically, ~100°C
(ii) the engineered barriers: compacted bentonite, cement, or concrete
(iii) the pore water in contact with the canister: its properties will likely change over time and, initially at least, differs from that of the ground water
(iv) the amount of available O_2, limited in deep geological formations to that trapped after sealing of the GDR
(v) the magnitude of the gamma (and neutron) radiation fields at the outer surface of the canister and the amounts of oxidising (and reducing) radiolysis products formed
(vi) the time for the GDR to saturate with ground water following closure, typically a few decades or hundreds of years
(vii) the rate of mass transport of reactants to, and of corrosion products away from, the canister, which is largely determined by the nature of the barriers
(viii) the possibility of microbial activity at, and away from, the canister surface.
(ix) the magnitude of residual and applied stress
(x) the permeability of the host rock and its transport capacity for any H_2 that may be produced by the anaerobic corrosion of the canister
(xi) the mineral content of the rock; the oxidation of pyrite can lead to the formation of thiosulphate and other oxidised forms of sulphur that can be deleterious for some candidate canister materials

The corrosion of container materials has been extensively studied under constant conditions, commonly those reflecting the long-term period of the repository. Thus, the extrapolation of experimental results to the evolving chemical, mechanical, and redox conditions of the early post-closure period, needs to be verified and complemented. Conceptually, four phases are identified for the temperature-relative humidity (RH) and, for aerobic/anaerobic conditions, at the canister surface from the time of emplacement up to one million years (Landolt et al., 2009 for the specific case of the NAGRA concept):

- Phase 1 – initial dry phase (oxic and dry conditions: first tens of years)
- Phase 2 – aerobic unsaturated phase (oxic and unsaturated conditions: few months to tens of years)
- Phase 3 – anaerobic unsaturated phase (anoxic unsaturated conditions: up to first hundred years)
- Phase 4 – long-term cool, anoxic phase (long term anoxic and fully saturated conditions).

Figure 7 shows a schematic representation of the evolution of the temperature and relative humidity at the canister surface after the time of emplacement. The establishment of anoxic conditions after an initial oxidic period is a key consideration. The corrosion behaviour in steady-state conditions after the consumption of oxygen has been the focus of EC research projects (e.g. NFPRO[2] and PEBS[3]) as well as several independent studies (Arcos et al. 2005; Arcos et al. 2008; Carlson et al. 2006). The role of the 'dry' period preceding re-saturation (not corrosive or slightly corrosive) and the transient period during re-saturation (potentially corrosive) should be also regarded. After facility closure, the saturation of the bentonite barrier during the thermal phase of the repository leads to swelling and the development of mechanical stresses on the container. Such transients can be further influenced by attempts at repository footprint optimisation (e.g., increased container heat production). Considering the time span of the processes we can presume that the characteristic timescales of the various environmental transients are oxygen consumption < saturation < chemical < temperature.

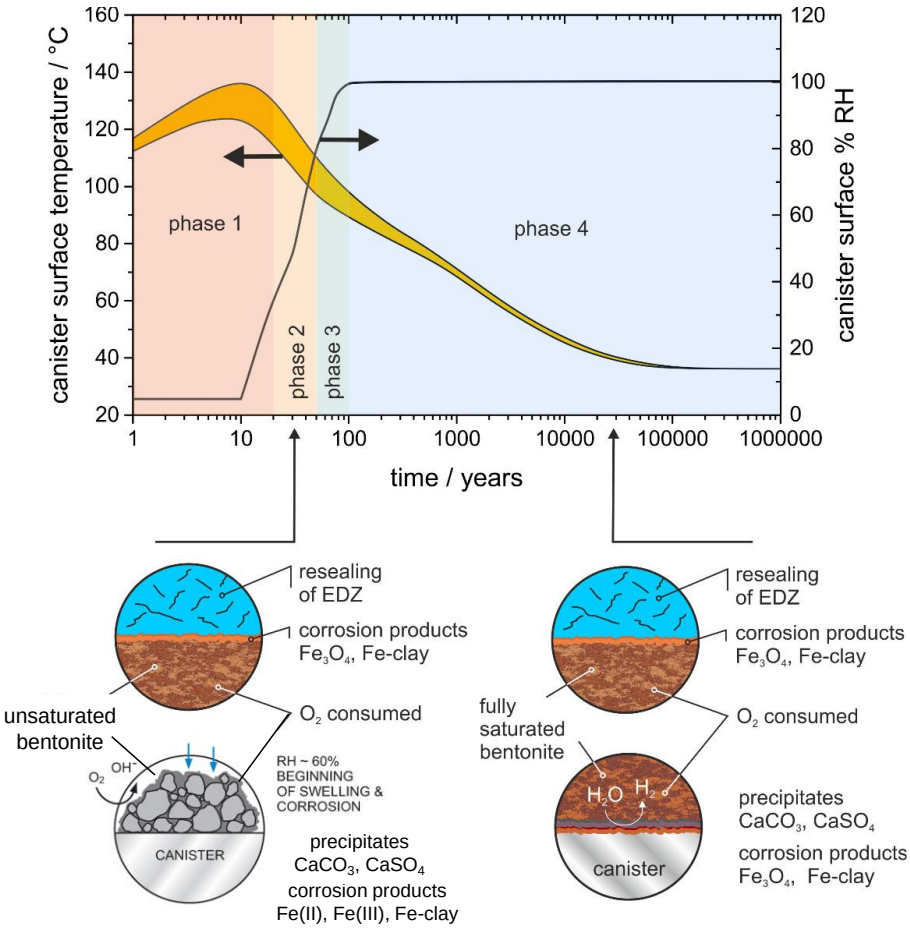

Figure 7: Evolution of temperature and relative humidity (RH) with time and the expected corrosion products and processes at the canister surface (lower diagrams) (adapted from Landolt et al., 2009). EDZ: excavation-damaged zone.

[2] https://cordis.europa.eu/project/id/2389
[3] https://cordis.europa.eu/project/id/249681/reporting/es

3.2 Redox transients

The redox conditions in the EBS constitute an important factor determining corrosion and the behaviour of radionuclide transport in the nearfield (Giroud, 2014). A redox system may involve gases (O_2, N_2, H_2, CH_4, CO_2), dissolved components (NO_3^-, NH_4^+, CH_2O (TOC), Fe^{2+}, Mn^{2+}, SO_4^{2-}, HS^-, H^+), as well as solids (FeOOH, MnO_2, $FeCO_3$, $MnCO_3$) and components (Fe^{2+}, Mn^{2+}, NH_4^+) associated with the solids by ion exchange (Christensen et al., 2000). The most important species that undergo redox reactions contain carbon, iron, sulphur, and nitrogen. Thus, the knowledge of the kinetics and reactivity of the redox-active species involved is important for the determination of the redox conditions.

In the case of an SF/HLW repository, the redox conditions will be determined by the inventory of O_2 trapped during closure and by the radiolysis of the pore water. The different processes that a priori can have a larger influence on the short and long-term redox evolution of the repository are a) metal corrosion, b) organic matter degradation, and c) microbial activity.

The corrosion evolutionary path (CEP) defines the time-dependent corrosion behaviour of the canister and is closely tied to the evolution of environmental conditions. A useful indicator of this evolution of the corrosion behaviour is the time dependence of the corrosion potential (E_{CORR}) of the canister (figure 8). During the early aerobic phase, E_{CORR} is relatively noble (positive) because of the cathodic reduction of O_2. At longer times, the corrosion potential falls to a value determined by the relative rates of Fe dissolution and the reduction of H_2O, resulting in E_{CORR} values close to the H_2/H_2O equilibrium potential during the long-term anaerobic phase. Between these two periods, the value of E_{CORR} undergoes a transition, during which Fe(III) corrosion products formed during the aerobic phase are reductively dissolved to Fe(II) species (Johnson and King, 2008). Although H_2O is an oxidant for some canister materials, the rate of corrosion processes in anoxic conditions is typically less severe than in aerobic environments (Shoesmith, 2006). The redox potential of the repository (Eh) will be determined by the most dominant redox couple. In aerobic systems, the Eh will be determined by the O_2/H_2O couple, whereas equilibrium between Fe^{2+} and $Fe(OH)_3$ or involving pyrite may determine the redox potential under anaerobic conditions. Certainly, in systems where sulphide is present (either naturally in the ground water or produced by the action of sulphate-reducing bacteria (SRB)), the Eh of the repository will become reducing. The expected nearfield redox conditions have been investigated in different EU Projects (NF-PRO, RECOSY) (Carlsson and Muurinen, 2008; Duro et al., 2014). Wersin et al. (2021) proposed a conceptual model of corrosion, the redox evolution and Fe-clay interaction processes in the ABM2 in situ test, and Hadi et al. (2019) in the FEBEX *in situ* test.

The establishment of anoxic conditions after an initial oxic period is a key consideration for evaluation of conditions for corrosion processes. Apart from the oxygen trapped in the pore spaces, the radiolysis of humid air or water also produces oxidising species, such as H_2O_2, resulting in an increase of the general corrosion rates of metals or to localised corrosion (Crusset et al., 2017). The effect of the radiolysis of water on corrosion, however, can be significantly attenuated in the absence of oxygen (Lapuerta et al., 2008).

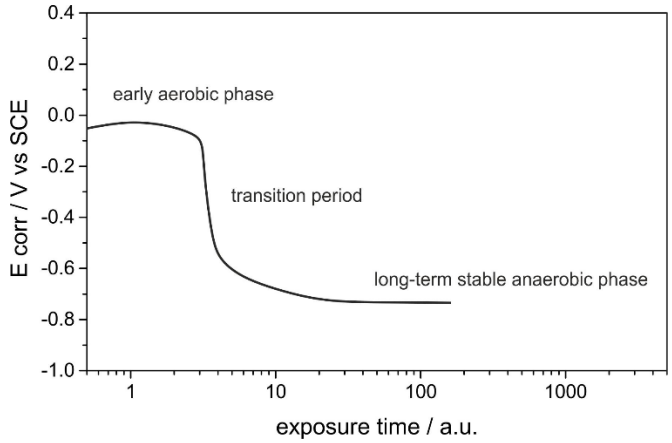

Figure 8: Schematic representation of the evolution of the open circuit potential of carbon steel during the aerobic-anaerobic transition. Potentials are given with respect to the SCE scale, which is +242 mV versus the normal hydrogen electrode (NHE). (Diomidis & Johnson, 2014; King, 2008a; Johnson & King, 2008).

Oxygen can be consumed by corrosion of the canister and of the steel mesh stabilizing the tunnel wall (for clay rock, see Landolt et al., 2009), oxidation of Fe minerals in the bentonite (Wersin et al., 1994), (Puigdomenech et al., 2001), (Grandia et al., 2006), (Giroud et al., 2018), or by microbial activity (fermentative microbially-mediated reactions or aerobic respiration) in bentonite (Kotelnikova and Pedersen, 1998) (Giroud et al., 2018). Corrosion conditions during Phase 1 supports a uniform dry oxidation yielding trivalent iron oxide (figure 7). Oxidation of sulphides in the backfill may contribute to oxygen consumption and would produce sulphate and thiosulphate (Landolt et al., 2009). All the oxygen is presumed to be consumed during Phase 2 (figure 7).

Wersin et al. (1994; 2007) proposed two ways for the O_2(g) consumption in the buffer: (i) diffusion into surrounding rock, and (ii) reaction with mineral phases existing in the buffer and backfill materials. They predicted that anoxic conditions would be re-established in the buffer after a period ranging between 7 and 290 years (Wersin et al., 2007) depending on the value taken for the most uncertain parameter: the pyrite reactive surface area. Giroud et al. (2018) considered gas exchange with bentonite pore water and adsorption on mineral surfaces as the most important processes controlling O_2 in the drift of the FE experiment, which was fully consumed after only a few months. According to Grandia et al. (2006) aerobic conditions can prevail for more than 5,000 years in the absence of geochemical processes (consumption of O_2 in the buffer).

Other authors (Kotelnikova and Pedersen, 1998) determined the period of consumption of O_2 by microorganisms to be in the range of 9 days to 4 years. Puigdomenech et al. (2001) also confirmed the short term of consumption of O_2 due to microbial involvement and organic matter degradation.

The Swedish research programme studied in more detail the consumption of O_2 trapped in the repository, reacting with rock minerals in tunnels and deposition holes. Malmström et al. (1995) studied the kinetics of dissolution of Fe(II)-bearing silicate minerals (biotite and chlorite) and presented a simple calculation of the time needed for oxygen consumption in fractured granite due to the oxidation of the Fe(II) contained in the silicates. Periods of time ranging from 50 to 300 years were estimated, depending on the type of mineral and on whether oxygen was considered to the depleted by direct consumption on the mineral surface or by oxidation of the Fe(II) previously released from the mineral.

During Phase 2, the environment is still aerated, and atmospheric corrosion takes place as the moisture starts to condense on the iron surface (figure 7). Atmospheric corrosion is an electrochemical

phenomenon and leads to a variety of corrosion products: in addition to Fe_3O_4 and Fe_2O_3, hydrated ferric species including different forms of FeOOH and green rust can be formed. Corrosion during Phase 2 may be influenced by the deliquescence of salts and by the presence of particulates on the surface, in a process not necessarily uniform (Landolt et al., 2009). Droplets of water can form by deliquescence of individual salt crystals, or collections of crystals, with surrounding areas either dry or wetted by microdroplets or thin layers of moisture. If O_2 is still present in the bentonite at this time, the regions around the deliquesced droplets will tend to become cathodic because of the greater access of O_2. The droplets themselves will tend to become O_2 depleted. Some degree of localised attack can be expected during this period (Diomidis and Johnson, 2014) (Johnson and King, 2008).

3.3 Saturation transients

The time-dependent degree of saturation of a repository will determine when and how corrosion will occur (King 2006, 2013a). Initially, the system may remain sufficiently dry to hinder aqueous corrosion. As the system cools and the RH increases, the surface of the canister becomes wet and aqueous corrosion is possible.

The time for complete saturation of a repository is estimated to be in the range of 100-1000 years (Johnson and King, 2008), although it may take tens of thousands of years in certain low permeability sedimentary host rocks. According to estimations using standard multi-phase flow process models, complete re-saturation occurs in 3-4 years in a permeable, fully saturated host rock (Rutqvist and Tsang, 2008). Different *in situ* experiments, such as the FEBEX experiment at Grimsel or the HE and FE Experiments at Mont Terri provide information about the saturation behaviour of the bentonite barrier (Villar et al., 2020).

The typical assumption applied to bentonite re-saturation is that groundwater is available in the host rock. Due to the high chemical suction in partially saturated bentonite (SKB 2006a), water is drawn in from the surrounding host rock into the bentonite. The rate at which re-saturation can occur will be controlled by the intrinsic permeability and water saturation state of the surrounding host rock.

The application of a thermal load on the inner (nominally ‘dry’) side of a bentonite buffer has a significant impact in terms of accelerating the generation and diffusion of water vapour. The water vapour migration is implicitly related to the water suction, and both vapour and liquid water are driven in proportion to the suction pressure. Therefore, water vapour mobilizes at the canister boundary and drives water away from the canister. Moving away from the heat source, some of this vapour returns to the liquid state. The condensate migrates back towards the low-water saturation, high-suction inner surface, creating a local water circulation pattern (figure 9).

However, if the availability of water from the host rock is low, or the heat source is relatively large, it is possible to dry large sections of the bentonite and to induce relatively high temperatures in the inner annulus. Intense desiccation can occur in the warmest part, causing a microstructural collapse. This leads to contraction of the stacks of ordered smectite lamellae, so that spontaneous expansion may be only partial when water finally enters. The affected part of the buffer may permanently lose some of its expandability and self-healing capacity, turning fine-fissured (Wilson et al., 2011).

These fluid processes would also lead to an accumulation of chloride and sulphate salts near the hot canister surface, whilst driving away dissolved silica. This induces the canister corrosion and a radial variation of clay density, resulting in changes of porosity (Couture, 1985).

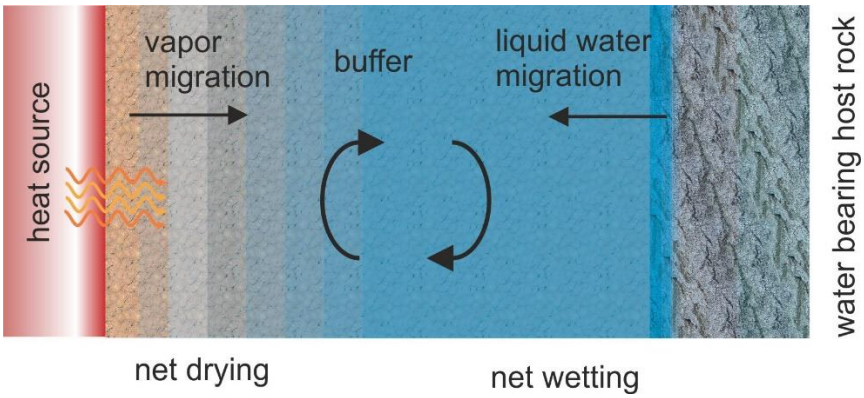

Figure 9: Schematic of the drying and re-saturation process of a clay buffer between a heat generating canister and the host rock (adapted from Wilson et al., 2011).

The processes observed during the evolution of the environmental conditions in a DGR are summarized in figure 10. Before saturation, localized corrosion is possible because surface salts wet (deliquesce) before the development of full saturation, leading to spatial separation of anodic and cathodic sites (King 2013a, 2017). With increasing RH, the surface of the canister becomes progressively wetter until it is uniformly wetted. The rate of supply of gaseous reactants (e.g., O_2) will be higher under unsaturated conditions, but the rate of removal of dissolved corrosion products will diminish, increasing the propensity for the formation of protective corrosion product films.

Aqueous corrosion requires an adsorbed water film on the metal surface able to sustain electrochemical reactions. Initially, corrosion may not occur if the relative humidity is lower than the Critical Relative Humidity (CRH). This is a threshold value above which vapour can condense and form aqueous films on the metallic surface. In the case of a discontinuous adsorbed water film, localized corrosive attack of the canister surface may occur. Such adsorbed films form when the surface temperature of the canister decreases below 100°C and the relative humidity rises to about 60% - 80%. However, an adsorbed water film can also form at relative humidity as low as 30% if particularly hygroscopic salts (such as $MgCl_2$ or $CaCl_2.xH_2O$) are deposited on the surface (King, 2006). Different studies have been performed on the corrosion of steel with time, as a function of RH, oxygen content and temperature, and how adsorption of water affects corrosion rates of different metals at different temperatures (Ben Lagha et al., 2007) (Dante and Kelly, 1993) (Lee and Staehle, 1997).

If the bentonite barrier is composed of compacted blocks and granular material, the blocks beneath the canister have a moisture content of 16 % while the granular material on top has a moisture content of about 5 % at the time of emplacement. Consequently, moisture initially flows from the partially saturated bentonite blocks beneath the canister into the drier granular material. While the bentonite close to the canister will not swell, the redistribution of water to locations away from the surface could lead to development of a swelling pressure around the periphery of the tunnel.

Dry conditions persist until cooling and an increasing level of saturation of bentonite causes the relative humidity to rise above the critical level for the formation of thin films of moisture on the metal surface. The resulting thin electrolyte layer can support aqueous corrosion and the formation of electrochemical corrosion cells. Wetting may also be facilitated by the deliquescence of salts. Progressive saturation by water inflow (Phase 2, figure 7) will cause swelling of the bentonite starting from the periphery of the tunnel and gradually progressing towards the centre (Landolt et al., 2009).

Swelling of bentonite continues during Phase 3. In the long-term anoxic Phase 4, bentonite is completely saturated and all oxidized corrosion products formed at the canister surface and the support structures

have been degraded. Over a period of a few hundred years, once complete saturation has been achieved, the groundwater pressure in the bentonite will slowly increase as the hydrostatic head is restored. Equilibration of the bentonite pore water with that in the surrounding host rock will take place over a longer period until the pore-water chemistry reaches a steady state.

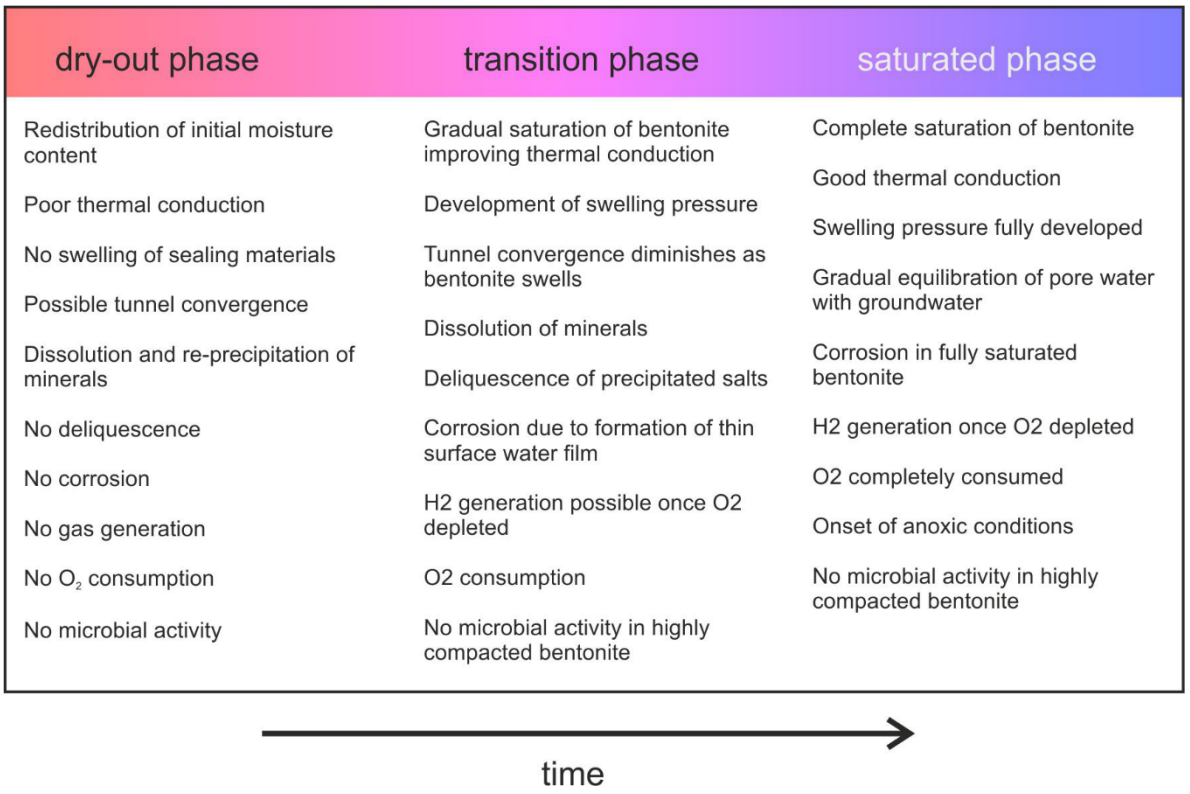

Figure 10: Evolution of Environmental Conditions in a Deep Geological Repository Characterized in Terms of the Stages of Saturation (King, 2005).

3.4 Thermal transients

In deep geological repositories, the engineered barriers are exposed to two separate sources of heat. One is the increase in ambient temperature with depth (temperature increases by 25-30 °C/km for dry rock formations, depending on geographical position). The second source is the heat released due to the decay of radionuclides. The heat dissipates into the nearby engineered structures and the host formation.

The temperature evolution within the bentonite barrier and the surrounding host rock depends on the reference concept for waste disposal in each country. It is a critical factor, as it may alter the properties of the multi-barrier system by acceleration of the corrosion of the waste form and of metal components of the containment systems. Further, high temperatures may degrade the bentonite or cement used as backfill materials, as well as argillaceous host rocks (Finsterle et al. 2019; King et al., 2017a). Temperature variations may also create driving forces that affect the migration of radionuclides in the nearfield of the repository. Chemical thermodynamics, kinetics and diffusion processes are temperature dependent. Thus, the maximum allowable temperature needs to be determined by analysing the acceptable impact on barrier functions.

The evolution of temperature is determined by thermal simulations (e.g., Finsterle et al., 2019). Heat generation from radioactive decay of the SF/HLW results in an initial period of elevated temperature (sometimes referred to as the 'thermal pulse'), followed by a period of slow cooling as the heat release from the waste decreases. The temperature evolution during the thermal pulse has been extensively studied for various disposal systems using both laboratory and field experiments as well as numerical analyses (Payer et al., 2019).

Large-scale, long-term heater tests for mined repositories in the saturated zone have been conducted in underground rock laboratories dedicated to nuclear waste research (HE-E Experiment: t>100°C, EB Experiment: isothermal, FEBEX *in situ* test: t_{max}=100°C, FE Experiment: t<120°C (see Villar et al., 2020). These studies reveal the importance of heat generation as it induces coupled thermal-hydrologic (TH) effects. Strong thermal perturbations also affect the geochemical conditions and corrosion products, as well as the geo-mechanical properties and stress state of the repository components, with complex feedback mechanisms to thermal and hydrologic processes (Nguyen et al. 2005, Zheng et al. 2011, Kumpalainen et al. 2016, Gens et al. 2009, Sánchez et al. 2012, Finsterle et al. 2019). An important thermally induced effect in low permeability media is the pore water pressurization that occurs upon heating (Delage et al., 2010) (Mohajerani et al., 2012). Such strong THM couplings were clearly demonstrated from both *in situ* experiments and laboratory tests performed in the TIMODAZ Project.

Most reported corrosion studies have been performed under defined and constant temperature. An increase of the corrosion rate with temperature is usually observed (e.g., Smart et al. 2002a). Only a few studies have been performed under fluctuating temperature conditions. The effect of decreasing temperature in iron-bentonite interaction experiments was investigated by Pignatelli et al. (2013, 2014), with focus on the nature of formed corrosion products. In these experiments, Callovo-Oxfordian claystone was contacted with metallic iron (present both as coupon and as powder) in autoclaves and heated to 90°C for 6 months before the temperature was reduced by 10°C every month until reaching 40°C. The pH measured after cooling to 25°C did not change considerably. Unfortunately, neither the oxidation-reduction potential nor the iron corrosion rate have been reported. In all samples, the presence of magnetite, cronstedtite and greenalite was detected. These studies also indicated that cronstedtite may not be stable below 50°C. In all cases, the formation of these iron silicates was directly linked to the dissolution of silicates present in the argillite, the solubility being dependent on the temperature.

3.5 Chemical (pore water) transients

In the early, non-isothermal and unsaturated period, thermal and hydraulic gradients influence the properties of the bentonite barrier and its performance. The bentonite pore water can be modified over time due to changes of the initial physicochemical conditions under different types of perturbations: a) interaction with groundwater (saturation phase), b) desaturation phase due to heating, c) perturbations linked to the interactions between the bentonite and the engineered solid materials (concrete, iron, steel, organics, etc.), and d) interactions with different gases produced and consumed in the system (CO_2, H_2, CH_4, etc.), due to mineral dissolution/precipitation, microbiological reactions and corrosion processes.

The impact of the different perturbations can be described in terms of: 1) modifications in the pore water chemistry and redox conditions, which may affect the smectite structural stability and speciation of dissolved ions, 2) mineralogical alteration: dissolution and redistribution of primary mineral phases and precipitation/neoformation of secondary minerals, 3) clay mineral stability and alteration of the clay mineral properties (especially cation exchange capacity, cation exchange population, crystallo-chemical structure, layer charge and swelling ability), and 4) modification of transport properties through

modifications of porosity, permeability and tortuosity by cementation processes. The perturbation processes may change the physical, hydraulic, and mechanical properties of the bentonite system.

The scientific challenge of predicting the long-term clay barrier behaviour consists in analysing the results from experiments conducted in underground research laboratories (URL) in real scales and conditions (Tournassat et al., 2015). Most of the bentonite barrier experiments described in the literature have been carried out under laboratory conditions (e.g., Cuevas et al. 1997, Fernández and Villar 2010, and references therein) to study the chemical evolution of the pore water and the alterations of the bentonite barrier. There are only a few large-scale experiments, such as LOT, ABM, FEBEX and FE *in-situ* experiments (Karnland et al., 2009) (Svensson et al., 2011) (Villar et al., 2017) (Müller et al., 2017). Several papers have reported results of geochemical and reactive transport modelling for the long-term analysis and nearfield evolution (Bradbury and Baeyens, 2002) (Fernández et al., 2004) (Curti, 2011) (De Combarieu et al., 2007) (Savage et al., 2010) (Wersin et al., 2003; 2004) (Itälä, 2009) (Červinka et al., 2018) (Jenni et al., 2019) (Zheng et al., 2015, 2020).

After repository closure, gradual saturation of the bentonite may lead to some redistribution of the water content, dry density, and salts during Phase 1 (figure 7). Precipitation of salts close to the canister surface may also occur, assisted by the desiccation of the bentonite (Landolt et al., 2009). Progressive saturation by water inflow causes re-dissolution of precipitated salts and the bentonite pore water equilibrates with the incoming water from the host rock. During Phase 3, Fe(III)-rich corrosion products formed during the previous periods can be reduced (Diomidis and Johnson 2014). Equilibration of the bentonite pore water with that in the surrounding host rock will continue until a steady state has been reached by approaching to Phase 4 (figure 7), a few hundred years after closure. Steady state conditions for the chemical composition of the pore water, however, have not been achieved before 10.5 years of experiment in the EB experiment (Fernández, 2019), nor before 18 years in the FEBEX in situ test (Fernández et al., 2018), and during the ABM5 Experiment (Fernández et al., 2022). In different tests, it has been observed that the most important parameter for pore water chemistry is the bentonite composition, independent of groundwater chemistry (deliverable D2.6 WP ACED) (Havlová et al., 2020). However, this is true if the infiltrating ground water is a diluted granitic pore water. Modifications in the pore water chemistry and in the cation exchange composition of the bentonites have been observed in the ABM5 experiment after the interaction of a saline granitic groundwater with Na- and Ca-bentonites during 4.4 years (figure 11), indicating an influence of the type of the infiltrating water and the type of bentonite (main cation at exchange sites) on the evolution of the pore water chemistry of the bentonite barrier (Fernández et al., 2022).

In the case of waste disposal concepts in clay formations, concrete structures are needed for supporting galleries. In this context, the pore water pH will evolve as the alkaline mineral phases are leached out over time (see Deissmann et al., 2021) (De Windt et al., 2020). There will be an interface between cement-based materials and metal supporting structures. Highly alkaline pH values during the thermal phase keep the carbon steel canister passivated, thus limiting the corrosion.

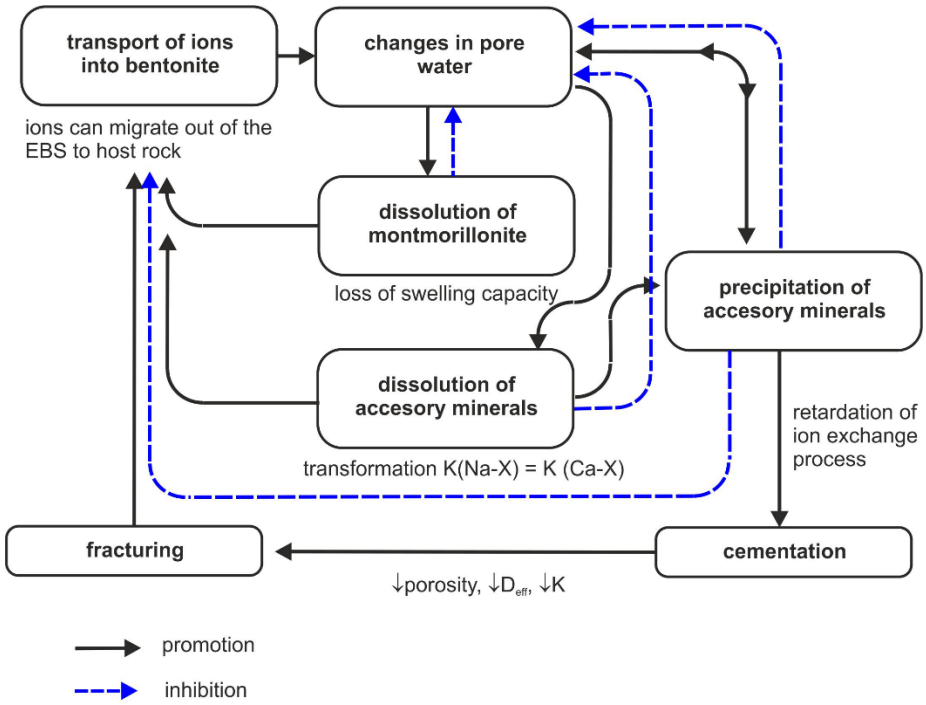

Figure 11: Water-bentonite interaction processes and possible buffer alterations after (Takase, 2004).

3.6 Mechanical transients

Canisters are exposed to residual and applied stresses and, hence, the possibility of environmentally assisted cracking (Shoesmith, 2006). The magnitude of the applied stress (~ 20-50 MPa) depends on the repository design, the depth, and the host rock formation. The external load will comprise the swelling pressure of the backfill (if used), the hydrostatic pressure, and the lithostatic load (the latter only for non-self-supporting rock, such as salt domes and sedimentary deposits).

For a bentonite-backfilled repository, the pressure on the canister depends on (Hasal et al., 2019):

1. the hydrostatic water pressure in the rock, which is transferred to the canister through almost fully saturated bentonite,
2. the swelling pressure of bentonite (Raikko et al. 2010),
3. the increase of temperature of the bentonite and surrounding rocks,
4. degradation of the canister and influence of corrosion products on the bentonite (if the Pilling-Bedworth ratio is >1),
5. the increase in pore pressure due to gas release,
6. chemical changes of materials, namely bentonite, and,
7. deposition hole deformation (Raikko et al. 2010).

The mechanical load on the canister develops with continuing saturation of the bentonite. The buffer swelling pressure increases with increasing bentonite dry density (figure 12a), decreasing temperature (figure 12b), and decreasing bentonite pore water salinity (figure 12c). After the bentonite barrier is completely saturated, the total pressure comprises the sum of the bentonite swelling pressure and water pressure. While the water pressure is isostatic, bentonite density variations in combination with imperfections in the deposition hole/disposal tunnel can impose an asymmetric pressure on the outer surface of the canister, which may be permanent, and may yield an over-stress affecting the canister integrity (Jonsson et al. 2018).

In the last few years, considerable research has been carried out to evaluate the behaviour of compacted clay-based buffer material in the framework of coupled thermo-hydromechanical (THM) processes in nuclear waste repositories (Villar et al., 2020). An important issue is the total time for saturation of the bentonite, the changes in dry density and porosity of the bentonite barrier, and the pressure exerted on the canisters. The time-dependent degree of saturation of the repository is an important factor in determining when, and in what form, corrosion can occur (King, 2006). The process of hydration depends on the hydraulic permeability and thermal conductivity of the bentonite and the host rock, the salinity, and temperature. In addition, hydration triggers the swelling of interlayer space in the clay particles and transforms the material from an initial heterogeneous to a homogeneous one, changing the local volume constraint conditions. The changes of macroscopic volume due to clay-water interactions is associated with the evolution of the microstructure and its interaction with the macrostructure, being described by dual porosity models and water retention behaviour. The changes in pore size distribution domains in terms of micro- to macro-porosity fractions are highly sensitive to the physicochemical processes involved in the applied loading paths (Schanz, 2016).

3.7 Influence of various transients on the corrosion process

The surface damage resulting from dry oxidation due to oxygen entrapped upon closure is expected to be very limited. Typical corrosion products are Fe_3O_4 and Fe_2O_3 (Terlain et al., 2001). The oxygen will be consumed after a certain time and the environment will become anoxic. This modification of the geochemical conditions influences the metallic corrosion as the reduction of higher oxides becomes the main cathodic reaction before water reduction starts to dominate the cathodic process during the anaerobic phase (Johnson and King, 2008).

In the framework of ConCorD, KIT-INE investigated the effect of the presence of ferric corrosion products (0.5 wt.% hematite) on the corrosion behaviour of spheroidal graphite cast iron in contact with MX-80 bentonite under anaerobic atmosphere. The addition of hematite brings about a significantly higher in-situ redox potential (Eh) and greater surface damage, as corroborated after 3 months by corrosion rates calculated by weight loss.

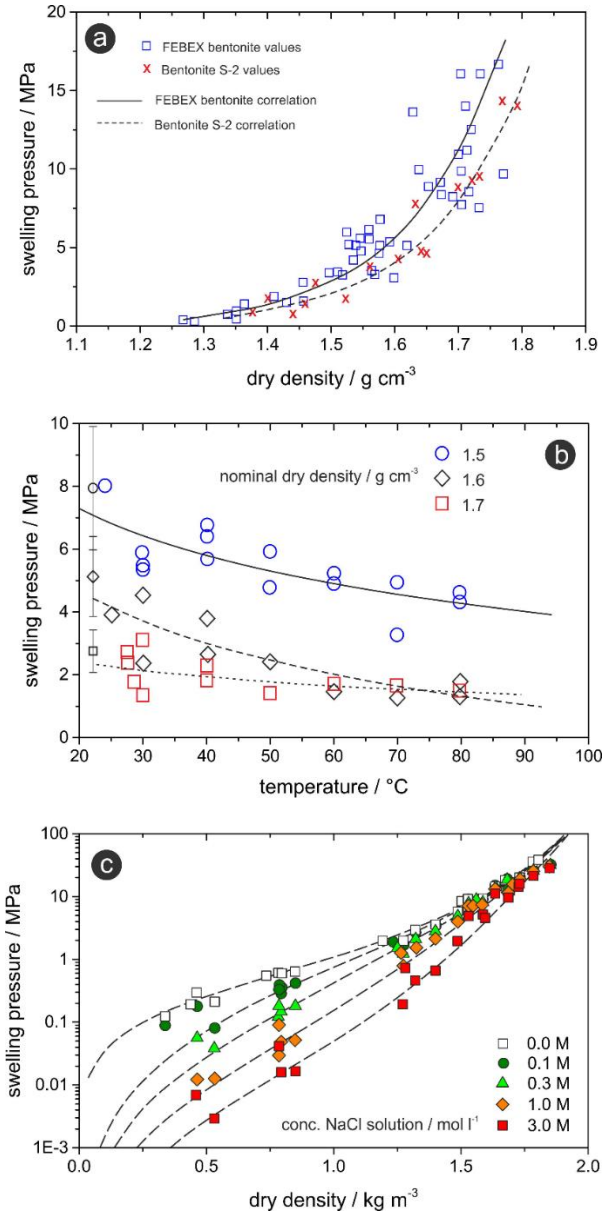

Figure 12: Dependence of the swelling pressure on (a) dry density (Gens, 2016), (b) temperature (adapted from Villar and Gómez-Espina, 2009), and (c) pore-water salinity (adapted from SKB 2006b).

An increase of temperature from 30°C to 50°C accelerates the corrosion rate, without changing the degradation mechanism significantly. The doubling of the reaction time to 6 months, on the other hand, resulted in a decrease of the corrosion rate and of the in situ Eh, which may be explained by ongoing release of Fe(II) ions interacting with montmorillonite and hematite. Indeed, the observed blue/green coloration at the coupon/bentonite interface suggests a reduction of structural Fe(III) in the bentonite. It is also known that the interaction of Fe(II) with hematite results in a Fe(II)-Fe(III) electron transfer (Williams & Scherer, 2004), which over time may lead conversion of hematite to a mixed Fe(II/III) compound such as magnetite. No magnetite, however, could be detected. But outcomes hinted at the formation of typical steel corrosion products such as layered Fe silicates of the kaolinite-serpentine group in experiments at 50°C and ferrous hydroxide. The nature of these detected secondary phases agrees with the measured low in situ Eh values.

Overall, findings suggest that the formation of oxic dry corrosion products would act as redox transient in the early repository post-closure phase. The consequence would be an initial relatively high corrosion rate that would decrease slowly until ferric compounds are converted to lower valence Fe oxides. After further reductive dissolution of Fe(II/III) oxides (Johnson & King, 2008), the steel canister surface would be exposed and corrode under the prevailing anaerobic water-saturated conditions. Most secondary phases forming under such initial transient redox conditions may not persist to the long-term.

A series of studies on the effect of changing oxidic/anoxic conditions have been published. For example, the effect of fluctuating redox conditions on the corrosion mechanism has been investigated by Saheb et al. (2011) using archaeological artefacts. In that study, a nail, which was exposed to an aerated unsaturated soil for several hundred years was reburied and exposed to anoxic and saturated conditions. Goethite and smaller amounts of magnetite and maghemite formed under aerobic and unsaturated conditions, while ferrous carbonates were detected in the corrosion layer after subsequent exposure to anoxic and saturated conditions. Based on experimental findings and aided with geochemical modelling, the authors concluded that phase transformation occurred rather than metallic corrosion progressing by direct formation of new phases. In the same study, an experiment was also conducted by applying the reverse sequence of changing conditions: a nail, which was exposed to anoxic and saturated conditions for several hundred years was immersed in an aerated carbonated solution for five weeks. Ferrous carbonate and iron oxides (magnetite, maghemite) formed as corrosion products upon exposure to anoxic water saturated conditions, and the subsequent exposure to aerated conditions resulted in the formation of an external goethite layer on the external part of the corrosion layer. In this last experiment (i.e., anoxic to oxidic transient), the authors also concluded that the presence of the ferric phase resulted from the transformation of the corrosion layer.

In the framework of ConCorD, CIEMAT investigated the corrosion of carbon steel in compacted bentonite for analysing the effect of water saturation, temperature (80 °C) and gas evolution in static experiments. The test was performed inside a PARR reactor, starting from oxic conditions. The unsaturated FEBEX bentonite (65.57 g, 14.3% water content) compacted at 1.4 g cm^{-3} was submerged in 200 cm^3 of groundwater (ionic strength I = $3.3 \cdot 10^{-3}$ mol dm^{-3}) and heated at 80 °C (relative water pressure of 0.4619 bar), for 135 days. At the end of the test, and prior to opening the reactor, gas and water samples were collected after several cycles of Ar flushing and vacuum inside the sampling lines. Then, the cell was dismantled, and the compacted block was transferred to an anoxic glove box for the analysis of the solid and the two coupons inserted in the middle of the bentonite block.

The corroded coupons were analysed by scanning electron microscopy (SEM), and the corrosion products adhered to the coupon surface were separated and analysed by XRD. The coupons presented a uniform generalized corrosion with a corrosion rate of 53.2 μm a^{-1}. Apart from magnetite as the main iron oxide product, other corrosion products and newformed mineral phases were detected: siderite, calcite, aragonite, pyrrhotite, anhydrite, gypsum, and a carbonate green rust.

The bentonite showed a colour change, from slight brownish to greenish, indicating a redox process. The pH of the contacting water decreased from pH 6.6 to 5.0 as a consequence of the bentonite/carbon steel/groundwater interactions. The sodium content increased from 5.6 to 656 mg l^{-1}, whereas calcium and magnesium decreased slightly (i.e., cation exchange reactions implying sodium desorption at exchange sites). Also, an increase of the concentration of chloride and sulphate as well as the alkalinity were detected in the contacting water (from 4.2 to 359 mg l^{-1}, 1.6 to 266 mg l^{-1}, and 1.9 to 2.24 meq l^{-1}, respectively), indicating an interaction of the FEBEX bentonite with pore water and carbonates dissolution. Dissolved total organic carbon increased up to 1792 mg l^{-1}, mainly as formate (1788 mg l^{-1}).

The gas analysis at the end of the test indicates a partial consumption of oxygen (up to 12.7 vol.%) and an increase of the content of H_2, CO_2, and CH_4 (8.3 vol.%, 9.3 vol.% and 71 vpm[4], respectively), and other hydrocarbons. This implies a gradual change in the redox conditions over time from oxidizing to reducing conditions. It seems that the degradation of organic matter contained in the bentonite consumes oxygen and generates CO_2, the content of which depends on pH and temperature. The consumption of oxygen generates local reducing conditions at the bentonite-Fe-coupon interface, favoring the anaerobic corrosion of carbon steel. The produced Fe(II) diffuses through the bentonite, precipitating magnetite, Fe-carbonates (siderite) and carbonates green-rush. Part of the generated Fe(II) reacts by ion exchange/edge sorption and/or exchange electrons with structural iron (Fe(III) reduction). However, not all the oxygen is consumed after 135 days of experiment. There is a counter diffusion of Fe(II) and oxygen outwards and towards the metal surface, respectively. The depletion of O_2 is controlled by diffusion and the kinetics of reduction reactions. The presence of H_2 implies the reduction of other species, for instance, sulphates, precipitating to iron sulphides, or the reduction of CO_2 generating CH_4.

Other corrosion experiments were performed under dynamic conditions by using convective water-vapor fluxes. In this case, different bentonites (FEBEX, SWy-3 and Czech bentonites) compacted at dry densities of 1.4 and 1.6 g/cm^3 and embedded with carbon steel coupons (Nagra reference and Czech reference steels) were saturated with water vapor at 80 °C. In contrast with the static experiment, the tests were not completely air-tight. Thus, a supply of oxygen was continuous during the test. After 286 days of experiment, all the bentonites were fully saturated and the metal coupons presented different degrees of corrosion, being higher when the dry density of the bentonite was lower. In addition, the corrosion rate changed with the type of bentonite, being higher for the FEBEX bentonite and lower for the SWy-3 bentonite, probably due to the highest salinity of the FEBEX bentonite pore water. The corrosion rates measured in all the coupons ranged between 23 and 341.7 μm a^{-1}, being lower for bentonites compacted at a higher dry density of 1.6 g cm^{-3}.

The main corrosion products observed in the coupons were not only magnetite but also other Fe oxy-hydroxides, such as hematite, goethite, lepidocrocite and akageneite, probably due to the permanent ingress of oxygen. Calcite, aragonite, and dolomite were the carbonates observed by XRD. Siderite was only observed by SEM. Gypsum and anhydrite were also detected by XRD. Sulphur species were only detected in SWy-3 and Czech bentonites. In some samples, iron calcium silicates, e.g., Hedenbergite type, were observed by SEM, indicating some dissolved silica available, favoured by the elevated temperature. In any case, the extent of alteration inside the bentonite at the metal contact was < 1-2 mm in all bentonite samples, corresponding to an increase of the iron content.

El Hajj et al. (2013) investigated sequential aerobic and anaerobic microbiologically induced corrosion of carbon steel. They found that the corrosion rate under anaerobic conditions is lower when specimens experienced a prior phase of aerobic corrosion. This outcome was attributed to the nature of the formed corrosion products and their adherence to the steel surface. The transition from aerobic to anaerobic conditions resulted in the formation of pyrrhotite as a single phase, while nanocrystalline mackinawite formed during direct anaerobic steel corrosion. The different results observed in this study were attributed to the stimulation of the activity of sulphate-reducing bacteria (SRB) and the hydrogen sulphide production upon transition from aerobic to anaerobic conditions.

Experiments performed at 85°C under *in situ* conditions showed that transient oxidic conditions can have substantial effects on steel corrosion. Fe^{2+}-bearing compounds in clay rock (e.g., pyrite) oxidise in the presence of oxygen (ingress due to loss of tightness), resulting in a decrease of pH of the porewater

[4] vpm: volume parts per million: 0.0001 vol.%

(Necib et al., 2016). These transient acidic conditions had, in turn, an impact on the corrosion rate, which were relatively important owing to the positioning of spatially decoupled anodic and cathodic areas (Schlegel et al., 2016). Galvanic coupling between areas exposed to different concentrations of O_2 in (sub)oxidic conditions can result in the formation of pits (Sherar et al., 2011; Refait et al., 2016). Areas more easily accessed by oxygen become cathodic while those less exposed may become anodic. The coupling is sustained by the precipitation of corrosion products and the driving force is the large difference in electrochemical potentials between O_2 reduction and Fe oxidation (Schlegel et al., 2018).

Romaine et al. (2015) showed that the reactions are in fact more complex and highly dependent on the mineralogical composition of the argillite used. Coupling of a bare electrode under argillite (anode) with a pre-corroded electrode covered by a bilayer of corrosion products (magnetite/siderite) under argillite (cathode) resulted in the formation of heterogeneous layers of corrosion products. The heterogeneity of these layers resulted from the variation of the galvanic effect along the surface of the initially bare electrode due to the variation of the distance from the initially covered electrode. Such variation of galvanic effects may also be associated to transient conditions affecting corrosion processes.

In anoxic groundwaters, anaerobic steel corrosion generates hydrogen, which results in a decrease of the E_h. However, with increasing reaction time, corrosion products will form a protective layer, which will result in a progressive lowering of the corrosion rate and thus of the hydrogen production (Smart et al., 2002a, Turnbull, 2009). The evolution of hydrogen is thus expected to decrease with time until reaching a lower constant value in the long-term (Smart et al., 2002a).

Several studies reporting the effect of hydrogen on selected reactions have also been reported (Truche et al., 2009; 2010; 2013). Under elevated temperature and calcite-buffered conditions, pyrite can be reduced by hydrogen through a coupled dissolution-precipitation mechanism and involves the generation of H_2S (Truche et al., 2010; 2013). Similarly, aqueous sulphate can also be reduced by hydrogen (Truche et al., 2009), but this reaction is kinetically slow under expected disposal conditions. Experimental findings reported by El Mendili et al. (2015) indeed showed the formation of a continuous iron sulphide layer covering carbon steel contacting Callovo-Oxfordian argillite in experiments performed at 90°C. The origin of this layer was attributed to the presence at the corroding interface of H_2S formed by reduction of pyrite by hydrogen. Iron sulphide was likewise detected in experiments performed at 30°C, but the corrosion layer was thinner than in experiments performed at 90°C. At this lower temperature, the origin was attributed to the activation of sulphate reducing bacteria (absorption of hydrogen and release of hydrogen sulphide).

In the absence of argillite, Smart et al. (Smart et al., 2002a,b) reported experiments performed in the presence of a hydrogen overpressure. In their studies, they could not detect any significant effect of this parameter on the anaerobic corrosion of carbon steel and cast iron in artificial groundwaters.

Reported studies showed that evolving redox conditions at the steel/bentonite interface can have a substantial impact on canister corrosion by changing the corrosion rate and mechanism. Among them, the presence of oxygen plays an important role and involves an increase in corrosion rate. Similarly, the presence of hydrogen may have an impact on the geochemical conditions of the canister nearfield, such as dissolution of selected minerals and formation of dissolved species, which in turn influence steel corrosion. The presence of hydrogen does not seem to modify directly the steel corrosion (e.g., no decrease in corrosion rate).

Geochemical conditions in a repository are also expected to evolve due to the metallic corrosion itself, which produces corrosion products and generates hydrogen. The accumulation of corrosion products at the steel/bentonite interface may influence the nature of the electrochemical reactions. For instance, the presence of magnetite at the steel-bentonite interface results in an increase of steel corrosion by acting as an external cathode coupled to the steel surface (Kojima et al., 1995; Taniguchi et al., 2003).

It was shown that the observed increase in corrosion rates was caused by the reduction of Fe_3O_4 itself. Consequently, because magnetite dissolves, such corrosion product may not necessarily play any role in the long-term, but it may influence corrosion processes between its formation and its dissolution.

Only a few studies of Cu corrosion under transient conditions have been reported. Smith et al. (2006) have reported electrochemical experiments on the effect of pre-oxidation on the surface attack of Cu by sulphides in 0.1 mol/L NaCl under anoxic conditions. Cu was pre-oxidized to mimic the formation of corrosion products during the warm oxic period. Depending on the extent of pre-oxidation, the surface was covered either with a thin film made of Cu_2O or Cu_2O covered by $CuO/Cu(OH)_2$ for longer reaction times. Samples were subsequently immersed in a sulphide-containing solution (30 µmol L^{-1}) and the evolution of the corrosion potential (E_{corr}) was recorded. For all samples, E_{corr} stabilized at a value slightly more negative than observed in the absence of sulphide, then decreased to a value between -0.5 and -0.6 V (SCE) before a sudden decrease to the equilibrium potential for the Cu/Cu_2S redox reaction. The time needed during the first decrease in E_{corr} increased with the extent of pre-oxidation and probably reflects the penetration of SH^- (the predominant species) to the Cu metal surface. The second drop was comparable for all samples and indicates that the redox conditions are dominated by the Cu/Cu_2S redox couple. Overall, outcomes pointed out a beneficial effect of Cu pre-oxidation, indicating that deposits could impede the reaction of Cu with aqueous sulphide.

The effect of a progressive increase of dissolved sulphide content on the corrosion of a cupronickel alloy (UNS C71500) in contact with MX-80 bentonite under anoxic conditions (25°C and 50°C) was investigated by KIT-INE within ConCorD. In the first approach, the sulphide content in the water flowing through the reaction cell was increased stepwise from 0 to 3 µmol l^{-1} (0-1-2-3 µmol l^{-1}). After 3 months, a Cu-rich layer composed of Cu oxides and Cu(0) had developed at the surface and covered a Ni-rich interface, mainly composed of (hydr)oxide compounds, with the pristine coupon underneath. No Ni was found associated with the Cu layer; only low amounts of sulphur were found associated with the Cu layer and marginal amounts with the Ni-rich layer. In the second approach, experiments were performed in closed vessels using a defined starting sulphide content of 3 µmol l^{-1}. In this series, results showed a comparable corrosion layer composition with mostly cuprite (Cu_2O) at the topmost layer, suggesting that water flowing through the reactor played no significant role. Corrosion rates were low and decreased with time, corroborating the formation of a protective passivation layer. Interestingly, in situ redox potentials were clearly positive. The nature of the formed products under prevailing pH/Eh conditions is in line with reported relevant thermodynamic data (Puigdomenech & Taxen, 2000).

Overall, outcomes reveal that the applied low sulphide concentrations, either a defined starting content or a stepwise Cu content increase, resulted in comparable very low effect on corrosion processes with the formation of an oxide layer probably formed due to residual oxygen. Because of the low sulphide content, it is probable that longer times are required for Cu sulphides to form assuming the surface reacts first with residual oxygen, and subsequently with dissolved sulphide. Alternatively, the low amounts of available sulphide adsorbed to the surface to form Cu(SH)ads (Chen et al., 2010) and the remaining dissolved SH- was too low to react with this surface species to form a Cu sulphide corrosion film.

In the context of Concord Project, CIEMAT has been performed corrosion experiments under dynamic conditions by using convective water-vapor fluxes. In these tests, different bentonites (FEBEX, SWy-3 and Czech bentonites) compacted at dry densities of 1.4 and 1.6 g/cm^3 were embedded with copper coupons (SKB Cu-OFP reference) and saturated with water vapor at 80 °C. The tests were not completely air-tight., a supply of oxygen being continuous. After 326 days of experiment, all the bentonite samples were completely saturated. The metal coupons present a degree of corrosion, which depends more on the type of bentonite than on the dry density. The corrosion rates ranged between 3 and 9 µm/year, the highest degree of corrosion being in the Cu coupons interacting with the Czech bentonite.

The main corrosion products observed in the coupons were cuprite, although tenorite was detected in minor amounts in the Czech samples compacted at 1.4 and 1.6 g/cm^3. The extent of visual alteration inside the bentonite was < 0.5-1 mm, only detected visually by a change of the color in the bentonite FEBEX at 1.4 g/cm^3, were azurite and cuprite were detected. Most of the bentonites remain unaltered, only malachite was observed in some samples at the bentonite/Cu coupon interface: FEBEX samples compacted at 1.4 and 1.6 g/cm^3, and SWy-3 compacted at 1.6 g/cm^3.

Senior et al. (2019) reported corrosion rates of copper in anoxic NaCl solutions at various temperatures by measuring the rate of hydrogen release. Copper exposed to 0.25 mol.kg^{-1} NaCl at 30°C or 50°C produced negligible amounts of H_2 below the detection limit. At 75°C, the H_2 release was in agreement with a corrosion rate of about 10 nm y^{-1}. When the temperature was returned to 50°C, the H_2 production immediately returned below the detection limit. Comparable findings were obtained for experiments performed in solutions containing up to 5 mol kg^{-1} NaCl. These results may suggest that the corrosion rate of copper in NaCl solutions up to 5 mol kg^{-1} is very low and decreases with temperature.

Smart et al. (2005) used electrochemical techniques to investigate the galvanic corrosion of the copper-cast iron couple in artificial groundwaters while changing the oxygen content. The context was an unlikely event of the outer copper canister being breached followed by water entering the annulus between the inner and the outer canister. In the presence of oxygen, copper was the cathode in the galvanic couple. In deaerated conditions, potentials were considerably more negative than in aerated conditions: the potential of the copper in deaerated conditions was within the thermodynamic domain of stability of copper, while that of iron suggested that the hydrogen evolution by anaerobic corrosion of iron was thermodynamically possible. Accordingly, copper plating was observed on the surface of iron in the experiment where conditions evolved from aerobic to anaerobic.

4. Microbial effects

4.1 Microbial corrosion in the context of nuclear waste disposal

4.1.1 Initial state of the art

In the literature, microbially-influenced corrosion (MIC), the process by which microorganisms impact the corrosion of a metal, directly or indirectly, is proposed to be categorised in two broad groups: chemical MIC (CMIC) that relies on corrosive chemical by-products of microbial metabolism and electrical MIC (EMIC) that entails the transfer of electrons from the metal to the bacterium (directly or indirectly) (Venzlaff et al., 2013) (Enning and Garrelfs, 2014). The latter is presumed to require biofilm formation (Jia et al., 2019) (Little et al., 2020), which, for nuclear waste, is only relevant in the absence of a bentonite backfill.

In the context of nuclear waste disposal, the major concern is the corrosion of the waste canisters, whether made of steel or copper. Here, we are exclusively concerned with anoxic corrosion and will not discuss MIC under oxic conditions. Anoxic corrosion will take place regardless of microbial activity, with an anodic and a cathodic half-reaction (Féron and Crusset, 2014):

$$\text{Anodic reaction: } Fe^0 \leftrightarrow Fe^{2+} + 2e^- \quad (2)$$

$$\text{Cathodic reaction: } 2H_2O + 2e^- \leftrightarrow H_2 + 2OH^- \quad (3)$$

The mechanism by which microbial activity accelerates this process was long attributed to cathodic depolarization, by which microbial activity can consume H_2 and thus accelerate the process but this theory has been already invalidated (Costello, 1974).

The major form of CMIC is through the production of corrosive by-products of microbial metabolism. A diversity of metabolisms has been identified in metal-corroding biofilms, including sulphate-reducing bacteria (SRB), sulphide-oxidizing bacteria, manganese-oxidizing bacteria, iron-oxidizing bacteria, iron-reducing bacteria as well as microorganisms producing acidic compounds (Amendola, 2022). Reductive metabolisms, such as sulphate reduction, iron reduction, acetogenesis, and methanogenesis, on the other hand, are expected in the repository if the appropriate electron donor (e.g., H_2) and acceptor (i.e., sulphate, ferric iron, and CO_2) are available.

Of the potential microbes in the repository, SRB are considered the most relevant for MIC because through dissimilatory sulphate reduction (DSR) they utilize sulphate as an electron acceptor and produce the corrosive compound, hydrogen sulphide (H_2S) or the bisulphide ion (HS^-), depending on the pH of the environment. Methane is not corrosive but could facilitate MIC through EMIC (Mand et al., 2016). Acetogens produce acetate that is acidic and that can fuel sulphate reduction and they likely also corrode via EMIC (Mand et al., 2016). Here, we will focus on SRB as they are the major players in CMIC.

DSR stoichiometry depends on the electron donor that is available (either H_2 or organic carbon) (eq. 4 and 5, respectively):

$$4H_2 + SO_4^{2-} + 2\,H^+ \rightarrow H_2S + 4H_2O \quad (4)$$

$$2CH_2O + SO_4^{2-} + 2H^+ \rightarrow H_2S + 2CO_2 + 2H_2O \quad (5)$$

Sulphide reacts chemically with zerovalent Fe (Fe^0) to produce mackinawite and H_2 (eq. 6).

$$Fe^0 + H_2S \rightarrow FeS + H_2 \quad (6)$$

The overall reactions (with H_2 or organic carbon as the electron donor) become (eq. 7 and 8, respectively):

$$3H_2 + SO_4^{2-} + Fe^0 + 2H^+ \rightarrow FeS + 4H_2O \quad (7)$$

$$2CH_2O + SO_4^{2-} + Fe^0 + 2H^+ \rightarrow FeS + 2CO_2 + H_2 + 2H_2O \quad (8)$$

Thus, sulphide-driven CMIC generates a layer of FeS that ultimately covers the surface of metallic iron, resulting in the formation of a film of FeS that serves as a protective layer (a passivation layer), precluding the diffusion of Fe^{2+} from the metal anode (Enning and Garrelfs, 2014). Thus, in the absence of other processes, the rate of sulphide-dependent CMIC is expected to decelerate over time. However, if the FeS film is interrupted, the corrosion rate will increase (Lv and Du, 2018). CMIC can take place in the absence of a biofilm as long as there exists a diffusion path for H_2S (or HS^-) to the metal surface.

EMIC depends on the transfer of electrons from metallic iron to SRB (or other microorganisms). Thus, iron serves as the electron donor for DSR (eq. 9) and the ferrous iron generated precipitates with sulphide as mackinawite (eq. 9) or, for instance, with carbonate as siderite (eq. 11) due to the production of CO_2 in heterotrophic sulphate reduction (eq. 5):

$$4Fe^0 + SO_4^{2-} + 10\ H^+ \rightarrow 4Fe^{2+} + H_2S + 4\ H_2O \quad (9)$$

$$Fe^{2+} + H_2S \leftrightarrow FeS + 2\ H^+ \quad (10)$$

$$Fe^{2+} + CO_3^{2-} \leftrightarrow FeCO_3 \quad (11)$$

However, because of the stoichiometry of the reaction, there is a single sulphide produced per four ferrous ions produced, which means that the production of mackinawite will be threefold lower than that of siderite (eq. 11):

$$4Fe^0 + SO_4^{2-} + 3CO_3^{2-} + 8H^+ \rightarrow 3FeCO_3 + FeS + 4H_2O \quad (12)$$

The different mineral products detected during EMIC and CMIC can be used to decipher which of the two mechanisms takes place, or even the relative contribution of each MIC mechanism in the presence of carbonate (Enning et al., 2012).

SRB can carry out both forms of MIC (figure 13), depending on the species considered. EMIC strains such as *Desulfovibrio ferrophilus* (Chatterjee et al*.,* 2021) or *Desulfopila corrodens* (Beese-Vasbender et al., 2015) are currently a minority. This is likely due to the use of organic carbon in the isolation of most SRB. In order to capture EMIC-specific SRB, it is necessary to consider a lithotrophic medium that requires metallic Fe to be the only electron donor and thus favours EMIC-SRB. The mechanism of electron transfer from the metal surface to the bacterium remains a matter of discussion (Liang et al., 2021). Sulphate-reducing bacteria are the most relevant organisms for CMIC, but other sulphide-producing microorganisms such as thiosulphate- or sulphite-reducing bacteria or sulphate-reducing archaea are also important. Furthermore, other organisms are likely to be capable of carrying out EMIC via the abstraction of electrons from the iron metal surface, such as nitrate-reducing bacteria and methanogenic archaea. There is increasing evidence of microbially-mediated electron transfer from mineral surfaces and this phenomenon of electrochemistry is likely to be underestimated to date.

In the context of nuclear waste disposal, particularly those concepts that require a bentonite backfill in direct contact with the waste canister, it is unlikely that biofilms will develop on canister surfaces. Thus, the main mechanism of concern is the formation of corrosive by-products of microbial metabolic activity

(CMIC). If information about biofilm formation on metal surfaces were to emerge, naturally, EMIC would become an important consideration.

Several studies have considered the corrosion of steel by exposing steel coupons to a solution unrepresentative of repository conditions (Shrestha et al., 2021) (Diler et al., 2021) (Rajala et al., 2015).

The study by Shrestha et al. (2021) was based on the exposure of metal coupons to a solution of synthetic bentonite porewater (sterilized) that was inoculated with groundwater from the Josef Underground Research Center. Pitting corrosion, and the formation of mackinawite and magnetite, was observed on the steel only in the biotic sample while the abiotic sample exhibited a uniform layer of magnetite. The biofilm that formed on the surface of the steel coupon included SRB but also nitrate-reducing organisms such as *Pseudomonas, Methyloversatilis* and *Acidovorax*, which is consistent with the presence of 10 mM nitrate in the water. Probably, a combination of CMIC and EMIC occurred here due to the absence of a solid phase and the formation of a biofilm. This type of study is only relevant for the French concept in which there is a gap between the carbon steel tunnel casing and the canister overpack which will become filled with groundwater (Diler et al., 2021).

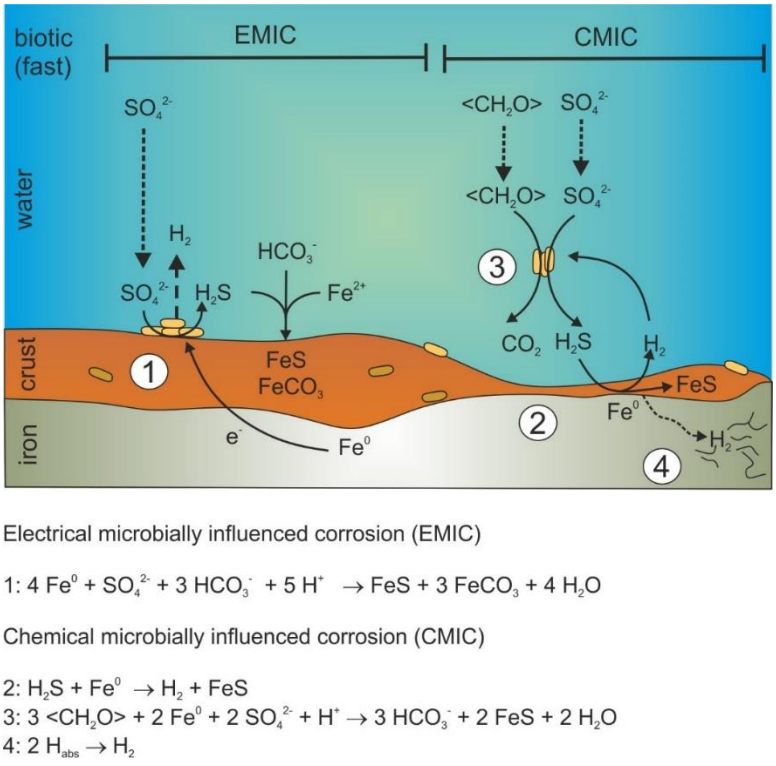

Figure 13: Microbially influenced corrosion pathways modified from (adapted from Enning & Garrelfs, 2014).

Similarly, Rajala et al. (2015) evaluated the corrosion of carbon steel in the presence of Olkiluoto groundwater (at RT and at 6ºC) and found that after 3 and 8 months, pitting corrosion occurs, and a biofilm developed at the surface of the coupons. Betaproteobacteria appeared to thrive in the presence of carbon steel perhaps through the utilization of H_2 as an electron donor (as they are known hydrogenotrophic bacteria). Additionally, iron oxidizers and reducers were observed, suggesting iron cycling. The electron acceptor for iron oxidation was not identified in this anoxic environment and it is

presumed that H_2 drove iron reduction. SRB were also observed in the biofilm and some genera (e.g., *Desulfopila*) were presumed to use elemental iron as an electron donor for sulphate reduction.

Also relevant to the French concept, an experiment (IC) (Necib et al., 2017) was performed at the Mont Terri Underground Laboratory. It consisted of test chambers placed within a core of Opalinus clay confined in stainless steel screens and introduced into a borehole within the same rock formation. The test chamber contained four steel electrodes, electrically insulated from each other with alumina, and mounted on a central tubing. Thus, the electrodes were close (~1 mm) to the Opalinus clay. A synthetic solution representative of Opalinus clay porewater was injected into the test chamber. The water flow rate was manually set to ensure circulation between the metallic electrodes and the Opalinus clay core. Electrochemical measurement on the electrodes allowed an estimation of the corrosion rate. After a total period of 7 years, the equipment was dismantled, and the iron was characterized. Inspection of the metal surface/Opalinus clay interface revealed several layers of corrosion products. Various iron-bearing minerals such as magnetite, goethite, lepidocrocite, akageneite, chukanovite, and siderite were observed. Fe sulphide with sulphur in various oxidation states (such as iron monosulphide (FeS) or iron disulphide FeS_2 (pyrite)) as well as elemental sulphur, were also observed and the original surface had been replaced by iron sulphide, likely pointing to MIC.

However, for the bentonite-backfilled repository environment, CMIC in the clay buffer is the more relevant question. A study by Grousset et al. (2020), investigated the sulfur isotopic fractionation during the exposure of steel embedded in Toarcian Argillite to a sulphate-rich water inoculated with a SRB isolate and an iron-reducing bacterium. The novelty of the study was the use of Nano-SIMS to spatially delineate the S isotope signature. Mackinawite was detected at the surface of the steel coupon, but it was not possible to conclusively determine whether its formation resulted from microbial processes due to the poor constraints on the isotopic signature of the sulphate source.

One study probed the corrosion of steel by exposing coupons to a solution representative of the Callovo-Oxfordian (Cox) rock formation in contact with cement-bentonite with or without uncompacted representative solid phases (Cox or Cox+cement/bentonite) and with or without Cox-derived microbial amendments (Diler et al., 2021). Corrosion was observed in the systems in which microorganisms were amended in comparison to the control systems that were left unamended (but not sterile). However, in the presence of a cement-bentonite mix, the extent of corrosion decreased considerably for 47 days. In addition, the embedding of the Cox clay rock in the cement/bentonite mix further decreased the extent of corrosion. These results are in line with expectations, as alkaline conditions are inhibitory to sulphate reduction. The microbial community was dominated by Firmicutes, including sulphate reducing bacteria (SRB) in the incubations with cement-bentonite and Cox as well as the incubation with Cox alone.

Another experiment (IC-A) carried out at the Mont Terri rock laboratory, was designed to measure the *in-situ* rate of iron corrosion. Metal coupons (carbon steel of various types) embedded in bentonite were deployed in a borehole by using stainless steel modules. The modules included holes and a sintered stainless-steel filter to allow for the exchange of pore-water with the host rock. The bentonite (MX-80) varied in its formulation (compacted or granular) and in its dry density. At time intervals, modules were retrieved, and the corrosion was evaluated along with the microbial community within the bentonite. This is an ongoing experiment. Findings do not point to any detectable microbial impact on corrosion (Smart et al., 2017). It was also observed that only aerobic microorganisms increased in number within the bentonite clay while sulphate-reducing bacteria were not detectable. This observation was the basis for the hypothesis that the growth of sulphate-reducing bacteria within the bentonite was inhibited due to the persistence of O_2 as SRBs are strictly anaerobic microorganisms (Burzan, 2021). The hypothesis is that O_2 trapped within the clay (perhaps in the interlayer space) is released upon influx of water and swelling, inhibiting anaerobic bacteria. Thus, this would suggest that longer deployment times are needed to reach conditions representative for a repository, i.e., to allow the consumption of O_2 and the

potential growth of SRB. Another scenario is that bentonite is fully saturated at the point in time at which O_2 is depleted, precluding SRB growth. The latter scenario would ensure the inhibition of SRB growth during saturation, providing an excellent protection against MIC. This experiment presents strong evidence that the borehole water microbial community did not colonize the bentonite significantly but that the bentonite microbial community grew initially and persisted.

The evidence presented above indicates the absence of CMIC in the bentonite backfill. However, the question remains as to whether the experiments conducted so far were carried out long enough to show that SRB do not grow within bentonite after depletion of the adsorbed O_2. In order to put to rest the question of whether the inhibition of SRB growth would persist in the absence of O_2, experiments should be conducted with bentonite from which O_2 was stripped. The bentonite, embedded with carbon steel coupons would receive H_2 as an electron donor and steel corrosion should be monitored over time.

4.1.2 New Insights into the role of O_2 in bentonite gained in ConCOrD

Experiments performed in ConCorD provided answers to the issue concerning the role of oxygen enclosed in bentonite for the growth inhibition of sulphate-reducing bacteria. Studies were performed with Wyoming bentonite MX-80 that equilibrated for a year:

(i) in anoxic atmosphere
(ii) in air with 21% O_2 and
(iii) in an oxic atmosphere with 100% O_2.

In addition, sterile bentonite exposed to air (21% O_2) was included. Carbon steel and copper coupons embedded in each of the bentonites were tested *in situ* in a borehole for 1.5 years using the set up described in e.g., Necib et al. 2017, Smart et al. 2017 and Burzan et al. 2022. The cores were recovered under anoxic conditions, sectioned under sterile conditions, and preserved at -20ºC for microbial analysis or embedded in a resin for mineralogical and corrosion characterization. A clear corrosion layer was observed in all steel coupons, but the bentonite equilibrated with the 21% oxygen concentration exhibited the thickest one, suggesting a possible contribution of both abiotic (oxic) oxidation and sulphate-reducing bacteria. This hypothesis is supported by the fact that both the 21% O_2 sterile and 100% O_2 exposed bentonites produced thinner corrosion layers than the non-sterile bentonite exposed to 21% O_2. An accumulation of sulphur was detected by XRF at the surface of the bentonite in all samples, it being more intensive in anoxic conditions and weak in bentonite equilibrated in 100% O_2, suggesting sulphate reduction. Additional analyses are ongoing, including the characterization of the microbial community in the bentonite sampled prior to resin-embedding, as well as further XRD and XRF analyses. Thus, the presence of oxygen in bentonite has a decisive influence on the growth of the microbial community in bentonite and work on the impact on microbial community and corrosion is still going on.

4.2 Impact of irradiation on microbial viability in the context of nuclear waste disposal

4.2.1 Initial state of the art

Microorganisms can cope with ionizing radiation to some extent. This depends on the type of microorganism. In the context of the safe long-term disposal of high-level radioactive waste the impact of the ionizing radiation on the microbial community structure, viability and activity is of concern because it affects the possible microbial processes. The expected radiation doses depend on various factors such as the disposal concept. The latter includes the radionuclide inventory, the distance from the source, the engineered barriers, especially the container material, the half-life of radionuclides and daughters (Černá and Bartak, 2019). In the case of the Swedish KBS-3 repository concept, a maximum dose outside the container of less than 500 mGy h^{-1} was calculated. The dose is dominated by Cs-137 (SKB 2006b). The gamma and neutron radiation are expected to be significant during approximately 1,000 years post deposition (SKB 2006b). Lundgren (2004) calculated an average dose rate outside the copper container of 100-150 mGy h^{-1}. On the other hand, the latest Canadian and Belgian HLW concepts predict a maximum surface dose rate of 1 Gy h^{-1} and 25 Gy h^{-1}, respectively (King and Behazin, 2021, Kursten et al., 2017). Therefore, a low ionizing radiation is expected for a longer period.

Radiation, independent of its source, affects biomolecules like nucleic acids, proteins, and lipids directly or indirectly (Jung et al., 2017). The ionizing particles can directly damage DNA. The indirect effect considers the impact of secondary reactive species produced by ionizing radiation. The indirect effect concerns the aqueous solution chemistry of water radiolysis products, which produces reactive oxygen species (ROS) – hydroxyl radical ($^{\bullet}OH$), ionized water (H_2O^+), hydrogen radical ($H^{\bullet}$) and hydrated electrons (e^-) followed by secondary ROS products superoxide ($O_2^{\bullet-}$) and hydrogen peroxide (H_2O_2) formed within one picosecond (10^{-12} s) after irradiation (Daly, 2009) (Jung et al., 2017).

Microbial radiation resistance includes a combination of diverse defence mechanisms. One of them is the DNA repair system, including unique DNA repair signalling components, constitutively activated, or expressed DNA repair machineries, or the presence of a polyploid chromosome set (Jung et al., 2017). Another mechanism is the enzymatic antioxidant system with a higher activity or expression of ROS-related proteins. Finally, the non-enzymatic antioxidant system, which comprises high intracellular concentration of inorganic solutes, high Mn/Fe ratios and pigments (Jung et al., 2017).

Microbial radiation sensitivity also depends on other factors (van Gerwen et al., 1999) (Shuryak et al, 2017). One factor is the type of ionizing radiation as an acute ionizing radiation (AIR) or chronic ionizing radiation (CIR) (Shuryak et al., 2017). Other factors are cell concentrations, physiological and genetic features, as well as the ability to apply defense mechanisms (Jung et al., 2017) (Shuryak et al., 2017). It was also demonstrated that certain resistant microbial cells can protect radiosensitive cell types (Shuryak et al., 2017). In addition, the vegetative state of the microbial cell has an influence on the microbial radiation sensitivity, because spores have many times higher radiation tolerance than vegetative cells (van Gerwen et al., 1999).

The radiation resistance of a microorganism is commonly measured by the decimal reduction dose (D10). This is defined as the radiation dose (kGy) required to reduce the number of that microorganism by one log (reducing 90% of the total number) (van Gerwen et al., 1999). The average D10 dose for most vegetative microorganisms was estimated to be 0.420 kGy, although it varies significantly between species and even strains (van Gerwen et al., 1999). Organisms with high radiation resistance were discovered within the three domains of life (Bacteria, Archaea, and Eucarya) (Jung et al., 2017). The most popular representative within the domain Bacteria is *Deinococcus radiodurans*, which was formerly named *Micrococcus radiodurans* and can survive high doses of gamma radiation (~ 17,000 Gy) (Daly, 2009). Studies on *D. radiodurans* revealed that in the non-enzymatic antioxidant defence system, high cellular content of manganous ions play a major role (Daly, 2009; Sharma et al., 2017). Another example of a radiotolerant bacterium is *Kinecoccus radiotolerans*, which was isolated from a high-level radioactive waste cell at the Savannah River Site in Aiken, South Carolina. This indicated high levels of resistance to gamma-radiation and desiccation (Philipps et al., 2002). The domain Archaea includes

microorganisms from extreme environments such as hydrothermal or highly saline. For example, the extremophile *Thermococcus gammatolerans* was isolated from an enrichment of hydrothermal chimney samples collected at the Guaymas Basin that were submitted to gamma-irradiation at a dose of 30 kGy (Jolivet at al., 2003). Halophilic archaea from the genus Halobacterium are highly resistant to desiccation, high vacuum, and Co-60 gamma irradiation (Kottemann et al., 2005). The *Halobacterium sp*. is able to repair extensive double strand DNA breaks (DSBs) in its genomic DNA within hours of damage induction. The gamma resistance depends on the growth stage with cultures in earlier stages exhibiting the highest resistance (Kottemann et al., 2005). Furthermore, membrane pigments, specifically bacterioruberin, offered protection of *Halobacterium sp.* against cellular damages induced by high doses of gamma irradiation (5 kGy) (Kottemann et al., 2005).

Within the domain Eucarya, a radiation resistant intraspecies of the filamentous fungus *Alternaria alternata* appears. Several strains originating from the highly radiation-polluted reactor of the Chernobyl (Ukraine) Nuclear Power Plant possess high radiation resistance. Genomic investigations showed that these strains are genetically adapted to this high radiation habitat by means of selection, thus providing a natural source of genetically homogeneous fungal lineages (Mironenko et al., 2000). Melanized fungi, such as *Cryptococcus neoformans*, also belong to the radiation-resistant fungi. It was even postulated that the melanin could employ γ-radiation as an energy source by converting electromagnetic energy into chemical energy and that this might enhance the growth of melanized fungi (Dadachova and Casadevall, 2008).

Taken together, organisms with high radiation resistance were discovered within all three domains of life (Bacteria, Archaea, and Eucarya) and the extreme ionizing radiation resistance originates in most cases from a combination of DNA repair systems and enzymatic as well as non-enzymatic antioxidant processes (Jung et al., 2017). In addition, tolerance to radiation might be a common phenomenon among extremophiles microorganisms (including thermophiles and halophiles), which must have evolved mechanisms to survive extreme environmental conditions such as desiccation. Furthermore, most of the organisms described above were detected in radioactive contaminated areas. Survival data from pure culture studies may not be fully applicable to the relatively nutrient limited environment of a DGR, where different species of the community will be competing, and where radiation is highly probably not the only selective stress (Černá and Bartak, 2019).

Gamma irradiation is also a common method to sterilize rocks, soils and sediments, when it is necessary to distinguish between biotic and abiotic processes in laboratory experiments (Otte et al., 2018). Such studies give us additional information about how a natural microbial ecosystem reacts to the presence of radiation. The effects of ionizing radiation exposure on soil biota were studied by exposing soil microcosms to weekly bursts of Co-60 gamma radiation over six weeks (three levels of exposure (0.1 kGy h^{-1} wk [low], 1 kGy h^{-1} wk [medium] and 3 kGy h^{-1} wk [high]). The results showed that the bacterial diversity decreased. The diversity of fungi and algae, however, increased unexpectedly and the functional gene diversity of algae, bacteria, fungi and total biota increased as well. In addition, large overall changes in community composition were observed after radiation exposure and several potential novel radiation-tolerant groups, such as Deinococcus-Thermus, phyla Chloroflexi (bacteria), Chytridiomycota(fungi) and Nanoarcheota (archaea), were identified (Ogwu et al., 2019).

Brown and colleagues (2015) studied the effect of ionizing radiation (8 weeks, 0.5 or 30 Gy h^{-1}) on microbial communities in sediment systems. Results indicate that biogeochemical processes are likely not restricted by dose rates in such environments, and electron-accepting processes may even be stimulated by radiation. The effect of gamma radiation on the viability of a soil microbial community under conditions similar to those in the Mars surface was investigated by Cheptsov et al. (2018). Doses of gamma radiation of 100 kGy under –50°C and 1 Torr were applied. In this case, the irradiation did not result in the death of the microbial community. On the contrary, the number of living cells, metabolic

activity, and functional diversity remained high. Most soil bacteria are eliminated by 20 kGy. A dose higher than 70 kGy, however, may be required to kill certain radio-resistant bacteria (McNamara et al., 2003). Furthermore, it was also mentioned that γ-irradiation may not be an appropriate method for all experiments as it can influence soil chemical properties, in particular soil nitrate and ammonium levels (McNamara et al., 2003). To sum up, low doses of radiation influence biogeochemical processes, microbial diversity and activity in natural rock, soil or sediment environments but these will not be completely restricted. However, a radiation dose higher than 70 kGy will effectively eliminate the bacterial presence in various soil materials. A high dose for a relatively short period represents only one aspect of radiation resistance. However, nuclear waste disposal in a deep geological repository is associated with chronic low-dose irradiation. Many microorganisms can grow under chronic gamma ionizing radiation dose rates of 13-126 Gy h^{-1}, but this does not mean that they can cope with acute ionizing radiation (Shuryak et al., 2017). Bacteria and fungi that exist in extremely radioactive waste and contaminated sites (e.g., Hanford, Chernobyl, Fukushima) have to cope with chronic ionizing radiation. The diversity of bacterial communities exposed to radioactive contamination in Chernobyl soils was examined by a combination of culture-independent and culture-dependent approaches (Chapon et al., 2012). Both highly and weakly contaminated soils contained highly diverse bacterial communities, suggesting that long-term exposure to radionuclides does not lead to the extinction of bacterial diversity (Chapon et al., 2012). Subsequent analysis based on next generation sequencing revealed profound changes in community composition at the phylum and operational taxonomic units (OTUs) levels and higher diversity in the trench soils as compared to the outside and identified specific phylotypes affiliated to the phyla Crenarchaeota, Acidobacteria, Dormibacteraeota (formerly AD3), Chloroflexi, Proteobacteria, Verrucomicrobia and Eremiobacterota (or WPS-2), which were unique for the trench soils (Theodorakopoulos et al., 2017).

In the multi-barrier concept, the buffer material, which is at the interface with the container, plays an important role regarding the radiation effects on the mineralogy and its barrier performance as well as the microbial communities. Bentonite is a suitable buffer material for clay and crystalline host rocks. Chemical and mineralogical analyses and physical testing of bentonite MX-80 after heating up to 130°C and with and without gamma radiation showed only insignificant alteration in the smectite content and physical properties (Pusch et al., 1992). The radiation sensitivity of naturally occurring microorganisms in bentonite and the sensitivity of *Bacillus subtilis* spores and *Acinetobacter radioresistense* in a buffer matrix was studied by Stroes-Gascoyne and colleagues (1995). The D10 values at dose rate 6,000 Gy h^{-1} was between 0.65 and 1.68 kGy in these experiments.

Within the EU-project Microbiology in Nuclear waste Disposal (MIND) the deliverables D1.1 and D1.3 reported the effects of radiation and microbial degradation of organic polymers and bitumen in low and intermedium level wastes (Abrahamsen et al. 2015, Mijnendonckx et al. 2015). Furthermore, in D2.15 the effect of gamma radiation and pressure on the indigenous microbial community in bentonite type BaM (Keramost, Czech Republic) enriched with granitic porewater VITA from Josef Undeground Research Center (Czech Republic), a natural source of anaerobic sulphate-reducing bacteria, was studied. Microorganisms that adapted and survived under harsh conditions underwent further selection caused by the gamma radiation. Notably, application of 19,656 Gy absorbed dose at a constant dose rate of 13 Gy h^{-1} did not completely eliminate bacteria in a bentonite suspension. A decline of the total microbial biomass was observed, but not of species richness. Minor changes in the microbial community structure were also noted (Černá et al., 2019). The results imply that some of the naturally present bacteria in bentonite are radiation resistant. However, the evolution of microbial communities under long-term low-level as well as high-level irradiation still needs to be investigated by long-term experiments under repository conditions including the effect of irradiation and compaction of bentonite.

4.2.2 New insights into the impact of irradiation and desiccation on microbial viability

Following the work performed in the MIND project, the evolution of microbial communities in bentonite under long-term weak and strong irradiation was investigated in WP Concord (subtask 4.1). In addition, the effect of bacterial communities in bentonite on the corrosion of metals, such as copper, were also studied. Sulphate-reducing bacteria (SRB) are commonly associated with copper corrosion, mainly because of their capacity of produce sulphide which could react with copper generating copper sulphides (corrosion products). Deep groundwater reservoirs may contain high concentrations of dissolved sulphate, providing an optimal environment for the survival of SRB (Hall et al., 2021). Apart from radiation, the effect of high temperatures on microbial survivability and future activity during the initial hot phase of the DGR needs to be evaluated. Early phases of the repository characterized by elevated temperatures, peak irradiation levels and low water saturations are considered to provide unfavourable physicochemical conditions for microbial activity. The evolution of a (nearly) sterile zone around the canister was predicted (Stroes-Gascoyne and West, 1997). However, long-term experiments under realistic repository conditions are missing and past long-term experiments indicated that bentonite microorganisms can survive long-term exposures to extreme heat treatments (Kašpar et al., 2021), but these data needed confirmation. In Subtask 4.1 of ConCorD, the long-term experiments were conducted under simulated repository conditions combining the effect of irradiation, temperature, water saturation, and the level of bentonite compaction, emphasizing the effect of irradiation and other repository-relevant stressors on indigenous microorganisms in bentonite.

The experiments of UGR and CIEMAT aimed to explore, for the first time, the impact of gamma radiation on the survival of microbial communities within 100% saturated compacted FEBEX bentonites. To achieve this objective, FEBEX bentonite was compacted to a density of 1.6 g/cm^3, fully saturated with artificial bentonite pore water following the recipe proposed by Fernandez & Rivas et al. (2005) and amended with 1.5 mM of sodium acetate. All the bentonite blocks contained in their core a pure copper coupon for corrosion analysis. Moreover, some samples were enriched with an SRB consortium to stimulate bacterial activity. The activity of SRBs is a very important issue for future repositories as these bacteria are the main drivers of copper corrosion (Hall et al., 2021). Prepared blocks were irradiated in several different ways: some were irradiated at a dose of 14 kGy at the beginning of the experiment and then incubated for 6 months. Other blocks were irradiated at the beginning and after 6 months incubation irradiated again with the same dose and then incubated for other 6 months, i.e., they received a double dose of gamma radiation (28 kGy). Some blocks were irradiated for the first time after 6 months of incubation by 14 kGy and then incubated for other 6 months. Unirradiated control-blocks were used to estimate the effect of irradiation. At the end of experiment, DNA extractions, amplification, and sequencing of the 16S rRNA gene and quantitative PCR (qPCR) were conducted to analyse the microbial diversity across various treatments. The viability of microorganism was also determined by the most probable number (MPN) method for SRB in Postgate medium and by counting the heterotrophic aerobic colony-forming units on R2A agar plates. The results have shown that the effect of gamma radiation on bacterial communities in FEBEX bentonite depends on the cumulative radiation dose received (14 or 28 kGy) and on the time at which the bacterial community receives the gamma radiation. An incubation period before and after the radiation seems to allow the microbial communities to adapt and recover since the results were quite similar to the unirradiated controls. Thus, a prior adaptation and subsequent recovery period seems to be key to the survival of the indigenous microorganisms in bentonite. Interestingly, in the case of compacted bentonite enriched with the SRB consortium, survival of this group of bacteria was severely affected at both 14 kGy and 28 kGy doses. The 6-month irradiated sample with the SRB consortium was the only irradiated sample that was slightly positive for the presence of viable SRBs.

Based on these results, it can be expected, that the activity of this group of bacteria would be very low in the early stages of DGR when radiation doses are still high. The extent of corrosion of Cu coupons

after 6 months of anaerobic incubation was in line with the microbial diversity and the bacterial viability. Copper oxides and copper sulphides were the main corrosion products. It is surprising to observe copper corrosion in 1.6 g/cm^3 compacted bentonite. However, the bentonite was pre-saturated before compaction, allowing a potential growth of SRBs. Moreover, the presence of the SRB consortium may have played a role in the corrosion of the coupons, as a sulphide signal, potentially associated with copper sulphide precipitates, was detected only in the treatments enriched in SRB. The results imply that corrosion is mainly attributed to biotic causes. In the 6-month irradiated sample with the SRB consortium (the only SRB positive sample after the irradiation), presence of small precipitates of possibly copper sulphides were detected. However, further investigations are necessary to confirm whether these precipitates are indeed copper sulphides.

The experiment performed by TUL + UJV in Subtask 4.1 focused on the combined effect of irradiation (dose rate of 0.4 Gy h^{-1}) and heat (90 °C and 150 °C). The values of both parameters were set as expected during the early hot phase of the repository evolution. Long term experiments (up to 18 months) with varying bentonite states (compacted bentonites BCV and MX-80 -1.6 g/cm^3/ powder/ suspension) and saturation level were carried out. A combination of molecular-genetic approaches (sequencing, quantitative PCR) with cultivation techniques and microscopic analyses was used to estimate microbial survivability in studied samples. The experiments indicate that the high temperature represents a crucial factor for microbial survivability. Long exposure to elevated temperatures (90 °C and 150 °C) was found to significantly reduce the viability of bentonite microorganisms to an almost complete sterilization, with consistent effects observed in both BCV and MX-80 bentonites. Effects of irradiation (repository relevant dose rate of 0.4 Gy h^{-1}) or additional factors such as bentonite state and water availability were insignificant, but their effects are probably underestimated due to the overwhelming influence of temperature. The study also emphasized the critical role of exposure duration in understanding microbial responses to the heat treatment. The potential for microbially-induced corrosion during the initial hot phase of the DGR is thus highly unlikely, mostly due to the detrimental impact of high temperatures on microbial viability. Elevated temperatures might be, however, associated with increased abiotic corrosion rates, with irradiation potentially mitigating corrosion (Bevas et al., 2024).

The experiments performed in Task 4.1 highlight the strong negative effects of both irradiation and heat on microbial activity and survivability in bentonite. Both effects will be the strongest during the initial hot phase of repository evolution and the formation of an abiotic zone in bentonite around the metal canister during this stage is thus highly likely. On the other hand, the analyses of untreated control samples across both experiments further revealed, that the dry density of 1.6 g cm^{-3} reduced but did not inhibit microbial activity in saturated compacted bentonite samples, and bacteria remained cultivable even after the 12 to 18-month incubation in compacted saturated state. The question of the possible reinoculation of the abiotic zone from the more distant layers of bentonite/surrounding environment is unresolved. Further long-term experiments at additional nearly limiting temperature ranges and in combination with mathematical predictions of temperature evolution in DGR are recommended to refine predictions of microbial effects in the bentonite buffer over the time. Furthermore, more experiments would be needed to accurately determine the radiation threshold total dose which significantly reduces the presence and activity of bentonite microbial communities, particularly for SRBs.

4.3 Inhibition of microbial activity and growth in bentonite

4.3.1 Initial State of the Art

Natural and commercial uncompacted bentonites harbor a diverse microbial community, including sulphate-reducing bacteria (SRB) (Matschiavelli et al., 2019) (Lopez-Fernandez et al., 2015) (Masurat et al., 2010). The number of culturable cells (SRB and others) differs among different types of bentonites. For SRB, this number was correlated with the initial water content of the bentonite (Haynes et al., 2018)

(Vachon et al., 2021). Cultivation-based approaches are biased to the species that can be cultivated and fail to detect viable but non-culturable species. Nevertheless, the indigenous bentonite microbial community is shown to be able to survive extreme conditions such as high pressures, high temperatures and high levels of gamma irradiation (Masurat et al., 2010) (Haynes et al., 2018) (Masurat et al., 2010). The number of culturable SRB depends on the treatment and the type of bentonite. Wyoming bentonite harbors the least amount of culturable SRB (Haynes et al., 2018).

The highly compacted bentonite buffer in a geological waste repository is expected to play an important role in precluding microbial activity due to its high swelling pressure and low water activity (Stroes-Gascoyne et al., 2010) (Pedersen et al., 2000). Microbial activity may be limited when the water activity remains below 0.96 (Pedersen et al., 2000). Desiccation results in membrane disruption, denaturation of proteins and enzymes and DNA damage. However, many bacteria have developed mechanisms to mitigate stress induced by desiccation by increasing production of exopolysaccharides, changing composition of the membrane, improving the stability of proteins, reducing oxidative stress, and repairing DNA damage (Esbelin et al., 2018) (Greffe and Michiels, 2020). There seems to be a large overlap between responses to desiccation and radiation. For example, mechanisms that govern tolerance to desiccation are believed to be responsible for the high levels of radiation resistance in *Deinococcus radiodurans* (D10 = 16 kGy), the model organism for radiation resistance (Daly et al., 2007).

The high swelling pressure generated at high bentonite densities imposes space limitations, which interfere directly and indirectly with microbial growth and activity. Direct effects occur if the pore spaces are too small to enable the presence of microbial cells. Pore throats with a diameter > 0.2 µm are essential to sustain microbial activity in subsurface environments (Rebata-Landa and Santamarina, 2006) (Fredrickson et al., 1997). A decrease of pore space results in diffusion-limited nutrient transport. As microorganisms themselves become immobile in such conditions, access to nutrients is restricted and microbial growth is inhibited (Kiczka et al., 2021). The decreasing rate of water inflow when the bentonite reaches its saturation state further limits transport. Full saturation of the bentonite, however, may take several hundreds or even up to several thousands of years (e,g, in the Swedish KBS-3 concept),and microbial growth was observed during the saturation phase. Nevertheless, no growth of sulphate-reducing bacteria was observed during this phase, putatively due to the persistence of O_2 (perhaps as an adsorbed species) in the bentonite (Burzan et al., 2022).

Both water activity and swelling pressure depend on the dry density of the bentonite (Stroes-Gascoyne et al., 2007) (Villar and Lloret, 2008). Water activity in bentonite decreases as the density increases in response to interactions with solutes and adsorption of water to mineral surfaces (Stroes-Gascoyne et al., 2007). On the other hand, swelling pressure increases with increasing dry density (Kaufhold et al., 2015). As long as the bentonite buffer maintains a uniform dry density ≥ 1600 kg m^{-3}, microbial activity is expected to be inhibited (Stroes-Gascoyne, 2010) (Stroes-Gascoyne et al., 2011). However, the fundamental determinants of the threshold bentonite dry density at which microbial activity is inhibited remain unknown. It remains unclear why different boundaries are observed between different bentonites (Pedersen et al., 2000) (Stroes-Gascoyne, 2010) (Bengtsson and Pedersen, 2017). Furthermore, the high density does not necessarily eliminate the viable microbial population in bentonite and upon expansion of compacted bentonite into a void, the resulting reduction in dry density stimulated or restored microbial cultivability (Stroes-Gascoyne et al., 2011). Microbial viability at interfaces is comparatively much higher than that in bulk clay material as interfacial regions provide a more favorable environment with increased access to nutrients and water (Pedersen, 2010) (Stroes-Gascoyne et al. 2002) (Jalique et al. 2016). Long-term persistence of microorganisms has also been observed in laboratory and in-situ experiments (Burzan, 2021) (Jalique et al., 2016) (Bengtsson et al. 2017a,b). Cultured species are often known as spore-forming bacteria, which could facilitate their long-term persistence (Haynes et al., 2018) (Vachon et al., 2021) (Jalique et al., 2016). Sporulation enables microorganisms to withstand unfavourable and potentially lethal environmental conditions, but spores

are metabolically inactive until conditions become more favourable for vegetative growth. The triggers that control endospore formation are still unclear (Hutchison et al., 2014).

Bentonite is considered a limited nutrient environment with very low amounts of available organic carbon, mainly composed of plant-derived waxes and highly aromatic carbon with low contributions from small molecules (Marshall et al., 2015). Based on the molecular-level analysis of the organic matter, it is believed to be recalcitrant for microbial reproduction. However, recent analysis showed the presence (in bentonite) of alkanes, toluene, and other aromatic compounds, which are known as potential energy sources for microbial metabolism. The amount of these more easily accessible electron donors, however, is not known (Matschiavelli et al., 2019) (Pedersen, 2017). A recent study showed that dissolved organic material from different types of bentonites is able to sustain a sulphate-reducing microbial community (Maanoja et al., 2020) (Maanoja et al., 2021). Another possible mechanism to fuel sulphate reduction is autotrophic growth with H_2 as an electron donor and CO_2 as a carbon source (Muyzer and Stams, 2008). In turn, heterotrophic microorganisms can use the organic carbon generated by autotrophic hydrogen-oxidizing SRB. Hydrogen can originate from radiolysis of water and the anoxic corrosion of steel but also from microbial metabolism such as fermentation processes (Bagnoud et al., 2016) (Smart et al., 2001a,b). Hydrogen has been shown to fuel sulphate reduction in bentonite microcosm experiments (Matschiavelli et al., 2019). However, H_2 consumption within bentonite as a function of dry density remains inconclusive.

Based on this literature review, it is tempting to design experiments that capture repository conditions to assess the potential for microbially influenced corrosion of canisters. Such experiments would consider either pre-compacted bentonite or bentonite at a target dry density and physically, chemically, and biologically relevant conditions. However, such experiments preclude the real-time monitoring of processes and require appropriate controls that detangle the role of microorganisms. Furthermore, the timeline is an important parameter as transient processes are expected that could impact the overall conclusion. Bringing together all these conditions in a meaningful way is a considerable challenge.

4.3.2 New insights into the impact of bentonite dry density

A novel diffusion reactor based on counter diffusion gradients of electron donors and acceptors was used at EPFL and HZDR to elucidate the impact of the dry density of MX-80 and Calcigel bentonites on microbial activity. The reactor is a modification of that from Luc Van Loon (Van Loon et al., 2003) (see Figure 14). The new design allows the establishment of opposing gradients of electron donor and acceptor within the reactor, precluding the growth of microorganisms within the filters keeping bentonite in place. By allowing only one of two components required for growth to be introduced at each end, the only possible location for growth becomes the centre of the reactor, that is, the bentonite.

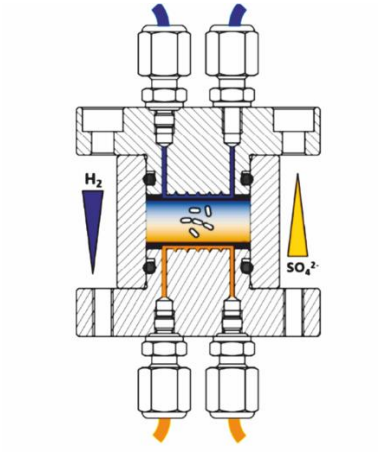

Figure 14: Schematic representation of the diffusion cell with counter flow to study the influence of bentonite on microbial activity.

The experiments included the dissolution of gypsum from MX-80 bentonite and the addition of H_2 and sulphate. The former was required to remove sulphate from the bentonite bulk and allow the abovementioned gradient to be established. The diffusion-controlled dissolution of gypsum took about 100 days, where, despite no addition of H_2, substantial microbial growth was detected. There was a large range of 16S rRNA copy number per gram of dry bentonite after the gypsum dissolution phase. Values from 5.0×10^4 to 4.3×10^5, some orders of magnitude higher than those obtained for the original bentonite were measured. Thus, a source of electrons like organic carbon might be present in the bentonite. Despite the addition of H_2 as an electron donor starting at time zero, no evidence of an increase in biomass or statistically significant change between times 0, 7, 14, and 21 days was observed. Probably, sulphate and H_2 have not yet diffused sufficiently to meet.

A similar experiment was carried out at HZDR with Calcigel bentonite including gypsum dissolution. It was observed that the sulphate concentration decreased majorly in the microcosms containing hydrogen in their atmosphere, Calcigel bentonite and metal coupons. In addition, the hydrogen content in the atmosphere of these microcosms was lower than that in sterilized bentonite. This suggests that hydrogen works as a potential electron donor and sulphate as an electron acceptor consumed in these microcosms by the present microorganisms. Microbial diversity analysis also showed that these samples were enriched with sulphate-reducing bacteria from the genus *Desulfotomaculum*, indicating that Calcigel bentonite harbours sulphate reducing bacteria that become active under the applied conditions.

The surface of the coupons in these microcosms showed a more intense corrosion at lower incubations times, probably because a protecting layer of Ca-containing minerals. Sulphide minerals were also found indicating activity of sulphate reducing bacteria. High corrosion rates were also observed in microcosms with hydrogen in the atmosphere and with sterilized Calcigel bentonite, indicating an abiotic type of corrosion.

The impact of bentonite dry density on microbial growth was also studied at SCK-CEN using oedometers. The experiments focussed on the inhibiting properties on H_2 consumption originating from the anoxic corrosion of carbon steel by the indigenous community and the impact of the produced sulphide on the corrosion of carbon steel. The oedometers included cold rolled mild steel coupons whose corrosion would generate H_2 that could stimulate microbial growth. An increase of hydrogen was observed in the first three consolidation cells (sterile bentonite without additional hydrogen). This increase was slower towards the end of the percolation. This suggests a faster corrosion in the beginning

of the experiment. Putatively, bacteria are still active in the consolidation cells and are consuming the hydrogen. This will be checked after dismantling of the consolidation cells in the near future.

The methods described above constitute an advance for investigating the impact of bentonite dry density on microbial community growth in a reliable, reproduceable, and statistically way. Due to its low sulphate content and the presence of naturally sulphate-reducing bacteria, Calcigel bentonite is an excellent substrate to study the impact of dry density on microbial activity and corrosion.

5. Novel technological concepts for nuclear waste disposal canisters

A number of different types of metallic and non-metallic materials have been, and continue to be, considered as candidate container materials. Each material has advantages and disadvantages (Table 3) which are briefly reviewed here, along with a discussion of the prospects for continued development.

Table 3:Summary of advantages and disadvantages of candidate materials for containers.

	Material	Advantage	Disadvantage
Metal	Cu-OFP	Excellent corrosion behaviour	High price
	Other Cu-grades	Price (compared to Cu-OFP), availability	Not yet as widely studied in repository conditions as compared to Cu-OFP
	Carbon Steel	Low price, mechanical integrity, weldability, suitable for use with bentonite-based or cementitious backfill	Higher general corrosion rates compared to other passive alloys
	Stainless steels	General corrosion resistance, availability	Susceptibility to localized corrosion in certain environments
	Titanium alloys	Corrosion performance in aggressive brine solutions	High price, susceptibility of some grades to localized corrosion in certain environments
	Nickel alloys	General corrosion resistance, availability, (improved pitting corrosion resistance compared to stainless steels)	Tendency for localized corrosion in certain environments
	Lead	Low price, corrosion resistance, availability	Toxic to environment
Ceramics	Alumina	Chemically inert with good mechanical properties	Feasibility of large ceramic pieces, sealing brittle nature
	Silicon Carbide	Chemically resistant for SSiC. feasibility of large pieces	SSiC vulnerable to leaching High temperature for sealing processes brittle nature
	Silicate materials	low porosity due to glassy phases	Glassy phases can reduce lixiviation properties, mechanical properties brittle nature
	Titanium Oxide	Less refractory than alumina, lower temperature sintering	Expensive, chemically inert except under very alkaline pH brittle nature
Coatings	TiO_2 coatings	High hardness coating, bactericidal activity	Ceramic coatings must be without defects
	CrN coatings	High hardness, excellent wear resistance, chemically resistant	
	Cu coatings	Cu corrosion well known, less expensive than Cu container	Risk of galvanic corrosion in case of defects
	Ti and Ni coatingss	Corrosion performance	Long term prediction is difficult, microbial induced corrosion cannot be excluded

5.1 Ceramic Materials and Coatings

5.1.1 Ceramic containers

The minimisation or complete avoidance of canister surface hydrogen generation is one of the reasons for the evaluation of alternative solutions such as that provided by bulk ceramic containers or ceramic coatings (Landolt, 2009).

The use of ceramics for nuclear waste disposal containers was first seriously considered in the 1970s (Mattson, 1980) (Bienek et al., 1984) and has continued to be an option since the early 2000's (Holdsworth, 2013) (Baroux and Martin, 2016) (Adams et al. 2000) (Wötting and Martin, 2007) (Kerber and Knorr, 2013), albeit apparently without a high level of commitment. There seems to be insufficient motivation to invest in the research which would be necessary to overcome known difficulties when feasible metallic solutions have already been recognised (Holdsworth, 2013). The reluctance of ceramic components manufacturers to invest without external support is almost certainly due in part to insufficient customer demand in the near future for large ceramic pieces. Nevertheless, there have been significant developments relating to the consideration of ceramics as a candidate nuclear waste disposal canister material.

While ceramics are an attractive option in terms of their high corrosion resistance and lack of gas production, their mechanical strength and toughness characteristics are low. Although the existing press and sintering furnace capacities around the world limit the size of the canister sections that can be manufactured, such limitations can be overcome with adequate investment. However, the main manufacturing challenges to be overcome through systematic development include: i) efficient handling of very large lumps in the green state just after shaping (before sintering), and ii) achieving adequate density (porosity levels) with section thicknesses ≥ 50 mm. Moreover, achieving effective sealing of thick ceramics will never be possible without significant research and development. With no demand for large diameter ceramic pressure vessels from any other industrial sector, funding for such R&D can only come from the nuclear waste disposal community. Recently, there have been significant changes related to the consideration of ceramics as a candidate material for containers for nuclear waste disposal (Holdsworth 2013), and they have been comprehensively analysed (Holdsworth et al. 2014). Potential ceramics candidates for overpack nuclear waste disposal canister applications are alumina (Al_2O_3), pure or in combination with silicon oxide (SiO_2) (Baroux and Martin, 2016) (Mattson, 1980), silicon carbide (SiC) (Wötting and Martin, 2007) (Kerber and Knorr, 2013), silicon nitride (Si_3N_4), partially stabilised zirconia (PSZ), and titania (TiO2), because of their chemical stability, reasonable mechanical properties, and ready availability (Wilfinger, 1994). At present, the main attention is paid to the alumina (Al_2O_3) and the silicon carbide (SiC) solutions.

5.1.2 Alumina

The development of an alumina or alumina-silica ceramic canister has been the subject of several studies.

SKB (Sweden)

A first patent by Larker (1980) presents a concept of a ceramic-metal capsule (figure 15). In this concept, the waste (in the form of spent fuel or vitrified waste) is placed in the alumina capsule, consisting of an open container and a cover fitting the open end of the container. These two parts are produced from ceramic powder material (alumina), which is then compacted by hot isostatic pressing (1,300°C - 1,400°C, 0.5 kbar - 2 kbar). The capsule is then enclosed in a gas-tight metal casing and joined by

means of hot isostatic pressing (at the same pressure and temperature conditions as described for the compaction of the container and the cover fitting) in order to obtain a homogeneous monolithic body. The developed capsule allows waste to be stored in a single cavity or multiple separate ones. A thermal insulating material can be placed between the waste and the body of the ceramic container in order to limit the temperature in the vicinity of the waste during the closure phase of the capsule. In order to mechanically reinforce the sealing area, a ceramic insert is placed in the lid of the container.

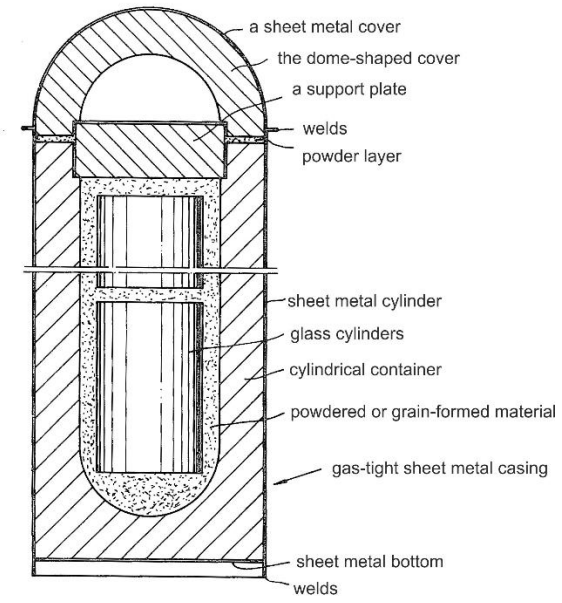

Figure 15: Scheme of a capsule containing several nuclear waste cylinders arranged for connection of the cover and the hollow cylinder by isostatic hot pressing. The ceramic powder layer is bound together with the container during sintering (adapted from Larker 1977).

Lawrence Livermore National Laboratory (USA)

In the early 1990s, the Lawrence Livermore National Laboratory was commissioned to study alternative solutions to metal containers for the geological disposal of radioactive waste at Yucca Mountain (Wilfinger, 1994). Two exploratory paths were chosen:

- solid ceramic containers
- composite containers: metal structure for mechanical strength and ceramic coating/liner for chemical durability

The specifications state that these cylindrical containers (5.50 m high and 1.80 m in diameter) have no transport function and will be placed “nose to nose” in horizontal tunnels dug into the rock. They must allow for the storage of spent fuel assemblies or vitrified waste and be identifiable and retrievable for 50 years, and leakproof for 300 to 1,000 years. The closure system of these containers must be feasible remotely in a radiation hot cell without thermal damage to the waste package. On the basis of these specifications, different selection criteria were identified for the materials and associated manufacturing processes:

- Good tensile strength and impact resistance of the material

- High toughness
- Dense material with no open pores or cracks
- Joint or weld areas must have the same properties as the body material
- Good chemical resistance of the material in the storage environment
- Sufficient thermal conductivity to remove heat from the waste
- Use of conventional processes requiring only minor adaptations

For the last two criteria, the difficulty of manufacturing large ceramic parts was highlighted. Cost was not the primary criterion but must be taken into account. The authors point out that these developments of large objects will require development time.

BNL/Nucon (USA)

In the late 1990s, the company Nucon developed containers for the transport and storage of nuclear waste in the USA (Rockhvarger and Khizh, 1998, 1999, 2000). These containers, based on the Russian doll system, were composed of a multi-layer system ensuring radiological, mechanical, and corrosive protection of the encapsulated waste both during transport and for geological disposal of the waste. The different liners used were:

- a first ceramic container that encloses the waste. This first structure acts as a thermal, chemical, and radiological protection,
- a second ceramic liner acts as a mechanical and corrosion barrier and,
- the space between these two ceramic bodies is filled with graphite or metal powder which acts as a radiation shield.

Two concepts were proposed depending on the size of the waste to be encapsulated (Rockhvarger and Khizh 2000).

The watertight sealing of ceramic containers made of $MgAl_2O_4$ is based on a microwave process. The sealing is carried out using a ceramic paste of the same composition as the parts to be joined. This paste is doped in order to promote the absorption of microwaves by the material (hydrogenation of the powder).

The switch to compounds doped with ceramic fibres is envisaged. In addition to the mechanical reinforcement of the container, the addition of ceramic fibers can favour the thermal treatment of the material (e.g. SiC, which has a high permittivity value and is preferentially heated during microwave heat treatment) or an increase in the radiological properties of the container (addition of boron nitride).

Andra (France)

The first part of the work (2007-2009) focused on the development and characterisation of alumino-silicate ceramics with leaching resistance and mechanical properties superior to conventional silicate ceramics (Baroux and Martin, 2016):

- the development of a ceramic with an alumina-rich composition that meets the required physical and chemical properties. After chemical characterization using pure water Soxhlet tests at 100°C and column tests in Callovian-Oxfordian deep groundwater at temperatures between 50 and 90°C, it was concluded that the chemical durability of the ceramic was suitable, with an effective thickness reduction of ~3- 4mm over a period of 1000 years.
- the design (shape and thickness) of a container for high activity nuclear wastes adapted to the ceramic material.

- the development of casting, drying and sintering processes adapted to these thick ceramic parts.

These developments have made it possible to demonstrate the feasibility of the body and lid of an ½ scale, 4 cm thick container (figure 16). This constitutes a real advance compared to the current state of the art in the industry.

The technological roadblock for these new silico-alumina containers remains the closure of such a system. Current studies focus on the development of a sealing technology adapted to the application, with constraints associated with the vitrified waste and the watertightness of the waste disposal container (Kalfayan, 2019). In order to preserve the containment properties of the glass matrix of the waste (maximum temperature 450°C), the sealing process will have to meet two major constraints:

- a maximum surface temperature of the ceramic container of 600-700°C
- a heating technology localised to the closure area.

One of the ways identified to assemble ceramic parts is to use the interaction of ceramic materials and microwaves to locally heat the joining area until the material melts, in order to achieve a tight weld. A lot of work is currently being performed on the sintering of ceramic materials, in particular for alumina (Clark, 1996) (Zymelka, 2013; Zhang and Datta, 2003). These works resulted in a better understanding of these microwave/material interactions. This process can now be considered for the welding of ceramic specimens with an alumino-silicate composition. The work carried out since 2014 made it possible:

- to improve the quality of the ceramic/glass sealing interface via a two-stage enamelling process: first firing in a conventional furnace, then sealing the enamelled parts by microwave heat treatment. The process can then be industrialized with this pre-firing, which can be carried out by the porcelain manufacturer supplying the ceramic container,
- to confirm that the selected and tested glasses have processing temperatures compatible with the constraints imposed by the presence of the primary package,
- to confirm the feasibility of sealing by microwave heating (no influence of the microwave frequency on the process, the sizing of a furnace will not be limited by the wave-material interaction),
- to make a clear improvement in the quality of the joints for heating under minimal load, and
- to verify the viability of the process: a study was carried out with an industrial manufacturer of microwave ovens. An industrial prototype was proposed, taking into account the size of the full-scale container and the localised heating constraint.

With a view to going further and designing and testing a first prototype to reinforce the proof of concept, the following avenues are being considered:

- to produce a prototype furnace for testing the annular shapes of test bodies and the localised heating of these parts,
- to understand the resistance of the ceramic to the thermal gradients resulting from localised heating, and
- to optimise the compositions of sealing glasses to reinforce their mechanical and leaching resistance (example: glass-ceramics).

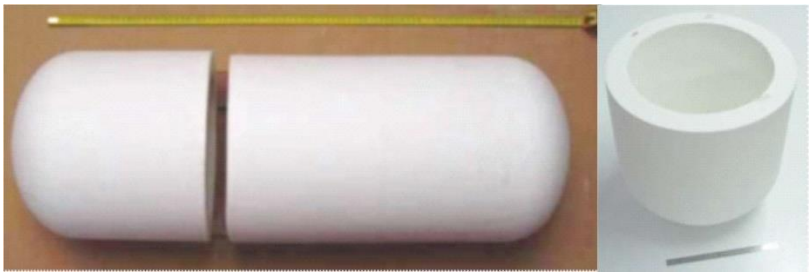

Figure 16: Andra half-scale model of Al_2O_3/SiO_2 VHLW canister (Baroux, 2016) (a) complete model, (b) lid.

5.1.3 Sealing of ceramic containers using microwaves: recent advances

Recently, the Institute of Ceramic Research (IRCER) and EMSE developed new sealing formulations, for alumina-based (*i.e.,* silico-aluminate materials with a high content of alumina) ceramic canisters. Their performance during the sealing using microwaves (MW) was tested. The major achievement was an unprecedented improvement of the microwave coupling allowing a fast sintering. In real conditions this will enable the limitation of the increase of the temperature in the core of the container containing the nuclear waste "parcel" during the sealing process. The new sealing formulations have also satisfied the mechanical and leaching resistance specifications.

In a first approach, the research was focused on the exploitation of the hetero-aggregation phenomenon in water-based suspensions between an alumina micro-powder and a silica nano-powder carrying opposite surface charges. The generation of surface charges was linked to the zeta potential resulting from the acid-base equilibria arising in water. This procedure permitted the preparation of very homogeneous and intimate blends of the two materials at the nanoscale. Since the blends are composed of two materials exhibiting different MW coupling efficiencies, materials achieving a local coupling enhancement (*i.e.,* at the powder grain level) for a localized, efficient, homogeneous, and fast heating process were explored.

The strategy was validated by initial MW sealing tests of hetero-aggregated alumina-silica blends, which showed an increased MW coupling. The addition of silicon carbide to the alumina-silica formulations in low quantities (maximum of 2 vol.%) was explored. SiC is well-known as one the best ceramics in terms of MW coupling. In another approach to previous unsuccessful studies performed with the addition of SiC micro-powders, we added nano-SiC (typical size of 20 nm). This SiC was covered with a native silica layer allowing the implementation of hetero-aggregation in the same way as with nano-silica and in a very homogeneous way. Figure 17a shows the temperature evolution of compacted SiO_2-Al_2O_3 powders with and without dispersed nano-SiC during their heating by applying microwaves. The fast increase of temperature observed in the presence of nano-SiC indicates an achievement of a strong boost of the MW coupling. Figure 17b shows the corresponding microwave forward power applied during the tests. A correlation of the heating efficiency with the vol% of SiC can be seen.

Apparently, the very positive effect of nano-SiC on MW coupling is not only due to the material itself and to its very homogeneous distribution throughout the volume. There might also be a "kind of pinning" of the electromagnetic field on nano-SiC. But, at this stage, it remains an assumption that has still to be confirmed. Another issue to be investigated is the oxidation of SiC during the sealing, which produces bubbles that may degrade the mechanical properties (to be studied in the future) and the leaching resistance.

Finally, based upon the determination of the permittivity of materials as a function of temperature at the working frequencies, modelling of the MW heating would help to understand MW heating selectivity and

the determination of compatible materials (ceramics *vs* sealing materials) for an efficient and selective heating of the sealing area.

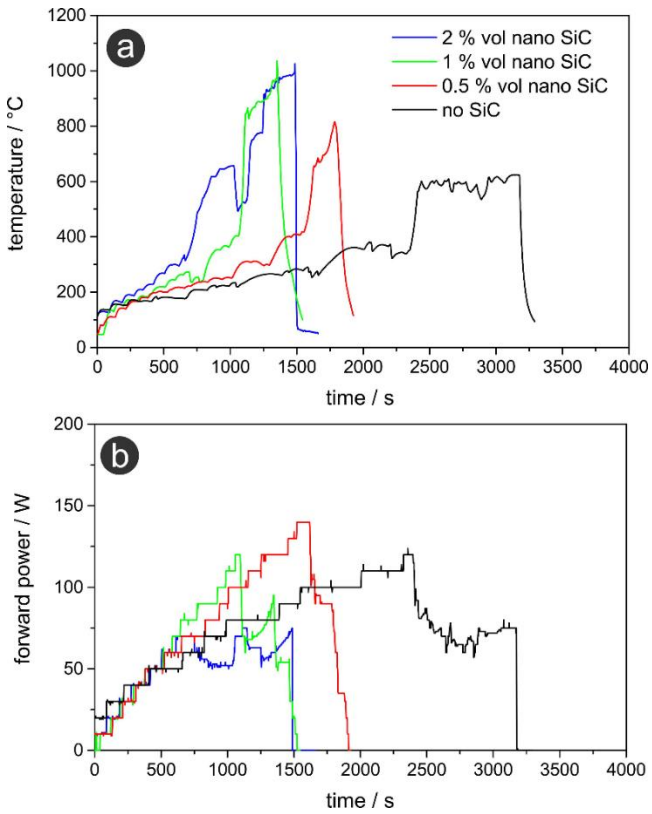

Figure 17: (a) Comparison of microwave coupling for samples containing different amounts of nano-SiC; (b) Corresponding forward power input during the microwave tests necessary to reach 400°C.

5.1.4 Silicon carbide

It has previously been shown that silicon carbide (SiC) is a viable option for container fabrication (Holdsworth, 2013) (Knorr et al., 2008). Until recently, it was only feasible to manufacture large pieces out of SSiC (silicon impregnated silicon carbide) and RSiC (recrystallised silicon carbide). However, there is now the possibility of making larger pieces from conventional SSiC (sintered silicon carbide) (see figure 18) and even high strength grades of SSiC (Wötting and Martin, 2007).

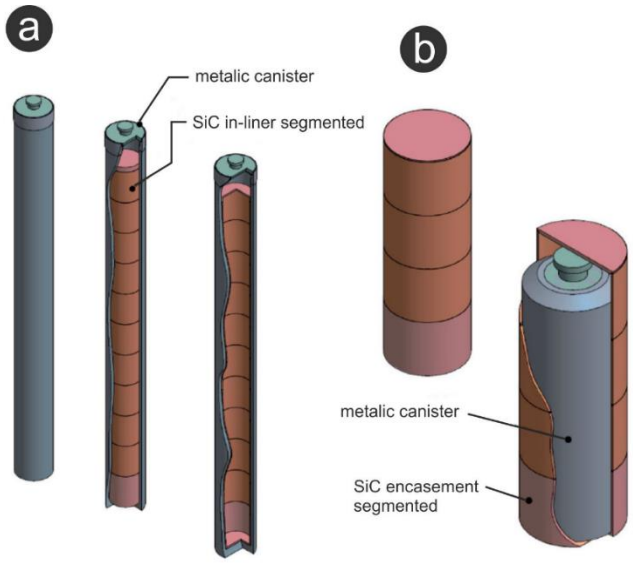

Figure 18: *Proposed SSiC encasement solutions for (a) SF rod disposal, with a diameter of 430 mm and a height of 4980 mm, and (b) VHLW disposal, with a diameter of 465 mm and height of 1,390 mm (adapted from Kerber and Knorr, 2013).*

The study of SiC behaviour (as a material for SF/HLW containers) under aggressive conditions is highly relevant. Nowadays the world's leading R&D centers make corrosion resistance tests of SiC and SiC with various alloying additions under conditions simulating the various environmental conditions.

In 2018 two companies "General Atomics" and "Westinghouse Electric" conducted corrosion tests of modern fuel pipes made of SiC/SiC composites (under conditions of normal operation of water-cooled reactors) (Deck et al., 2018). The composition of the liquid in the autoclave during the tests corresponded to different types of coolants; the tests were carried out for 3 months. Results obtained indicate that SiC has a high corrosion resistance; the authors calculated the dissolution rate of 1 μm per year, which is approximately 1% of the total thickness of the fuel cladding.

The positive effect of Cr on the corrosion resistance of SiC ceramics (Lobach et al., 2020) was experimentally shown under conditions simulating the inner environment of a VVER-1000 reactor. It is shown that doping of SiC with Cr decreases the dissolution rate of SiC(Cr) compared to SiC without additives, due to the formation of corrosion-resistant products (Cr_2O_3), which significantly affect the ability of SiO_2 films to passivate the surface of the samples. Also, it should be noted that the authors in (Lobach et al. 2018) showed the effect of Cr additives on the mechanical properties of SiC and found that doping of SiC with 0.5 wt.% Cr leads to an increase in fracture toughness (K_{Ic}) by 25–50% (from 4.2 to 6.2 MPa·$m^{1/2}$), while maintaining a high level of hardness with a value of 28.0 GPa.

The results of scientific research indicate that SiC-based ceramics have high corrosion resistance in hydrothermal conditions and are promising for use as a material for fuel claddings. Despite the fact that the leaching tests of SiC were carried out under severe conditions (350°C, 16.8 MPa), there is a need to study the mechanisms of corrosion processes in the system (SiC - compound - SiC) under the conditions simulating geological disposal (t = 90°C), because the interconnection of SiC segments is an important issue. There are two most promising approaches:

- The laser joining method (Knorr et al., 2008), which is based on a combination of pure oxidic braze filler (trademark: CERALINK ®) and a laser beam. The filler inside the joining zone is melted locally by using a laser beam. CERALINK ® shows an ideal wetting of the ceramic

surface and high oxidization resistance. The ceramic joint surface does not need pre-treatments (no metallization). This paper indicates that the joints obtained are gas-tight, have high mechanical strength and have no cracks. Joining surfaces does not require preliminary treatment, and,

- Soldering based on various materials (for example, glass-ceramic). Wang et al. (2020) joined SiC/SiC composites using the material Y_2O_3-Al_2O_3-SiO_2 (YAS). Shear strength tests showed an increase in the strength of the joining with increasing soldering temperature; maximum strength reached 51.7 MPa at a soldering temperature of 1400°C.

Within the ConCorD project, the optimal parameters of the high-pressure sintering process for obtaining the high-density SiC samples were determined (T = 2050 °C; t = 30 min; P = 40 MPa; heating rate of 200 °C/min). SiC ceramic composites with Cr additives (from 0.3 to 0.9 wt%) were prepared and investigated. Structural studies have shown that the obtained SiC(Cr) samples belong to the 6H-SiC polytype with a high density. Silicon carbide samples with chromium concentration from 0.3 to 0.5 wt% have higher micro-hardness (25.5 GPa) and nano-hardness (37.8 GPa) than pure SiC (22.8 and 31 GPa, respectively).

Samples of pure SiC and chromium (0.3 wt% and 0.5 wt%) doped SiC were tested for long-term (4200 hours) corrosion resistance in distilled water at 90 °C. The corrosion test results show that pure SiC samples are soluble in water. Chromium alloyed (0.3 wt%) samples dissolve two times slower than pure SiC after 3500 hours of testing. The leaching rate for these materials is 1.6-3 µm/year.

5.2 Ceramic Coatings

The main requirement of a ceramic coating applied to a carbon steel (or cast iron) nuclear waste disposal canister is the prevention over a period of ≥ 10000 years of access of bentonite and/or clay pore waters to the substrate via cracking or leaching (Holdsworth et al., 2018). Ceramic coatings for SF/HLW disposal canisters appear to be less mature than metallic coatings. The main issues to be addressed are related to the inherent brittleness of ceramics, the mismatch of thermal expansion coefficient with the underlying steel, the requirement for relatively large thickness and very low porosity. Nevertheless, yttria-stabilised zirconia or graded multilayer coatings of alumina and titania appear to be promising options that would require additional development before their feasibility can be better assessed. Irrespective of the selected ceramic coating material, methods for covering the lid-to-canister weld and for coating repair would also have to be developed.

Physical Vapour Deposited (PVD) coatings have good corrosion protection compared to coatings that are deposited by traditional spraying. Despite the smaller thickness of the PVD coatings, they have much lower porosity than the coatings deposited by spraying. Also, a significant advantage of the PVD methods over electrochemical deposition is the environmental friendliness of the process.

Titanium oxide-based coatings

The most-studied class of high-hardness coatings formed by the PVD methods (magnetron sputtering and cathodic arc evaporation) are titanium nitrides and carbides. Problems in the synthesis of various metals oxides by the vacuum arc method were discussed in the review (Tay et al., 2006). Previously, KIPT had developed vacuum-arc nanostructured TiO_2-based coatings (structure - anatase) with

controlled bactericidal activity for orthopaedic implants (Belous et al., 2013). The influence of the negative bias potential of the substrate was investigated by the authors (Belous et al., 2018). It is shown that titanium coatings deposited in an oxygen medium under pressure of 0.03 Pa produce a dispersed system of oxides, the composition of which depends on the magnitude of the bias potential on the substrate. Results of electrochemical measurements show that the current density characterizing the dissolution of steel coated with titanium nitrides and oxynitrides thickness of ~ 6 μm is one half to one order of magnitude lower than for uncoated steel. With the increase in the coating thickness to 12 μm the samples corrode more slowly, which correlates with a decrease of the coating porosity, with the corrosion current density decreasing by 2 to 3 orders of the magnitude. The highest corrosion resistance is observed in the samples with coating thickness of ~12 μm deposited using an oxygen and nitrogen mixture at an oxygen pressure P_{O2} = 3×10^{-2} Pa. These coatings provide high corrosion resistance of steel close to that of a pure titanium nitride coating in a 3 % aqueous solution of NaCl (Belous et al., 2018). The anodized and thermally oxidized Ti samples with TiO_2 coatings showed relatively high corrosion resistance in 4M HCl and 4M H_2SO_4 solutions at 100±5°C and the passive current density of the thermally oxidized samples was five orders of magnitude lower under the electrochemical testing condition compared with that of the anodized titanium sample (Minhas et al. 2021). The protection against corrosion provided by the conversion layer combined with TiO_2 coating on stainless steel in pure water and saline solution was quite good (Bamoulid et al., 2008). According to the corrosion test results, it was shown that TiO_2 films deposited on $MgCa_2Zn_1Gd_3$ effectively protect this alloy from corrosion in Ringer's solution at 37°C (Kania et al., 2021). While it is difficult to relate these qualitative electrochemical corrosion data to long-term repository performance, it can be assumed that titanium oxide coatings deposited by PVD methods are promising for corrosion protection of carbon steel containers. Additional studies are needed on the mechanisms of long-term corrosion processes in the TiO_2 coating-steel substrate system under conditions simulating geological disposal.

Chromium nitride coatings

Chromium nitride (CrN) has proven to be one of the most successfully and extensively used PVD coatings in industry due to its high hardness, excellent wear resistance and remarkable stability against corrosion (Milošev et al., 1997). The CrN coating deposited on AISI 304 stainless steel possesses high corrosion resistance in 0.5M H_2SO_4 solution and 0.5M NaCl solution (Milošev and Navinšek, 1993). The demand for high quality coatings in recent years has led to intensive research into the further evolution of chromium-based coatings (Cedeno-Vente et al., 2021). Daub et al. (2015) provided comparative analysis on the corrosion resistance of 2–4 μm-thick CrN-, TiAlN- and AlCrN-coated Zry-4 alloy. It was shown that CrN demonstrates better overall performance in both aqueous and steam environments. CrN coatings on Stellite™ (Cobalt based alloy) samples showed excellent wear and corrosion resistance in high temperature and high-pressure water when exposed to γ-irradiation at a dose rate of 100 Gy/h using a ^{60}Co source (Kawana et al., 1996). The Co elution rate from stellite decreased drastically with film thickness, up to about 4 orders of magnitude for a CrN coating thickness of 7 μm. This is the only publication known to us where the effect of γ-radiation on the corrosion resistance of coatings has been studied. Chromium nitride coatings are promising for corrosion protection of carbon steel, but additional studies are needed on the long-term corrosion processes in simulated geological disposal conditions.

In the ConCorD project, the effect of cathodic arc evaporation (PVD method) parameters (bias potential) on the structure and properties of ceramic coatings CrN and TiO_2 on steel has been studied. The CrN coatings of 30 μm thickness have a crystalline structure; with the crystallite size depending on the bias potential, with the smallest crystallite size of 43 nm obtained at a potential of -150 V. These coatings have superior mechanical properties (H=23 and E=320 GPa) and a high adhesion (HF1) to the steel substrate.

TiO_2 coatings with a thickness of 30 µm, deposited at a bias potential of -150 V, have an anatase structure and acceptable mechanical properties: hardness of 12 GPa and good adhesion to the steel substrate (HF2).

The CrN coating deposited under bias - 150 V with the smallest crystallite size of 43 nm has the best protective properties: after 296 hours of testing at 20 °C in 3% NaCl solution, no traces of corrosion were found. Electrochemical studies have shown that in this solution, the potential and corrosion current of the coating (E_{corr}= -187 mV, I_{corr}=0.85 µAcm^{-2}) are much lower than those of steel (E_{corr}= -548 mV, I_{corr}=29.6 µAcm^{-2}), and no traces of pitting corrosion were found. For the TiO_2 coating on steel substrate the corrosion current is 0.0815 µAcm^{-2} and E_{corr}= -33 mV. After subjecting steel samples with CrN and TiO_2 coatings to near-disposal tests in water at 90°C for 4200 hours, it was observed that the steel corroded intensely with rust formation and dissolution. The TiO_2 coatings showed weight loss and pitting, while the CrN coatings exhibited minimal weight loss and no pitting on the surface, indicating the best corrosion resistance.

5.3 Metallic Materials and Coatings

5.3.1 Metallic containers

The concepts for deep geological disposal in Finland, Sweden, Canada, Korea and Switzerland, propose copper as the outer barrier material for containers. Also, several other metallic materials have been investigated as candidates for containers, such as carbon steel, stainless steels, nickel and titanium alloys. Several extensive review reports and articles have been made comparing the metallic candidate materials (King et al. 2016) (Padovani et al. 2017). In these reports, the key properties of candidate materials are extensively presented as well as their engineering aspects together with the interactions with certain geological environments. This chapter aims to summarise the main aspects of scientific interest in these material candidates and give background for the motivation behind studies on corrosion of new materials and material grades.

Commonly considered corrosion phenomena impacting metallic containers are general corrosion, pitting corrosion, hydrogen-induced cracking (HIC) and stress corrosion cracking (SCC). The materials planned to be used in the final disposal may be subject to these corrosion phenomena and it is recognized that their susceptibilities vary between materials and environments. The corrosion phenomena listed above do not necessarily occur simultaneously, but merely become relevant during the different phases of the final disposal.

Regarding mechanical aspects, tensile strength, ductility, compressive strength, creep resistance and thermal resistance are properties that are required during the disposal phase. Sufficient tensile strength and ductility are required against external stresses that may be applied on the waste canister. Sufficient compressive strength is required against external isostatic pressure e.g., from hydrostatic loads.

In addition to this, metallic materials may be exposed to creep due to the elevated temperature and load from the swelling bentonite, isostatic pressure of the groundwater or residual stresses (e.g., in welds).

Properties that are required prior to the disposal phase include resistance to mechanical impact, grain size, weldability, and machinability. The waste canister should withstand a mechanical impact without fracturing if the canister is accidentally dropped during handling. The material should have a certain grain size for enabling non-destructive testing by ultrasonic inspection (Raiko and Salo, 1999).

Weldability and machinability are required for proper sealing of the canister and to produce the desired surface finish, respectively.

Low alloyed steels

Along with copper, steels are among the most studied material options for the canister material. Conventional carbon steels have several benefits as they are widely available at a reasonable price and are easy to machine (Landolt et al. 2009). This enables construction with relatively thick walls that result in good mechanical strength and radiation shielding. Compared to copper, the corrosion resistance of carbon steel is low, although during the anaerobic phase the corrosion rate of steel is low. The SCC risk for low alloyed steels exists in carbonate-bicarbonate environments that may arise as the container cools. However, SCC could occur not only at neutral pH but also in highly alkaline environments. A carbon steel overpack is considered for example in the French concept (Crusset et al. 2017).

Lead

Lead is studied to some extent as candidate material for canisters in waste programs of Argentina, Brazil and Russia, although the technical feasibility is still unclear (Xiong et al. 2021). The superior radiation shielding ability and low cost of lead is an asset. However, uncertainties lie in the corrosion behaviour, mechanical strength, and especially environmental aspects of using lead. Therefore, it is not considered as a potential candidate, at least, not in the near future.

Stainless steels

Stainless steels are passive materials for which the corrosion resistance is based on the thin passive film formed on the surface of the metal (Landolt et al. 2009). They exhibit very low uniform corrosion rates, with the major concern being localized corrosion. It is known that stainless steel is susceptible to localised corrosion in chloride-containing solutions. Additionally, the self-healing properties of the protective passive film on stainless steel are only effective in oxic conditions.

Titanium

Titanium alloys are also passive alloys that are extremely corrosion resistant in waste disposal environments (Braithwaite et al., 1980). The uniform corrosion rate is practically negligible due to the inertness of the titanium oxide passive layer. The alloys are immune to pitting in most aqueous environments (Landolt et al. 2009). The corrosion related challenge of titanium alloys is the crevice corrosion risk during the oxic phase that was considered as critical failure mechanisms in early studies and the need for further research in this area is recognized (Padovani et al. 2017). However, it is also stated that the risk of crevice corrosion of titanium alloys can be avoided by using alloys with Pd or Ru (Schutz, 1996) (Landolt et al. 2009). Hydrogen induced cracking (HIC) has been considered also as a potential risk for titanium alloys under anoxic conditions. The absorption of hydrogen can be enhanced by the presence of intermetallic phases in the alloy.

Nickel alloys

There are six major groups of Ni alloys, each characterised by the principal alloying elements: Ni-Cu, Ni-Mo, Ni-Cr, Ni-Cr-Mo, Ni-Fe-Cr, and Ni-Fe-Cr-Mo alloys. All of the alloys selected in the various international HLW/SF programmes belong to either the Ni-Cr-Mo group (i.e., Alloys 625 and 22, Hastelloy C-4, and C-276) or the Ni-Fe-Cr-Mo group (Alloy 825), primarily because of their resistance to corrosion under both oxidising (due to the presence of Cr) and reducing (due to the presence of Mo) conditions. Furthermore, Mo (and W in Alloy 22 and Hastelloy C-276) provides improved resistance to localised corrosion. Silicon can improve the corrosion performance under high-temperature oxidising

conditions through the formation of protective Si-O films. Manganese is added as a deoxidant, but it can increase the susceptibility to localised corrosion because of the tendency for film breakdown to occur at MnS inclusions (King 2014a).

Copper

There is a wide range of copper alloys with an equally wide range of corrosion properties. Up until this point, oxygen-free copper has been primarily considered as a container material, typically with a purity of ≥99.3 wt.% (Hall et al. 2021). Almost all research to date has been focused on the custom OFP-copper, which is oxygen-free copper with the addition of phosphorous and further described later in this chapter.

The copper material selected for the KBS-3 concept is specified so that it has to fulfil standard EN 1976:1988 (UNS C10100) for the grades Cu-OFE or Cu-OF1 with additional requirements for the concentrations for critical elements/impurities (Andersson et al. 2004). The requirements for critical elements are as follows: 0<5 ppm, P 30–70 ppm, H<0.6 ppm and S<8 ppm (Andersson et al. 2004). The EN standard has a lower limit for the phosphorous content and therefore the name “OFE+P” has been used for the selected alloy. Table 4 lists a number of commercial phosphorus-containing copper alloys that could be suitable alternatives to OFP copper.

The benefits of copper are its superior corrosion resistance and convenient mechanical properties. The downside, especially for highly pure copper grades, is the high cost.

Table 4: Properties of proposed alternative(?) copper alloys (Aurubis, 2022).

	Cu-OFP	**Cu-XLP**	**Cu-DLP**	**Cu-HCP**
		UNS 103000 CW020A	UNS C12000 EN CW023A	UNS C10300 EN CW021A
Description	Very pure, oxygen-free copper	Low phosphorus content	Deoxidized, oxygen-free copper, low residual P content	Deoxidized, oxygen-free copper, low residual P content.
Composition	Cu (min. 99.99 wt.%) Bi (max. 0.0005 wt.%) Pb (max. 0.005 wt.%) O (max. 0.001 wt.%)	Cu (min. 99.95 wt.%) P (0.001-0.005 wt.%)	Cu (min. 99.90 wt.%), P (0.005-0.013 wt.%), Bi (max. 0.0005 wt.%) Pb (max. 0.005 wt.%)	Cu (min. 99.95 wt.%) P (0.002-0.007 wt.%)
Typical use	Current canister material in national concept	Telecommunication cables, Terminals, Clad products, Busbars, Electrical conductors	Architecture, roofing, components of electrical engineering, cladding band, wire, heat exchangers, transistors, air conditioners, air-, hydraulic and oil-pipes	Telecommunication cables, terminals, clad products, busbars, base plates for power modules, electrical conductors, pressure vessels

In the ConCorD project, the impact of impurities on corrosion of commercial copper alloys for the Finnish disposal concept was explored, regarding factors such as improved availability, corrosion resistance and lower cost. VTT evaluated the absorption and diffusion of hydrogen, as well as the susceptibility to

stress corrosion cracking (SCC) by means of experiments with artificial groundwater containing ammonia as an aggressive species. Two copper grades, oxygen-free phosphorus-doped copper (OFP) and high conductivity phosphorous-doped copper (HCP), were studied in two deformation states (flat and curved) and with different rolling parameters (hot and cold), resulting in a total of six test materials. Immersion tests on U-bend, flat mass loss and electrochemical specimens were conducted in autoclaves, providing sufficient data to (i) calculate uniform corrosion rates, (ii) investigate the microstructure of the samples, (iii) analyse the chemical composition of the samples, and (iv) assess the presence of any SCC.

The results showed similar electrochemical behaviour for all the alloys after one month of immersion. While OFP copper initially exhibited higher corrosion resistance, the average corrosion rates for the 3-month immersion test showed very similar behaviours for HCP. Hydrogen content measurements showed that the copper grain size (ranging from 85 to 152 µm) did not correlate with the hydrogen uptake, and, in fact, hydrogen intake was not detected in this environment contrary to expectation. Applying different potentials to the U-bends resulted in various oxidation states. The highest anodic applied potential (-50 mV vs. SCE) leads to the highest oxidation of copper ($Cu(OH)_2$) with a distinctive blueish layer (figure 19a). Although small features suggesting intergranular corrosion were observed, they were either cracks in the oxide film (figure 19b) or the features were relatively blunt leaving the underlying metal mainly intact (figure 19c). These observations point out that HCP copper performed equally well as compared to OFE+P in NH_3 containing groundwater. While the results are encouraging, it is noted that several other aspects (such as the effect of hardness in different environmental conditions, especially on creep or alternative environments, e.g., sulphides) need to be taken into account before HCP can be considered as an alternative canister material.

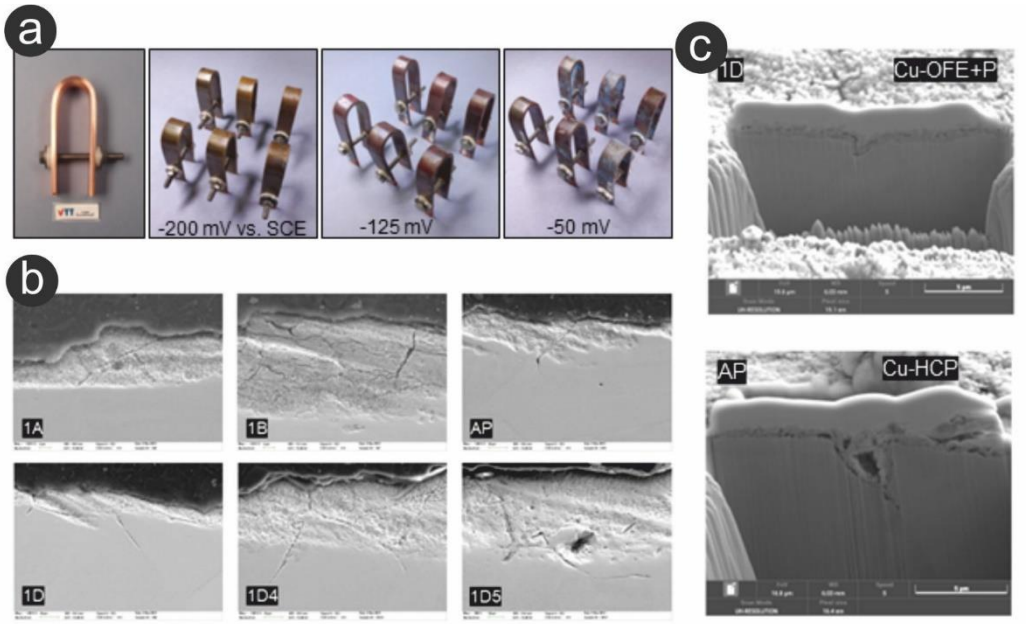

Figure 19: a) Copper U-bend sample before immersion; three sets of six alloys after 3 months immersed in simulated groundwater with 100 mg/l NH_4OH having constant potential applied (-200 mV, -125 mV and -50 mV vs. SCE, respectively); b) Cross-sectional images of Cu U-bends after immersion with application of -50 mV (AP, 1A, 1B: Cu-HCP and 1D, 1D4, 1D5: Cu-OFE+P); c) FIB micro cross sections of both alloys imaged by FEG-SEM.

5.3.2 Coatings

Titanium, chromium, and copper are well known materials for corrosion protection (Ahmad, 2006). The use of copper as a corrosion barrier has been considered for many years by many WMOs, including SKB and Posiva, and by Canada's Nuclear Waste Management Organization (NWMO) (Keech et al., 2014). In the Canadian program, the copper coating methods are still under development and the exact composition and property requirements of the copper are not yet established.

Candidate titanium coating solutions for application to carbon steel nuclear waste disposal canisters are immune to microbially induced corrosion. Open questions for the use of titanium, chromium, and copper as protective coatings on steel substrates include: the required thickness to exclude through porosity, the effect of through defects and the effect of irradiation on corrosion resistance.

Nickel alloys are widely used in industry as corrosion barriers and specific alloys, such as C22 proposed as the waste package material for Yucca Mountain, can provide extremely low corrosion rates. Also, coating with Ni-based alloys is well developed and numerous options exist. However, even though nickel alloys tend to be resistant to microbially induced corrosion, they are not immune and MIC can enhance the rate of general corrosion (King, 2020). Consequently, inherent uncertainties associated with MIC rates and mechanisms would be eliminated completely by adopting a different material which is known to be immune to MIC.

Titanium alloys are known to be immune to MIC (King, 2020). They also exhibit extremely low general corrosion rates, high resistance to corrosion under irradiation, and certain alloys are also immune to localised forms of corrosion (Hua et al. 2005). Titanium coatings deposited by PVD were studied mainly by electrochemistry methods (Zhou, 2012). Titanium coatings possess better corrosion resistance in corrosive media (0.5 N NaCl and 0.5 N Na_2SO_4 + 0.1 N H_2SO_4) than uncoated steel (Zhujing, 1991). Hydrogen absorption as a result of anaerobic general corrosion under disposal conditions will occur. However, such processes are generally predictable and long canister lifetimes can be expected with confidence. No corrosion resistance study of titanium, copper and chromium PVD coatings on the carbon steel under specific nuclear waste repository environment conditions has been published to date.

The concept of manufacturing a dual-shell container with a copper coating for corrosion protection directly on the steel structure was raised to avoid the drawbacks related to classical manufacturing approaches including machining/forging (Lee et al., 2011) (Keech et al., 2014) (Legoux, 2014). There is also the possibility of creep and stress corrosion cracking of the copper shell in the case of a gap between the outer copper corrosion barrier and the steel insert with the conventional dual-shell container design (King 2017). The benefits of a copper-coated design are as follows: no issues with tolerance of fabrication of copper part; the copper layer is produced directly on the steel part without any gap between layers; welding joint could be covered by copper after welding the steel vessel. Several deposition processes are available.

The method reviewed here is the cold gas dynamic spray, which satisfies the requirements of the dual-shell container concept: able to produce thick layer of copper on steel surfaces, guarantee low level of copper oxidation during treatment, able to deposit copper coating on localized surface, able to be applied in radioactive environment. The principles of cold spray are described in the following references (Alkhimov et al. 2012a,b) (Sova et al., 2013a-c).

While the corrosion behaviour of solid copper in waste repository conditions is well known and guarantees a very long-life containment (King, 2017, 2020), some further development work is required on copper cold spray coating materials both on the process itself and the materials obtained.

From a general point of view, the quality of coatings (density, absence of porosity) contributes to an increase in both the mechanical and resistance to corrosion properties. This quality is strongly dependent on the cold spray coating (CSC) process parameters.

One of the first parameters of CSC is the nozzle displacement, in particular the influence of nozzle traverse speed and distance between deposited tracks. It has been shown that cold spraying copper-silicon carbide powder at low nozzle traverse speed leads to the formation of thick tracks with quasi-triangular cross-section (Matts et al., 2019). Consequently, the particle impact angle on the sides of the spraying track increases. Thus, the particle deformation at impact on the track periphery becomes insufficient and local porosity arises. An increase of nozzle traverse speed allows increasing coating density and mechanical properties due to amelioration of particle deformation conditions. Compressive tests revealed significant anisotropy of the mechanical properties of copper-silicon carbide cold spray deposits. In particular, the compressive strength measured in the vertical direction (perpendicular to the substrate) was significantly higher than one measured in the horizontal plane (parallel to the substrate). This anisotropy can be explained by the orientation of the particle deformation pattern during impact.

Carrier gas velocity and its nature also have a significant effect on copper cold spray coating quality (Jakupi et al., 2015). The grain size and number of coincident site lattice grain boundaries increased, and plastic strain decreased, with carrier gas velocity. Post-annealing treatment (4h at 400°C) improved the quality of the coatings by increasing texture and coincidence site-lattices, but also increased the number of physical voids, especially when a low-temperature cold spray carrier gas was used. Tensile testing showed a better adherent coating to the steel substrate when He carrier gas is used instead of N_2 gas.

The mechanical performance of bonded thick copper coatings on steel have been assessed by Boyle and Meguid (2015). They showed the mechanical performance of the annealed cold spray coatings was comparable or exceeded that of the reference wrought copper and are suitable for the container design with adhesion strengths exceeding 45 MPa. In general, cold spray is used for production of metal deposits. However, the possibility of deposition of metal-ceramic composite coatings by spraying of different mixtures of metal and ceramic powders has also been studied (Yin et al., 2017) (Sudharshan Phani et al., 2007) (Ogawa et al. 2008) (Lee et al. 2017) (Fernandez and Jodoin, 2018) (Koivuluoto and Vuoristo, 2010). In this case, the adhesion of the metal to the substrate as well as primary matrix formation is ensured by the plastic deformation of metal particles, whereas the ceramic particles stick to the surface by a mechanical anchoring mechanism and form hard inclusions in the softer metal binder (Koivuluoto and Vuoristo, 2010) (Triantou et al., 2015) (Wang et al., 2014). Previous studies showed that the addition of ceramic powder to the metal increases the coating adhesion and density, ameliorates its mechanical properties and corrosion resistance in comparison to the cold spray deposits of the pure metal without ceramic inclusions (Yin et al. 2017) (Sudharshan Phani et al., 2007) (Ogawa et al., 2008) (Lee et al., 2017) (Fernandez and Jodoin 2018) (Koivuluoto and Vuoristo, 2010) (Triantou et al., 2015) (Wang et al., 2014). Several studies also revealed increased performance in wear resistance behaviour. For example, in the work of Triantou et al. (2015) devoted to comparison of pure copper and copper-alumina cold spray deposits, the authors found that wear resistance of composite deposits is higher due to the presence of alumina in copper matrix. In addition, the hardness, the density and the corrosion resistance were also improved.

No corrosion resistance study of CSC under specific nuclear waste repository environment conditions has been published to date. The environments selected for corrosion studies are NaCl solutions under anoxic or oxygenated conditions to simulate the long- and short-term redox conditions (Keech et al., 2014; Lee et al., 2011), and more or less acidic environments to quickly screen the corrosion resistance between wrought copper and cold spray copper coating (Lee et al., 2011). The corrosion behaviour of Cu cold spray coatings and wrought Cu in 3 mol/L NaCl under both sets of conditions are similar (Keech

et al., 2014). No evidence was observed to suggest the particle boundaries in the cold sprayed coating were preferential corrosion sites. In more concentrated NaCl solution and acidic 10% HCl solution, the corrosion rate was a little higher in the CSC coppers than the commercial wrought coppers. The authors indicated however that to further clarify these findings, more experiments, such as a field test for the CSC copper would be beneficial.

5.3.3 Metal coatings: recent advances

In the ConCorD project, EMSE studied Cu + 32 vol.% Al_2O_3 composite coatings deposited by the cold spray process. This study focused on the microstructure of the deposits, their mechanical properties, corrosion resistance, and creep resistance. Microstructural analysis, for a given set of process parameters (gas temperature of 500°C, nitrogen gas nature, spray distance of 40 mm, gas pressure of 35 bar, deposition line spacing of 4 mm), and two deposition speeds (20 mm/s and 40 mm/s) investigated, showed little effect of this speed on porosity. A low porosity is observed within the deposition lines, around 0.37% regardless of the deposition speed, while the overlap zones of the deposition lines exhibit significantly higher porosity, ranging from 1.68% to 2.52%. The EBSD analysis revealed a gradient of plastic deformation within the copper particles between the peripheral zones and the core of the particles. This results from both an increased effect of hammering by the ceramic particles and the phenomenon of recrystallization of the copper matrix. However, no crystallographic deformation texture is induced by this process.

Mechanical properties evaluated under uniaxial compression show a behaviour similar to that of cold-worked solid copper, with a yield strength close to approximately 300 MPa. Nevertheless, the apparent strain hardening rate is significantly lower, and the maximum strength exhibits dispersion among the different tests conducted. This result arises from the presence of porosities, which tend to close during compression and contribute to reducing the strain hardening rate. Damage to the deposits beyond the ultimate tensile strength results in the fracture of specimens along zones of high porosity density, namely, the overlap of deposition lines. Ultimately, these defects govern the mechanical strength of the deposits beyond a loading exceeding the yield stress.

The electrochemical behaviour characterized at 90°C in a synthetic medium representative of groundwater at the Bure site (France), through dynamic polarization tests, shows no significant difference between tests on solid copper and composite cold spray deposits. The corrosion rates extracted from the curves using the Tafel method are in the range of 10 to 15 µm/year. However, these corrosion rates are relatively high compared to those expected in anoxic environments for copper. The anodic branches of the polarization curves indicate that the materials are in an active state, although there is a pseudo-passivation plateau over a potential range of 200 mV beyond the corrosion potential. Subsequent measurement of the oxygen content in the medium revealed a residual content of about 50 to 100 ppb, contrary to the targeted anoxic test conditions. The results obtained are therefore representative not of the long-term anoxic conditions of underground storage, but rather of the transitional phase in the first years of storage.

The corrosion rate measurements by mass loss during immersion tests under these same test conditions for a maximum duration of 6 months show values in the range of 30 to 50 µm/year. Examination of the sample surfaces by X-ray diffraction and Raman analysis mainly revealed the predominant presence of copper oxide Cu_2O, along with some islands of carbonates and silica.

The creep tests at 90°C intended for tensile loading could not be conducted due to very low mechanical strength in this mode of loading. Failure occurs rapidly by decohesion along the strings of porosities in the overlap zones of deposition lines. Consequently, these tests were carried out in compression under

air at 90°C. The creep behaviour was characterized for three stress levels: 85%, 100%, and 115% of the yield strength. For the two highest loadings, the three phases of primary creep, steady-state creep, followed by final rupture, are observed. The steady-state creep rate is greater with higher stress levels. Creep at 85% yield strength shows, after the primary creep phase, a stable level of deformation as long as the deformation does not exceed 4% plastic strain.

No test in a corrosive environment could be conducted under compression to study the effect of dissolution on these creep rates. A specific setup needs to be developed.

The main original findings of this study on composite cold spray coating Cu+32vol.%Al_2O_3 concern both the corrosion resistance in a synthetic environment representative of underground storage conditions at 90°C and approximately 50-100 ppb of dissolved O_2, corresponding rather to the transient phase of underground deposition, and the creep resistance at the same temperature. The corrosion resistance of Cu/$A_{l2}O_3$ composite coatings deposited by cold spray is identical to that of pure cold-sprayed copper and wrought copper. An active corrosion state was observed with similar corrosion rates among these materials. The pores present in the cold-sprayed deposits do not appear to cause localized corrosion. The use of Al_2O_3 ceramic particles instead of SiC contributes to the same hammering, densification and bounding effects of the deposits, while eliminating the risk of galvanic coupling between Cu and SiC depending on its purity, or SiC dissolution. Regarding mechanical strength, the persistence of porosities in the coating contributes to locally weakening its tensile mechanical resistance, especially at the overlap areas of the deposition tracks. This finer analysis of distribution of pores had not yet been highlighted in the literature. Although the presence of pores is inherent to the manufacturing process of these materials, it has been observed that porosity decreases with the coating thickness. Increasing the thicknesses by a few millimeters could thus improve the mechanical strength by reducing the porosity. This result is important with regard to the tensile and/or creep stresses that may affect the containers.

In addition to the Cu+32vol.%Al_2O_3 composite coatings, in the ConCOrD project a number of metallic coatings (i.e. Ti, Cr and Cu) was studied by KIPT. The study investigated the effect of bias potential on the structure and properties of copper, titanium, and chromium coatings deposited by cathodic arc evaporation (PVD). The coatings deposited at the optimum bias potential showed good mechanical properties and a high degree of adhesion to the steel substrates. Coatings of Ti, Cu, and Cr with a minimum thickness of 30 µm exhibit l corrosion resistance without pitting when subjected to potentiodynamic testing in a 3% NaCl solution.

Long-term corrosion testing (4200 hours) of Ti, Cr, and Cu coatings on steel substrates under disposal conditions (water, T=90°C) showed weight loss and small pits in the Cr coating. The Ti and Cu coatings show high corrosion resistance as evidenced by their minimal weight change during the test period. However, after 3000 hours of testing, some pitting and rust corrosion products from the steel substrate are observed on the surface of the Ti coating.

6. Prediction tools for the assessment of long-time barrier integrity

6.1 Process and performance assessment models

In radioactive waste disposal, the main aims of modelling corrosion processes of SF/HLW disposal canisters are to:

- predict the durability of the disposal canister (and the uncertainties associated with durability estimates), to provide a key input into performance assessments (PAs), and

consolidate and demonstrate scientific understanding of the processes involved in the evolution of the disposal container and, more broadly, engineered barrier system (EBS), to underpin the treatment of container durability PAs, which are typically very simple, even if the results of the models are not used directly in PAs in any calculations of risk. A diverse range of approaches has been taken in the field to modelling corrosion processes, mechanisms and underpinning experimental results. These so-called process models have been reviewed by King (2014b), in the context of spent fuel/HLW disposal containers. Reviews focusing on corrosion, and the associated gas generation processes, of materials relevant to the disposal of intermediate level waste, including of metallic materials present in some wastes, are also available (Hoch et al., 2010; Smart and Hoch, 2010).

6.2 Process models

6.2.1 Copper containers

Among the process models that have been developed for predicting the uniform copper corrosion of spent nuclear fuel canisters located in deep geological repositories, the Copper Corrosion Model (CCM) (King et al. 2008) has been the most complete approach to the phenomenon. The model accounts for electrochemical processes at the container surface together with reactive transport and heat transfer in the nearfield, which provide a continuous description of the corroding environment. The equations are solved in a 1D domain using finite difference methods. The first version included the 10 most relevant species when focusing on chloride and oxygen transport-controlled corrosion (figure 14). The model has been progressively updated (King et al., 2010) and extended to long-term anoxic corrosion due to sulphide with the Copper Sulphide Model (CSM) (King, 2008b; King and Kolář, 2019).

Next, several relevant issues for a proper estimation of corrosion of copper containers are presented. Some of them have been already widely addressed by the CCM and CSM models, such as microbial sulphide production or the interaction of sulphide with Fe-bearing mineral phases, but some others still need to be further analysed and modelled. In this sense, alternative transport models in compacted bentonite have been reviewed, along with the impact of two-phase flow on sulphide fluxes in the nearfield at the early transient stage during groundwater intrusion into the repository. Finally, the last sub-section is fully devoted to irradiation-induced corrosion, which might be relevant in the short-term for dose rates over 100 Gy h^{-1} according to King (King et al., 2010).

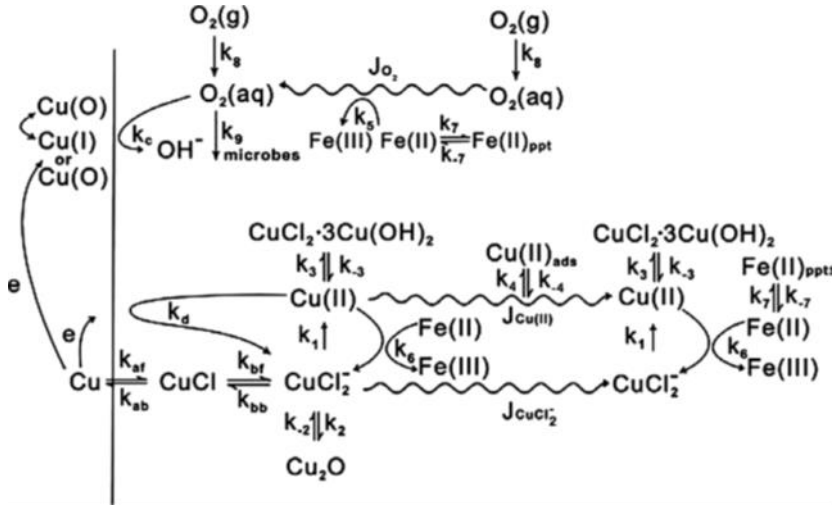

Figure 20: Schematic representation of the uniform corrosion sequence of copper in O_2 saturated bentonite containing saline groundwater. The letters j and k refer to diffusive fluxes and rate constants for various processes, respectively (King et al., 2008).

6.2.1.1 Reactive transport models in compacted bentonite

The diffusion coefficient of dissolved species in compacted bentonite is known to strongly influence corrosion due to the limited mass transport rate of corroding agents from the nearfield to the metal surface. According to Wersin et al. (Wersin et al., 1994), values of pore diffusivity have an uncertainty of a factor of 10 (Brandberg and Skagius, 1991). In the CCM (King et al., 2008), Fickian diffusion is considered with an effective diffusivity that is directly proportional to empirical values of tortuosity and effective porosity of the medium. The latter assumes that a relevant fraction of available porosity corresponds to dead-end storage pores (King and Kolář, 2019). In the case of sulphide, diffusivity has been estimated experimentally (King et al., 2010).

The definition of effective porosity and the assumptions regarding different types of porosity have led to several mechanistic and empirical approaches for describing diffusion of ions through compacted bentonite. Idiart and Coene (2019) tested these models by quantifying the diffusion of the radionuclide $^{36}Cl^-$ across the bentonite backfill in the SFL repository (Sweden). The multi-porosity model (Appelo, 2013) considered three porosity types: free, electrical double layer (EDL), and interlayer, which was assumed to be inaccessible to anions due to its structural negative charge. The size of the EDL porosity was coupled with the porewater ionic strength, which made this model more computationally demanding than the alternatives. In this sense, Wersin et al. (2014) simplified the formulation by deriving an empirical expression for the effective diffusion coefficient as a function of bentonite dry density and ionic strength and considering that the interlayer porosity was also devoid of anions.

Van Loon et al. (Van Loon et al., 2007) proposed an empirical approach which related the available porosity to the ionic strength of the external solution for the range between 0.01 and 1 mM before applying Archie's law for the effective diffusion coefficient. On the other hand, Ochs and Talerico (Ochs and Talerico, 2004) proposed a table of values of available porosity, effective diffusivity, and distribution coefficient for 38 different elements and oxidation states.

Finally, the Donnan equilibrium model (Birgersson and Karnland, 2009) assumed a single interlayer porosity with net positive charge to compensate the structural negative charge of the smectite sheets. Consequently, a concentration jump appears at the clay-water interface, thus leading to limited transport of anions through the bentonite (anion exclusion) as observed in the results obtained by Idiart and Coene (2019). This hypothesis posed a new uncertainty for the calculation of chloride and sulphide fluxes in the oxic and anoxic corrosion of copper canisters, respectively. In this sense, the CSM model was

recently extended with a dual porosity transport model accounting for Donnan equilibrium (King and Kolář, 2019), leading to higher corrosion rates. Idiart et al. (2019) and Pękala et al. (2019a) also applied dual continuum approaches to assess copper corrosion in the canister of a KBS-3V repository due to the presence of sulphide. While the former implemented a model in the reactive transport modelling framework iCP (Nardi et al. 2014), an interface coupling Comsol Multiphysics (COMSOL, 2020) and PhreeqC (Parkhurst and Appelo, 2013), the latter adapted PFLOTRAN to include dual porosity according to the approach proposed by Gimmi and Alt-Epping (2018) (see below). It was found that it had a relatively small effect on the results as compared to the traditional modelling approach, only observing a slightly reduced mackinawite precipitation and increased sulphide fluxes reaching the canister. However, this model did not account for the barriers outside the bentonite buffer, where significant sulphide generation is expected to take place. In both cases, it was concluded that further research was needed for a proper understanding of the impact of considering Donnan equilibrium on the transport of sulphide through compacted bentonite.

In terms of numerical tools for a complete electrochemical description of corrosion, Gimmi and Alt-Epping (2018) derived a Nernst-Planck equation accounting for immobile charge and Donnan equilibrium, which allowed a coupled transport simulation of all components while preserving the different diffusivities depending on their charge and the concentrations in the electrolyte. Note, however, that in that work there is no analysis of corrosion processes, and the scope is restricted to bentonite.

6.2.1.2 Modelling of sulphide fluxes in the early transient stage

Sulphide is considered the main corroding agent for copper canisters during the long anoxic phase in a nuclear waste repository. The flux of sulphide depends on different sources distributed in the host rock, the backfill and the buffer. Sulphate-bearing waters, gypsum in the bentonite, and sulphate reducing bacteria (SRB) are the main factors in sulphide generation, whereas the formation of iron sulphide phases (mainly mackinawite) though the dissolution of Fe-bearing minerals is expected to be the main sink.

According to the models developed as part of the work in Wersin et al. (2014) with FASTREACT (FrAmework for Stochastic REACtive Transport, Trinchero et al., 2014) and PFLOTRAN (Hammond et al., 2014), the concentration levels foreseen in a repository are too low for significant corrosion to occur. Severe damage of the copper coating was only predicted in a few extreme cases that applied multiple conservative assumptions. Similar outcomes were obtained by Cloet et al. (2017), Wersin et al. (2017), Pękala et al. (2019b), Pękala et al. (2020) and the CSM (King et al., 2011). However, these models did not consider a hypothetical early transient stage, during which higher sulphide concentrations may reach the container surface. This scenario, although restricted by the low microbial activity in the buffer materials due to its low porosity, would be possible in the case of relevant sulphide sources together with limited iron availability.

Wersin et al. (2014) analysed the maximum sulphide fluxes that could reach the buffer and the canister assuming that the reduction of sulphates takes place at the backfill/rock interface and no precipitation of iron sulphides occurs, although the early transient phase was not specifically considered in this study. First, the evolution of the gypsum inventory in the backfill and the corresponding sulphate fluxes were calculated with a 1D diffusion-reaction model implemented in PhreeqC (Parkhurst and Appelo, 2013) for both saline and brackish groundwaters in Olkiluoto (Finland). Then, the maximum sulphide flux was derived analytically as a balance between diffusion to the buffer and flow transport to the host rock. It was found that 5-11% of the generated sulphide reached the canister surface, which is enough to induce corrosion failure. However, it was also stated that the transport of all the sulphide to the container surface was totally unrealistic as ferrous minerals would capture a significant part of the sulphate inventory.

Besides the geochemistry, the thermal and hydrological conditions in the repository also need to be assessed, which can significantly affect both diffusive and advective transport of sulphide. For example,

Briggs et al. (2017) developed a 3D model with COMSOL Multiphysics of sulphide diffusion within the Canadian repository concept (NWMO) and concluded that the isothermal assumption was not realistic as changes in the saturation profile around the canister during the initial thermal transient might have a strong influence on the transport of sulphides until the systems reaches the cool and anoxic state. In this sense, the effect of two-phase flow during the early water intrusion in the repository should be analysed. Significant vapor and liquid fluxes are expected due to the high temperatures at the container surface and the heat dissipation in the nearfield. This, together with the motion of trapped gas bubbles, might lead to less regular sulphide fluxes in the short-term than those predicted by Wersin et al. (2014) or by the CSM model (King and Kolář, 2019), which only consider transport under the stable saturated conditions expected during the long-term anoxic period. A key concern that arises for this is the potential for gaseous H_2S to be transported during the unsaturated period. H_2S is corrosive to copper in dry atmospheres, even at comparatively low concentrations (>3 ppb) and becomes increasingly more corrosive at higher temperature and higher relative humidity. H_2S is also corrosive to carbon steel and under certain conditions can lead to localised corrosion and environmentally assisted cracking.

6.2.1.3 Modelling of microbial sulphide production

In the early non-saturated phase of the repository, oxygen consumption by aerobic microbes, which is expected to limit corrosion, was already implemented in the first version of the CCM model with a rate constant derived from in situ tests (King et al., 2008). This protective effect of microbes is removed when the system turns anoxic and microbial reduction of sulphate becomes dominant. In this sense, this model was updated by King et al. (2010) with 15 processes, including microbial sulphide production, and a mass balance for each organic agent (CCM-MIC), so the microbial population could be tracked in space and time. According to King and Kolář (2006), who used the model to predict the microbial population in a Canadian repository, the presence of microbes in the nearfield was minimal and the sulphide concentrations reaching the canister were predicted to be small due to mackinawite precipitation in the buffer and backfill. Moreover, the elevated temperatures and lack of water foreseen for the initial thermal-hydraulic transient were expected to suppress most of the microbial activity.

The definition of the kinetic rate constant for microbial sulphate reduction was addressed by the joint SKB-Posiva Integrated Sulphide Project. Bengtsson et al. (2017a) quantified this parameter (6.1×10^{-11} s^{-1}) after monitoring radioactively labelled sulphate in an experimental setup consisting of copper test plates buried in compacted bentonite with groundwater containing SRB (Pedersen, 2010). Results showed no SRB activity for bentonite wet densities of 1900 kg/m^3 and above, whereas iron sulphide precipitates were observed on the plate surface at a wet bentonite density of 1750 kg/m^3. The maximum sulphate reduction rate determined in MX-80 bentonite was 8.2×10^{-7} mol s^{-1} m^{-3} in bentonite porewater. The experimentally measured kinetic rate constant was used to feed a transport model using finite differences as a next step towards the quantification of the amount of sulfide reaching the surface of the test plates.

The CSM model has been recently extended by King et al. (2021) with two different pathways for microbial sulphate reduction: organotrophic (dissolved organic carbon as electron donor) and chemotrophic (H_2 as electron donor). It has also been applied to the KBS-3 concept for the disposal of spent nuclear fuel, leading to the precipitation as mackinawite of 98.5% of the microbially generated sulphide due to the dominance of siderite over organic matter in the buffer and the backfill. As a result, only 3 µm of copper would be corroded after one million years. However, this outcome might be less beneficial in repositories with higher amounts of organic material and gypsum and lower reactive Fe(II) contents, since a smaller fraction of the microbially produced sulphide would precipitate before reaching the canister.

The most recent 3D reactive transport sulphide model developed for the KBS-3 repository in Olkiluoto, Finland (Posiva 2021b) also considers organic carbon and H_2 as pathways for microbial sulphate

reduction, which is represented with a kinetic Monod model. The selected maximum sulphate-reducing bacteria (SRB) activity rate constants were defined as 5×10^{-5} and 10^{-4} mol sulphide/L of porewater, respectively, based on experimental and field studies from the literature. The simulations showed corrosion depths below 1 mm averaged over the whole copper canister surface after one million years. The maximum cell-resolved depths, however, were higher, in the range of one to a few millimetres.

6.2.1.4 Modelling the interaction of sulphide with Fe-bearing mineral phases

In the SR-Site safety assessment, it was assumed that pyrite dissolution could lead to the corrosion of the canister (SKB, 2010). The extent of corrosion was estimated according to mass-balance and mass-transport, leading to a maximum depth of canister corrosion of 0.1 mm and 0.9 mm for MX-80 and Ibeco-RWC bentonites, respectively. However, when the limited solubility of pyrite and the low diffusivity of sulphide were considered, it was found that only the pyrite within 2 cm of the canister surface contributed to corrosion after one million years, resulting in 1 µm of corrosion for the reference values of solubility and diffusivity (SKB 2010). Simulations using the CSM (King et al., 2011) predicted long-term corrosion rates of the order of <1 nm/year, of the same order of magnitude as those predicted for the SR-Site safety assessment (SKB, 2010), with the contribution of pyrite dissolution being less than 5% of the total extent.

Similarly, Marty et al. (2010) used the reactive-transport code KIRMAT to predict the alteration of bentonite for the French nuclear waste programme. In this case, as well as in the model developed with CRUNCH by Bildstein et al. (2006), the rate constant for the anaerobic dissolution of pyrite was taken to be that of the oxidative dissolution. In a later extension of the CSM (King and Kolář, 2019), the rate constant for the anaerobic dissolution of pyrite was excluded from the model after a review of its properties by King (2013b) due to its extremely low solubility. Instead, the CSM provided a wider description of the interaction between sulphide and ferrous minerals, especially the precipitation of FeS leading to reduced sulphide fluxes. In this sense, four Fe(II) solid phases were included in the reaction scheme: biotite ($K(Mg_{0.6–1.8}Fe(II)_{2.4–1.2})(Si_3Al)O_{10}(OH,F)_2$), which is initially present in the backfill and rock layers, and which undergoes temperature-dependent dissolution releasing Fe(II), pyrite (FeS_2), which is expected to be fully oxidized during the aerobic phase, iron carbonate ($FeCO_3$), which is initially present in both the buffer and backfill materials, and which precipitates reversibly in the presence of excess Fe(II), and finally mackinawite (FeS), which precipitates if the dissolved Fe(II) and HS^- concentrations exceed the value of the solubility product. With all these considerations, and assuming the expected conditions in a KBS-3 repository, the long-term corrosion extent was predicted to be less than 10 µm after one million years.

An alternative hydrogeochemical model using PhreeqC (Parkhurst and Appelo, 2013) was presented by Wersin et al. (2014a). A similar outcome was obtained, including copper corrosion limited to 1-1.7% of the total inventory, and sulphide fluxes controlled by mackinawite precipitation.

In the 3D reactive transport model used for the recent safety case of the spent fuel repository in Olkiluoto, Finland (Posiva 2021b), the main sources of iron reacting with sulphide are ferric (oxyhydr)oxides present in the buffer and backfill as accessory minerals. The reaction of sulphide with Fe(III) follows a complex redox reaction scheme leading to oxidized sulphur species (elemental sulphur, polysulphides) and Fe(II). The latter reaction products further react with sulphide to form iron sulphide (mackinawite).

6.2.1.5 Modelling irradiation-induced corrosion

The radiation from a spent fuel canister could affect the chemical conditions in the nearfield. The ionizing radiation will produce both molecular and radical oxidants and reductants through radiolysis. The concentrations of the different species formed during radiolysis depend on the type of radiation, the dose

rate, the composition of the aqueous solution, and the material of fabrication and wall thickness of the canister (King 2020). In the gamma-irradiated system, the reducing electron and hydrogen radicals (e- and H·), formed with yields higher than oxidizing species, rapidly react with both H_2O_2 and O_2, decreasing the concentrations of the corroding species (Soroka et al., 2021).

In addition to extensive experimental work, a number of numerical simulations have been performed of the effect of water radiolysis on iron and copper corrosion (Soroka et al., 2021; Wada et al., 2016). Soroka et al. (2021) performed numerical simulations using MAKSIMA-CHEMIST and considered the full set of chemical reactions describing the radiation chemistry of water together with a reaction of Cu oxidized by O_2. The simulations showed that the amount of molecular oxygen produced directly via γ-radiolysis of water and via catalytic decomposition of radiolytically produced H_2O_2 on the oxide surface could account for the amount of corrosion observed in the experiment. Wada et al. (2016) performed radiolysis calculations with the radiolysis code SIMFONY and determined the temporal evolution of the generated O_2, H_2 and H_2O_2 by gamma radiation (no comparison with experimental data was included). Recently, the complete set of kinetic reactions dealing with recombination of water radiolysis species have been modelled in Comsol Multiphysics in the context of spent fuel corrosion (Riba 2020).

6.2.2 Steel containers

6.2.2.1 Modelling of steel canister corrosion

Modelling studies on iron canister corrosion in contact with different geotechnical barriers (i.e. bentonite, cement) or pure clay minerals (i.e. montmorillonite) performed in the last 15 years (Savage, 2012) have been mainly simulated by mechanistic reactive transport models in porous media, including more or less simplifications (Montes-H et al., 2005; Bildstein et al., 2006; Wilson et al. (2006a, 2006b); Hunter et al., 2007; Wersin et al., 2008; Samper et al., 2008, 2016; Peña et al. 2008, Savage et al., 2010; Marty et al., 2010; Lu et al., 2011, Bildstein et al. 2012; Mon et al. 2017, Chaparro et al. 2021). Most of the works mentioned are related to long term simulations (> 10 000 years) and predict that magnetite is the principal steel corrosion product in contact with bentonite, along with significant alteration of the clay minerals to a mixture of non-swelling silicates, such as chlorite, berthierine or cronstedtite and zeolites (Ngo et al., 2014; Wilson et al. 2015). Although, some authors have focused on the principal reaction products (i.e., magnetite) considering sorption of Fe on clay surfaces (Hunter et al., 2007; Samper et al., 2008; Lu et al., 2011), others have tried to model the growth of iron-bearing aluminosilicates (Wersin et al., 2008; Savage et al., 2010; Marty et al., 2010). On the other hand, Peña et al. (2008) modelled the attenuation of the corrosion of carbon steel canisters due to the influence of diffusive transport through the corrosion product and compared it with data from Smart et. al. (2006) that studied the corrosion rate of steel in bentonite under a wide range of conditions. Table 5 provides a comparison of the main assumptions and results obtained in the previously explained modelling exercises at the disposal scale and below is given more detail of each work. However, all of these models are inherently geochemical models designed to predict the consequences of steel container corrosion on the buffer material and host rock. These are not corrosion models in the true sense of the term and, indeed, the corrosion rate is an input to these models, rather than an output.

Bataillon et al. (2010) were the first to develop a true corrosion model for steel containers aimed at predicting the corrosion rate. They developed the Diffusion Poisson Coupled Model (DPCM) as a tool to investigate the corrosion processes at the surface of the carbon steel canisters. The numerical scheme was implemented in the simulation code CALIPSO. This code was coupled with a geochemistry-transport code, Kirmat (Gerard et al. 1998). This makes it possible to give a realistic representation of both the corrosion behaviour of iron as well as the alteration of clay base material.

More recently, another model (Marion, 2014, Mohamed-Said, 2017) has also been developed to predict the evolution of the corrosion rate of carbon steel under a protective deposit. This model was proposed

to describe the oxidation of iron in anaerobic neutral or slightly alkaline conditions. These chemical conditions correspond to those expected in the French HLW disposal concept. The model allows the assessment of the evolution of the carbon steel corrosion rate (reduction by oxide layer formation), the chemical species released and the characteristic time of these processes. The model assumes that the solution is in contact with a dense disordered spinel-like oxide layer which covers the iron. Two interfaces bound the oxide layer: (1) the inner interface which corresponds to the metal/oxide layer; and (2) the outer interface which corresponds to the oxide layer/solution interface. The metal (an electronic conductor) could be charged either by accumulation or depletion of electrons. The solution (ionic conductor) could be charged either by accumulation of cations or anions. The oxide layer is a mixed electronic and ionic conductor. The outer and the inner interfaces could move with time. The model considers the electrostatic and kinetic effects and accounts for moving boundaries. The electrostatic module gives the potential profile in the solution-oxide layer–metal system. The kinetics module gives the concentration profiles; one per each charge carrier. The moving boundaries module gives the locations of the two interfaces which bound the oxide layer. These three modules are coupled because each module involves the solution of the others. Bataillon et al. (2010) tested the DPCM in a simplified situation where the locations of the outer and the inner interfaces are fixed and after that with moving boundaries. These data could be used to estimate the lifetime of the carbon steel overpack and the pressure rise resulting from hydrogen release. The convergence of the scheme was studied by Chainais-Hillairet et al. (2015) for the two-species model on a fixed domain. Chainais-Hillairet and Gallouët (2016) presented an updated version of the model of Bataillon et al. (2012) by studying the pseudo-stationary state for a corrosion model. The approach implemented in the CALIPSO code has the potential to be coupled with multicomponent reactive-transport models to study the interactions at the steel/iron-bentonite interface and the effects of corrosion products on the bentonite.

King et al. (2014) have developed a mixed-potential model for the anaerobic corrosion of carbon steel containers in contact with bentonite buffer. Using a similar approach to that used for copper containers and the CCM, the Steel Corrosion Model (SCM) couples interfacial electrochemical expressions for the dissolution of Fe (as Fe(II)) and for the cathodic reduction of H_2O and/or HCO_3^- to the transport of reactants and products towards and away from the corroding interface through various mass-transport layers representing the buffer and backfill materials and surrounding host rock. The model also incorporates the impact of the precipitation of corrosion products (as $Fe(OH)_2$, Fe_3O_4, or $FeCO_3$), both on the buffer material (via precipitation in the buffer pores or adsorption of Fe(II) by the bentonite) and, more importantly, on the interfacial electrochemical reactions. The effect of gas production (in the form of H_2) and transport through the buffer is also predicted, as is the periodic release of H_2 as the build-up of pressure exceeds the gas breakthrough pressure for the engineered barriers.

6.2.2.2 Modelling gas generation due to corrosion

One of the main concerns about the anaerobic corrosion of ferrous materials in a repository, is the production of hydrogen, due to its potential implications for damage to the structure of the EBS and the possible transport of gaseous radionuclides to the biosphere. A model known as SMOGG (Simple Model for Gas Generation) has been developed, with the aim of predicting the amount of gas that may arise due to both corrosion and radiolysis, under various conditions. Literature reviews and assessments of the corrosion rate data for steel and Zircaloy (Smart and Hoch 2010), and reactive metals (Magnox, uranium and aluminium, Hoch et al. 2010) have been prepared to identify corrosion data that should be applied in the SMOGG model to predict the amount of gas produced by anaerobic corrosion.

A similar model, referred to as the Gas Generation Tool (Poller et al. 2016), has been developed for the calculation of generated gas in the Swiss deep geological repository. The model covers both the corrosion of steel SF/HLW disposal canisters and the generation of gases in the L/ILW (due to corrosion and degradation of organics). The output of the model is used as input to 2-phase flow modelling for the

demonstration of the fate of repository-generated gas and the performance of the disposal system (Diomidis et al.2016).

Table 5: Comparison of steel corrosion modelling for deep geological disposal.

Reference	Type of interface	T (ºC)	Simulation time (years)	Corrosion rate	Assumptions	Main corrosion product	Main secondary minerals	Maximal perturbation extent	Relevant results
Bildstein et al. (2006)	Fe-MX80 bentonite	50	10.000	Constant (4,3 µm/y)	1D diffusive model Porosity feedback effec	Magnetite	Cronstedtite Berthierine	5 cm	Porosity clogging after 5.000 years
Wersin et al. (2008)	Fe-MX80 bentonite	100	500.000	Constant (1 µm/y)	1D model (Test case D0) Porosity update Clay reactions are considered Use of cation exchange and surface complexation	Magnetite	Cronstedtite Berthierine	Few cm	The interaction of Fe with bentonite remains spatially limited for very long times mainly because of Fe clay re-precipitation and diffusional limitation
Samper et al. (2008)	Fe-FEBEX bentonite	25	300.000	Constant (0.2 µm/y)	1D and 2D model No reactivity for clay minerals Use of cation exchange and surface complexation	Magnetite	Siderite Goethite	7 cm	Bentonite porosity decreases due to magnetite precipitation (no clogging) Proton surface complexation is highly effective in buffering pH in bentonite
Savage et al. (2010)	Fe-MX80 bentonite	-	1.000.000	Constant (~2 µm/y)	Time-dependent variation of reactive surface areas for the Fe-bearing minerals The sequence of the alteration of the clay by Fe-rich fluids may proceed via an Ostwald step sequence	Sequence of precipitation: magnetite-cronstedtite-berthierine-chlorite	Cronstedtite Berthierine	-	The secondary minerals evolution is different to that predicted by the fixed surface area model
Marty et al. (2010)	Fe-MX80 bentonite	100	100.000	Non-constant (decreases from 5 to 0.2 µm/y)	Porosity update Clay reactions are considered	Magnetite	Fe-chlorite Fe-saponite	15 cm	Porosity clogging after 100.000 years
Lu et al. (2011)	Fe-FEBEX bentonite	25	300.000	Constant (0.1 µm/y) and non-constant (max. of 0.7 µm/y)	1D model Use of cation exchange and 3 types of sorption sites in the bentonite	Magnetite		-	Accounting for kinetically-controlled canister corrosion leads to a significant reduction in the corrosion rate The concentration of dissolved Fe computed with kinetic

Reference	Type of interface	T (ºC)	Simulation time (years)	Corrosion rate	Assumptions	Main corrosion product	Main secondary minerals	Maximal perturbation extent	Relevant results
					Kinetically-controlled canister corrosion and magnetite precipitation				magnetite precipitation is smaller than that obtained at equilibrium
Ngo e al. (2014)	Fe-MX80 bentonite	100	10.000	Non-constant (decreases from 5 to 0.2 µm/y)	Similar to Marty et al. (2010) Porosity update Clay reactions are considered With and without accounting for the influence of the reactive surface areas of the primary minerals	Magnetite	Greenalite Fe-saponite Fe-chlorite Berthierine	10 cm	The large surface area of the primary clay minerals provides a significant decrease in porosity in the zone in contact with the steel overpack, which in turn limited the diffusion of the aqueous corrosion products toward the bentonite barrier. This induced an important porosity reduction and intense mineralogical transformation in the bentonite zone close to the bentonite/steel overpack interface.
Wilson et al. (2015)	Fe-bentonite	70	100.000	Constant (1 µm/y) and non-constant (diffusion limited)	Model 1: fixed steel corrosion rate Model 2: diffusion-limited corrosion rate Model 3: corrosion cell approach	M1 and M2: - M3: Magnetite Siderite	M1: Berthierine Fe-saponite Greenalite M2 and M3: Berthierine	2 cm	The extent and nature of the alteration predicted by the models is sensitive to model conceptualisation
Samper et al. (2016)	Fe-FEBEX bentonite	Non-isothermal	1.000.000	Constant (2 µm/y) and non-constant corrosion rate (T and chemical conditions dependence)	1D model Use of cation exchange and 3 types of sorption sites in the bentonite Kinetically-controlled canister corrosion and magnetite precipitation Smectite dissolution is considered	Magnetite	Analcime Cronstedtite	7 cm	Magnetite precipitation reduces significantly the porosity of the bentonite near the canister (7 cm thickness of the zone of reduced porosity at 1 Ma) The thickness ranges from less than 5 cm for a corrosion rate of 5 µm/year to nearly 12 cm for a rate of 0.5 mm/year. The thickness increases significantly when the corrosion rate dependence on the chemical conditions is considered and decreases 3 cm when smectite dissolution and analcime

Reference	Type of interface	T (ºC)	Simulation time (years)	Corrosion rate	Assumptions	Main corrosion product	Main secondary minerals	Maximal perturbation extent	Relevant results
									precipitation are taken into account
Mon et al. (2017)	Fe-Febex bentonite	Non-isothermal	1.000.000	Constant corrosion rate (2 µm/y)	1D model Use of cation exchange and 3 types of sorption sites in the bentonite. Smectite dissolution is considered	Magnetite	Gypsum Sepiolite	1 cm	Pore clogging at the canister-bentonite interface Narrow alteration zones Limited smectite dissolution after 1 Ma

6.3 Performance assessment models

6.3.1 PA models for copper containers

6.3.1.1 Introduction

Oxygen-free copper has been considered as the canister material in several European and international waste management programmes. Key countries of interest include Sweden (SKB, 2010a), Finland (Posiva, 2007), Switzerland (Johnson and King, 2003), the United Kingdom (RWM 2016), and Canada (NWMO 2016). The furthest developed disposal concept in Europe is the KBS-3 concept which utilises a ~50 mm thick barrier layer of phosphorus-doped oxygen free copper (SKB, 2010a). It is worth noting that performance assessments typically indicate expected depths of corrosion substantially less than that container wall thickness. However, the assumed wall thickness is currently conceived to both sustain the canister under its own weight (including during manufacture) and to ensure sufficient resistance to the risk of creep rupture. An alternative copper canister design comprises a copper coating, a few mm thick, applied to a carbon steel substrate as is considered in the Canadian (NWMO, 2016) and Swiss concepts (Johnson and King, 2003). For coated designs the corrosion allowance is considerably less than for the thicker copper canister designs, consequently for coated containers a greater certainty regarding the prevailing corrosion mechanisms is required. Currently electrodeposition and cold spray are being considered as possible coating methodologies.

Copper canisters used to dispose of SF and HLW are designed to be emplaced within a bentonite buffer. Unless specific environmental conditions are present in the groundwater (e.g., high carbonate and/or sulphate content, and low chloride content), copper would not be expected to passivate in a repository environment and much of its lifetime can be predicted based on a general corrosion occurring with moderate uniformity. For a particular corrosion process (e.g., oxic corrosion, anoxic sulphide-driven corrosion, microbiologically influenced corrosion, pitting) the loss of material is either bounded by a maximum loss of material that is distributed over an area or is ascribed a rate of loss of thickness that is applicable over a particular phase in the repository lifetime. (e.g., early aerobic post-closure conditions, long-term anaerobic conditions) (RWM, 2016; Scully and Edwards, 2013).

Early in the repository lifetime and for a comparatively short-lived period (previously estimated at decades (Johnson and King, 2003) but more recently estimated as shorter based on the results of full-scale field testing experiments (Huertas, et al., 2005)), the corrosion of copper is governed by the concentration of oxidants within proximity to the canister, including trapped O_2, radiolysis products and Cu(II) species produced by the oxidation of Cu(I) corrosion products. Over time, these species are consumed and not replaced (or not replaced at the same rate), leading to a reduction in the oxidising power of the environment and a change in the dominant corrosion mechanisms that are predicted to prevail over the long-term. In this phase, the corrosion of copper is expected to be governed by the flux of sulphide to the copper surface from outside the nearfield. This process is expected to be transport limited by the low solubility and slow diffusion of sulphide through compacted bentonite (Scully and Edwards 2013). In the absence of other degradation processes, which are not expected to occur, provided the swelling pressure of the buffer is maintained, copper canisters are predicted to last more than 10^5 years (Johnson and King 2003, RWM 2016) and potentially over 10^6 years (Keech et al. 2020).

The main types of corrosion affecting copper-based canisters, and which need to be considered in any performance assessment, are as follows:

- Corrosion under unsaturated conditions
- General corrosion
- Localised corrosion
- Microbiologically influenced corrosion

- Radiation assisted corrosion
- Environmentally assisted cracking

6.3.1.2 Corrosion in unsaturated conditions

Corrosion of the copper overpack during the unsaturated phase (including any corrosion before emplacement in the buffer and within the buffer before groundwater resaturation occurs) has been evaluated for a KBS-3 repository environment. Based on empirical evidence from the literature, corrosion rates are expected to be negligible (Posiva, 2013; SKB, 2010a). In these conditions it is assumed that the elevated surface temperature of 50 °C will ensure that the relative humidity close to the canister surface is lower than the critical relative humidity required to cause corrosion, generally considered to be around 50-70% RH (SKB, 2010a). In dry air, the corrosion rate of copper increases with temperature and is predicted to be of the order of 10s of nm/y at temperatures between 50 -150 °C (SKB, 2010b; Roy and Sircar, 1981; Pinnel et al. 1979). These values are consistent with measurements made at the underground Äspö Hard Rock Laboratory in Sweden, which indicated corrosion rates <0.1 μm^{-1} at 75 °C (Taxén, 2003). Consequently, the atmospheric corrosion of copper canisters awaiting disposal is pessimistically bounded by assuming the corrosion will not exceed 1 µm and will produce a copper oxide surface film (SKB, 2010a, SKB 2021).

6.3.1.3 General corrosion

For copper canisters emplaced within clay buffer materials, after closure of the repository oxygen is assumed to be present within the void space in both the buffer and backfill materials. A pessimistic assumption is that all the oxygen present in the buffer material reaches the canister surface and is consumed uniformly by corrosion (Keech et al. 2020, SKB, 2010b). A more realistic assumption, applied to the Swedish KBS-3 repository design, is that oxygen will also diffuse towards the oxygen-free rock and away from the canister, hence only around 50% may reach the canister surface, which equates to an expected corrosion loss of approximately 17 µm and bounded at 36 µm. The backfill is estimated to contain a greater amount of trapped oxygen than the buffer owing to its greater total volume, however, it is assumed that a smaller fraction of the oxygen trapped in the backfill would reach the canister. This fraction has been estimated for the KBS-3 design by considering the ratio of the canister diameter in relation to that of the deposition hole, with the assumption that the oxygen is consumed as it diffuses downwards by reaction with only the canister lid and the top 10% of the canister height. Under these assumptions a further corrosion loss of approximately 106 µm is anticipated, which gives a total expected loss of 123 µm (SKB, 2010b). In the Swiss program, the amount of copper corrosion arising from trapped O_2, assuming all the trapped O_2 reacts with the canister to form Cu(I), was estimated at around 70 µm (Johnson and King, 2003). No credit was taken for the consumption of oxygen by reaction with steel rock supports, microbial activity or oxidation of Fe(II), making the approach conservative.

Once oxygen has been consumed, sulphide will be the primary oxidant remaining in the repository (or, more precisely, copper will corrode with the evolution of hydrogen in the presence of sulphide). There is an initial inventory of sulphide that is present as minerals (e.g., pyrite) within the buffer and backfill that may dissolve and diffuse toward the canister surface during hydration of the borehole. The corrosion of copper by sulphide will lead to the formation of copper sulphide [Equations (13) and (14)], although other reactions are also possible). Sulphide is also produced by microbial activity, as previously discussed.

$$2Cu(s) + HS^- + OH^- \rightarrow Cu_2S(s) + H_2O + 2e^- \quad \text{anodic process} \quad (13)$$

$$2H_2O + 2e^- \rightarrow H_2 + 2OH^- \quad \text{cathodic process} \quad (14)$$

The contribution of the sulphide present as pyrite in the buffer can be pessimistically bounded by a mass balance estimate as for the residual oxygen. The contribution of the dissolution of pyrite and the diffusional transport of sulphide from the pyrite to the canister surface has been considered as a source of corrosion in the KBS 3 repository design (SKB, 2010b), however, an allowance is not currently made for it owing to the low solubility of sulphide in the buffer.

In PA models, the corrosion rate due to the diffusion of corrosive species towards the canister surface is typically treated using the assumption that they react immediately upon contact with the canister surface, and that any future reaction rate is unhindered by the formation of corrosion products. In the case of the copper/bentonite system, this assumption is justified by the slow rate of transport of sulphide in compacted bentonite in relation to the inherent reaction rate of copper with sulphide. Under these conditions, the corrosion reaction is treated as being transport-limited and the rate of corrosion is proportional to the flux of species reaching the surface (SKB, 2010b). It has been demonstrated that for copper corroding due to reaction with HS^-, the shift from kinetic limitation to transport limitation occurs at HS^- fluxes lower than 2×10^{-12} mol cm^{-2} s^{-1}, which is considerably greater than the anticipated long-term sulphide fluxes through an intact bentonite buffer (~10^{-14} mol cm^{-2} s^{-1}) (King et al. 2017b). The lack of impact of corrosion product formation on the subsequent corrosion rate is supported by experimental observations that copper sulphide corrosion product layers are porous and non-protective at the pH and sulphide concentration anticipated within a bentonite buffer (Keech et al. 2020, King et al. 2017b). The mass transport approach can be applied as well to any oxygen that is trapped in the buffer and backfill materials, although in conventional disposal scenarios (DGR tunnels sealed effectively) the treatment based on mass balance is considered both cautious and sufficient. On the other hand, whilst this approach is still conservative (as the consumption of oxygen by other sources is also not considered), this approach could be used to treat the corrosion of disposal canisters in relevant scenarios, including either deliberately or inadvertently unsealed tunnels during the DGR operational period (i.e., whilst operations in other tunnels are still taking place) or access of glacial-melt water (see below) (King et al. 2011).

Corrosion of copper by sulphide transport in groundwater is evaluated by mass transport limitation. The equilibrium concentration of sulphide in the groundwater is determined by the source (i.e., sulphate reduction by microbial activity) and sink (i.e., oxidation and precipitation with metals) terms (SKB, 2010b). Mass transport modelling has been used to evaluate the effect of buffer erosion on the sulphide transport from flowing groundwater, supplied from a rock fracture to the canister surface for a KBS-3 repository (SKB, 2010b). For an intact buffer and a sulphide concentration of the order of 0.01 mM, corrosion rates lower than 0.001 µm $year^{-1}$ have been predicted for all conditions modelled, with vastly lower corrosion rates predicted for most cases. For a partially eroded buffer, predicted corrosion rates are much higher, and under the most pessimistic combinations of flow rate and sulphide combination (≥0.161 m/s and 0.12 mM) failure of a canister (taken as 47 mm of corrosion or greater) could occur within 10^5 years (SKB, 2010b). However, for a more realistic sulphide concentration (0.01 mM), failure is only predicted to occur after around 850,000 years, even at a high flow rate of 0.251 m/s (SKB, 2010b). Likewise, similar hydrogeology models are used to evaluate oxygen transport from glacial melt water. This can be done by assuming an upper limit of oxygen concentration (1.5 mM) in the groundwater that is supplied to the canister surface from rock fracture intersecting a deposition hole over a fixed exposure period of 1,000 years, resulting in a corrosion loss of less than 6 mm (SKB, 2010b). In the Swiss disposal system, the corrosion loss based on the diffusion of HS^- to the container surface has been estimated as 80 µm over 10^6 years. This is based on reactive transport modelling of sulphide in bentonite (Cloet et al. 2017).

6.3.1.4 Localised corrosion

Pitting of copper canisters is only considered viable during the aerobic early post closure phase, while conditions are oxidising, but water chemistry is still quite dilute as the groundwater will have not yet reached the disposal container (or buffering by the initial- porewater still occurs) (RWM, 2016). Based on short-term laboratory testing in simulated DGR conditions and in situ corrosion testing in disposal programmes considering the use of the material, copper has been shown to exhibit non-uniform general corrosion rather than formation of discrete 'classical' pits that are characterised by a small, fixed anode spatially separated from a supporting cathode. Consequently, the relative non-uniformity in the extent of corrosion across the surface is anticipated to reduce over time (RWM, 2016). Therefore, predictions of pit depths based on the assumption of a fixed anode that corrodes at a greater rate than the mean corrosion rate are unrealistically pessimistic (e.g., empirical pitting factor and extreme value statistical analysis).

Another form of localised corrosion that has been evaluated in some disposal programmes, for example the Canadian disposal concept, is under-deposit corrosion (Scully and Edwards 2013). The specific mechanism of concern is a form of crevice corrosion that proceeds underneath a precipitated surface film. The film would act as a selective ion exchange membrane and enable the development of a locally aggressive solution chemistry, forming a permanent anodic region. Such a mechanism would preclude the use of a surface roughening factor to account for local attack in favor of the more conservative pitting factor (Scully and Edwards 2013). Localized corrosion including under deposit corrosion has been considered by ascribing a 0.1 mm corrosion allowance to this mechanism, on the assumption that anodic and cathodic sites will not remain permanently fixed but will change with time within the overall anodic region (under the deposit) (Keech et al. 2020, Scully and Edwards, 2013). The assumption is underpinned by measurements of the surface profiles produced from corrosion of copper underneath precipitated films in simulated Canadian repository conditions. The results showed a depth of attack of around 50 µm, following 18 months exposure under conditions that were conservative, with respect to oxygen concentration, in comparison to those anticipated during the aerobic phase in the DGR (King et al. 1992, Scully and Edwards, 2013).

Empirical pitting factor

Pitting factors for buried copper and copper alloys have been found to vary between 0 and 25 but exhibit a tendency to decrease with time. The longest exposure durations used to determine pitting factors are those of bronze-age artifacts (~3,000 years) reported by (Bresle and Arrhenius, 1983) and gave pitting factors between 2-5. These values are broadly consistent with measurements made of buried lightening conductor plates, which exhibited pitting factors of between 0 and 5 following exposures between 50 and 80 years (Hallberg et al. 1984). Hence, for buried copper canisters, a pessimistic pitting factor of has previously been assumed (SKB, 2010a). A pitting factor of 5 was applied to give a conservative estimation of the maximum depth of penetration of a copper canister in a Swiss repository due to sulphide flux (Johnson and King 2003). However, the use of a pitting factor for copper is, in general, considered to be overly conservative when applied to DGR performance assessment. This is due to a shift to less oxidising conditions (i.e., decreasing concentrations of O_2 and Cu(II)), and the progression of general corrosion into the surface, both of which act against the separation of anodes and cathodes (SKB, 2010a). Consequently, it is anticipated that a measured pitting factor would decrease with increasing time of exposure, consistent with archaeological observations. Currently, SKB makes an allowance for pitting due both residual oxygen and radiolysis of water and are based on empirical measurements of maximum pit sizes as well as probabilistic modelling SKB, 2021).

Empirical extent of surface roughening

Previously, roughening of ±50 µm was applied for copper corrosion due to initially entrapped oxygen (SKB 2010a, b), based on observations by Brennenstuhl et al. (2002) and Litke et al. (1992), but has since been updated to consider mass balance of oxygen plus maximum pit depths to give an allowance of 2.5 mm (SKB 2021). Similarly, in the Canadian system, a corrosion allowance of 100 µm has been assigned to address surface roughening during conditions where the oxygen level is still relatively high (Keech et al. 2020, Scully and Edwards 2013) and is based on arguments supporting the switching of anodic and cathodic regions (Kwong 2011).

Extreme-value statistical analysis

Pitting data generated by (Bresle and Arrhenius, 1983, Hallberg et al. 1984, Romanoff 1989) were analysed by King and Kolář (2000) and King and LeNeveu (1992) and fitted to an extreme-value distribution (Equation 15). Application of these data to a copper canister in the KBS-3 type repository environment led to the prediction of a 10^{-6} chance of a pit exceeding 7.5 mm after 10^{6} years and a 10^{-6} chance of a pit exceeding 5 mm after just 10 years (SKB, 2010a).

$$F(x) = \exp\left[-\exp(-ax + b)\right] \quad (15)$$

An underpinning observation that indicates that long-term prediction of pit depths making use of extreme value statistical analysis (and empirical pitting factors) may not be particularly meaningful is that copper will not passivate under anticipated repository conditions, as passivation is required to cause pitting (King and Lilja, 2014). In the early oxic period where pitting is more feasible, the presence of Cl^- ions tends to promote general active corrosion at near-neutral pH, with passivation occurring more readily in more alkaline solutions with a lower salinity (Briggs et al., 2020; Qin, et al., 2017). In the long-term, corrosion proceeds via the formation of copper sulphide, which has been shown to form porous non-protective films under anticipated repository conditions in Canada, Sweden and Finland (King et al., 2017b).

Comparison of corrosion potential to critical potential for localised corrosion

For copper in neutral conditions, when the oxygen concentration is sufficiently low that hydrogen evolution is the dominant cathodic reaction, the anodic overpotential required to cause pitting is estimated as being approximately 600 mV based on the potential at which copper oxide formation occurs. Pitting of a copper oxide film is expected to occur more readily with increasing chloride concentration, and less favourably with increasing HCO_3^- concentration, due to their destabilising and stabilising influence on passivity, respectively (Drogowska et al., 1992). When sulphide is present, the pitting potential of the protective sulphide film was shown to shift in the negative direction with increasing HS^- concentration (de Chialvo et al., 1985). For copper, in the presence of 0.01M HS^- an anodic overpotential of around 200 mV is assumed necessary to induce pitting corrosion based on corrosion potentials reported in Escobar et al. (1999). Whilst pitting of copper oxides and sulphides has been shown to be possible under certain conditions, the potentials at which such pitting occurs are hundreds of mV more positive than anticipated in repository environments (King et al., 2010).

6.3.1.5 Radiation assisted corrosion

Radiation assisted corrosion is considered separately for the saturated and unsaturated environment as the prevalent corrosion mechanisms in each case are quite different. In unsaturated conditions, the

major corrosion mechanism considered in safety case assessment is that caused by radiolytically produced nitric acid that arises from irradiation of the humid air trapped within the buffer. Once saturation is complete, radiolysis of the anoxic porewater leads to the production of oxidants, primarily H_2O_2, which in high enough concentrations can influence the corrosion rate and shift the corrosion potential in the positive direction (King and Behazin, 2021).

Mass balance of radiolytically produced oxidants

In the unsaturated phase, the influence of radiolytically generated oxidants on the corrosion of copper canisters within a bentonite buffer has been estimated by calculating the radiolytic yield within a given volume around the canister (liquid or gas phase) and assuming the oxidants produced will react with the canister surface to give a bounding value (SKB, 2010b).

This approach is adopted to take account of the formation of nitric acid from gamma irradiation of the humid air present in the canister-buffer gap during the buffer saturation phase. The total amount of nitric acid generated is calculated from the G-value for NHO_3 generation, the total absorbed gamma dose and the irradiated volume (e.g., 1 cm gap around canister) (SKB, 2010b).

Radiolysis of water is considered to form hydrogen and oxidants that will react with the canister material causing corrosion. It is assumed that there exists a volume around the canister in which all radiolytically generated oxidants will reach the canister surface (e.g., 5 mm gap around canister) and that there is a fixed stoichiometric ratio between the moles of oxidant produced and the moles of metal that are corroded uniformly from the surface of the canister (SKB, 2010b). Overall, the effect of radiolysis on the corrosion of copper in the Swedish system (KBS-3 type repository), after taking into account the aforementioned contributions, is around 7 nm (SKB, 2010a, SKB 2021).

In the KBS-3 concept it is assumed that of water radiolysis will contribute ca. 3 µm based on modelling of general corrosion depths and experimental of localised observations corrosion features.

Reasoned argument for exclusion

Intact canisters provide shielding against alpha and beta radiation with only gamma and neutrons penetrating through the walls to cause radiolysis of the porewater and groundwater. Due to the shielding afforded by the canister, the surface radiation dose is greatly attenuated; for the thinner-walled Canadian design the surface dose rate is approximately 1 Gy hr^{-1} (Keech et al. 2020), whereas, for the thicker KBS-3 containers the average surface dose is around 0.055 Gy hr^{-1}. At these dose rates, it is anticipated that there will be no enhancement of the corrosion rate (Pusch et al. 1992, Posiva, 2013). This perspective is supported by the work reported on in the review article by King and Behazin (2021), who compared the general corrosion enhancement by gamma radiation at dose rates from 0-20 Gy hr^{-1} and total absorbed doses from 1,000 to 50,000 Gy. At dose rates relevant to repository conditions (<10 Gy hr^{-1}) there was either no effect, or an inhibiting effect of radiation. At dose rates >10 Gy hr^{-1} there is no consensus within the literature, with some studies showing an enhancement in corrosion and others showing an inhibition of corrosion, when compared to uninhibited rates. These studies also showed that for all dose rates considered there was no consistent effect of increasing cumulative radiation dose.

Of the papers considered by King and Behazin (2021) the only studies that demonstrated an increase in corrosion rate due to gamma radiation were conducted at dose rates considerably greater than those anticipated at a copper canister surface during emplacement within a DGR. Moreover, King and Behazin (2021) draw attention to the mechanistic impacts of radiation dose rate on the corrosion potential, which

supports the suggestion that radiation dose rate is a critical factor in determining the influence of gamma radiation on the corrosion rate of emplaced canisters. Consequently, laboratory studies at dose rates far in excess of 10's Gy hr^{-1} are not expected to accurately simulate the corrosive conditions encountered within a DGR.

6.3.1.6 Microbiologically influenced corrosion

Reasoned argument for exclusion

It has been shown that microbial activity is suppressed in highly compacted bentonite above a certain density due to the low water activity (≤0.96) (Scully and Edwards, 2013), the high swelling pressure and the lack of physical space. In the Swedish SR-Site safety case, microbial activity leading to sulphide production via sulphate reduction was not considered within the intact saturated bentonite buffer whose saturated density exceeds1,850 kg/m^3 (SKB, 2021), based on the findings of Bengtsson et al. (Bengtsson 2017a). In the Finnish safety case for the disposal of spent fuel at Olkiluoto, a bentonite dry density greater than ~1650 kg/m^3 was considered the upper threshold for microbial activity (Posiva, 2013). Consequently, microbial corrosion is generally not considered feasible within the bentonite buffer provided it remains compact and retains its density. Microbial activity is instead considered away from the nearfield (e.g., in the backfill) (Johnson and King 2003, Scully and Edwards 2013, SKB 2010a, Posiva 2013).

Mass transport

Corrosion of copper by microbiologically generated sulphide outside of the nearfield in a KBS-3 repository environment is pessimistically bounded by the supply of nutrients for microbes (SKB, 2010a). The amounts of nutrients available have been estimated in several ways. The backfill contains an abundance of organic matter, but it would be unrealistic to assume the whole inventory is available for dissolution and could be used to produce sulphide that could reach the canister surface within the lifetime of the repository. Bounding calculations based on 1D diffusion of sulphide formed at the same location as the organic matter predict that only a fraction of the sulphide that could be produced would reach the canister surface within 10^6 years. A bounding corrosion loss from sulphide in the backfill is obtained by 1D diffusion modelling using pessimistic values for diffusivity and sulphide concentration (10^{-4} M) and applying the assumption that sulphur transported from the backfill is consumed by corrosion of the top 10% of the canister uniformly and gives a depth of penetration of 2 mm (SKB, 2010b). In the Canadian system a corrosion allowance for microbial activity of 1 mm is considered sufficient provided the buffer remains intact (Scully and Edwards, 2013) (Wolfaardt and Korber, 2012).

The contribution of H_2, generated via anaerobic corrosion of rock bolts and other iron components, to the formation of sulphide via acetogenesis and sulphate reduction has also been considered and bounded for specific repository conditions based on the amounts of steel present (SKB, 2011) if a conservative mass balance approach is adopted that assumes that all of the sulphide produced by acetogenesis reacts with the canister, then an upper bound corrosion loss of 300 µm is obtained (SKB, 2010b).

Empirical rates of sulphide formation

Another method to estimate bounding rates of sulphide production has been based on experimental studies performed in conditions that are more favorable for microbial activity than expected in a repository environment. The rates of copper sulphide production were measured in bentonite at different densities that was supplemented with lactate to act as a source of organic carbon and nutrient (Masurat et al. 2010). Previously, the experimentally determined rates of sulphide production were converted into an equivalent corrosion rate and the wall thickness loss after 10^6 years was extrapolated linearly to give a pessimistic estimation of thickness loss of about 3 mm (SKB, 2010b). This approach has now been revised and considers hydrogen production from corrosion of rock bolts and other iron components, and decomposition of organic material, that could promote sulphide via sulphate reducing bacteria; assuming mass balance against the maximum sulphide that could be produced from these processes the corrosion loss (assuming corrosion on the canister lid and 10 % of the cylindrical surface) would be 4.2 mm (SKB 2021).

6.3.1.7 Environmental-assisted cracking

Reasoned argument for nonsusceptibility

A combination of stress, aggressive ions and oxidising conditions are required for SCC of copper to occur. Even in the early oxic period where temperatures are elevated it is unlikely that sufficient concentrations of aggressive ions would be available within the KBS-3 type repository. There are no mechanistic arguments known that can justify the assumption that cracking of copper could be sustained long-term in the anaerobic phase of the repository environment (SKB, 2010b) (King et al. 2010), (Posiva, 2013).

This argument has been further underpinned by experimentally validated mixed-potential modelling of the anticipated E_{corr} of copper, evaluated over a repository lifetime based on the interfacial chemistry as predicted by reactive transport modelling. Modelling of E_{corr} and the surface pH demonstrated that a CuO_2/CuO surface film is not thermodynamically stable, which is a requirement for the SCC of copper (Maak and King 2006) beyond the initial aerobic period (Posiva, 2013).

In the Canadian concept, SCC is not considered to be likely during the steady state conditions encountered during deep geological disposal. Specifically, the interfacial pH and corrosion potential are expected to be far from the range in which SCC is a feasible corrosion mechanism, given the lack of aggressive species. Certain species, such as ammonia, nitrite ions, acetate and sulphides are known to promote SCC of copper, however, the concentrations in groundwater are below the threshold levels for which they have been shown to promote SCC. It has been acknowledged, that activities such as mining could lead to an increase of such species, however, the increase in SCC susceptibility is somewhat offset by the presence of Cl^-, which reduces the risk of SCC by promoting general corrosion (Kwong, 2011).

The risk of gradual embrittlement of copper by long term anoxic exposure to HS^- at concentrations of around 10^{-4} mol, has been highlighted as a risk to copper canisters (Scully and Edwards, 2013). However, it has also been argued that HS^- transport in bentonite is sufficiently slow that corrosion by sulphide could be transport-limited, resulting in surface or crack tip concentrations approaching zero, assuming that Cu(I) will sequester sulphide by precipitation of CuS_2 (Jacobs and Edwards, 2000). It was similarly concluded that for the KBS-3 concept, the possibility of SCC of copper, even at high sulphide fluxes is not anticipated and even if copper were susceptible to SCC in the presence of sulphide, the sulphide fluxes in the repository environment are not at the level that would be possible to induce SCC (SKB, 2019).

6.3.1.8 *Mechanical degradation and combined corrosion-mechanical effects*

There are a number of modes of mechanical degradation that could potentially affect the integrity of waste containers, specifically fracture, plastic deformation and creep. It is also possible that there could be detrimental interactions between mechanical factors and corrosion processes (figure 15). These issues have been discussed in detail by King et al. (2016). Fracture processes can be sub-divided into brittle fracture, characterised by cleavage or intergranular failure, and ductile fracture, resulting in the typical 'cup and cone' dimpled fracture surface. Brittle fracture is normally caused by some form of embrittlement process, such as radiation embrittlement, solute segregation within the metal or hydrogen embrittlement. Plastic deformation can occur when a metal is overloaded past its yield strength, eventually leading to ductile failure if the load is sufficiently high. This form of failure is avoided in container design by choosing wall thicknesses that are appropriate to the expected loads. If the load tolerance is exceeded, deformation of the container may occur.

Creep involves the slow deformation of a material under the influence of an applied static load below the yield stress. In the case of copper, this problem is ameliorated by the use of oxygen-free, phosphorus doped copper, which has a higher creep ductility.

It is possible that some forms of corrosion may have an effect on the mechanical performance of the container, and vice versa. This includes environmentally assisted cracking, which is considered in the previous section, where the mechanical factors affect the corrosion susceptibility, and conversely corrosion processes such as general corrosion will cause wall thinning, leading to a loss of wall strength and load-bearing capacity, and hence an increased risk of wall deformation or buckling. These interactions have been examined in detail by King et al. (2016) and are summarised in the figure 15. Other corrosion phenomena of note in this context are hydrogen-induced degradation of mechanical properties, since hydrogen may be generated by the anaerobic corrosion of iron, or may be present in the geological environment, and expansive corrosion due to the formation of a corrosion product with a larger volume than the original metal. The latter effect has been examined experimentally by Smart et al. (2003) and by comparison to analogues, such as archaeological artefacts (Smart et al. 2004, 2006b).

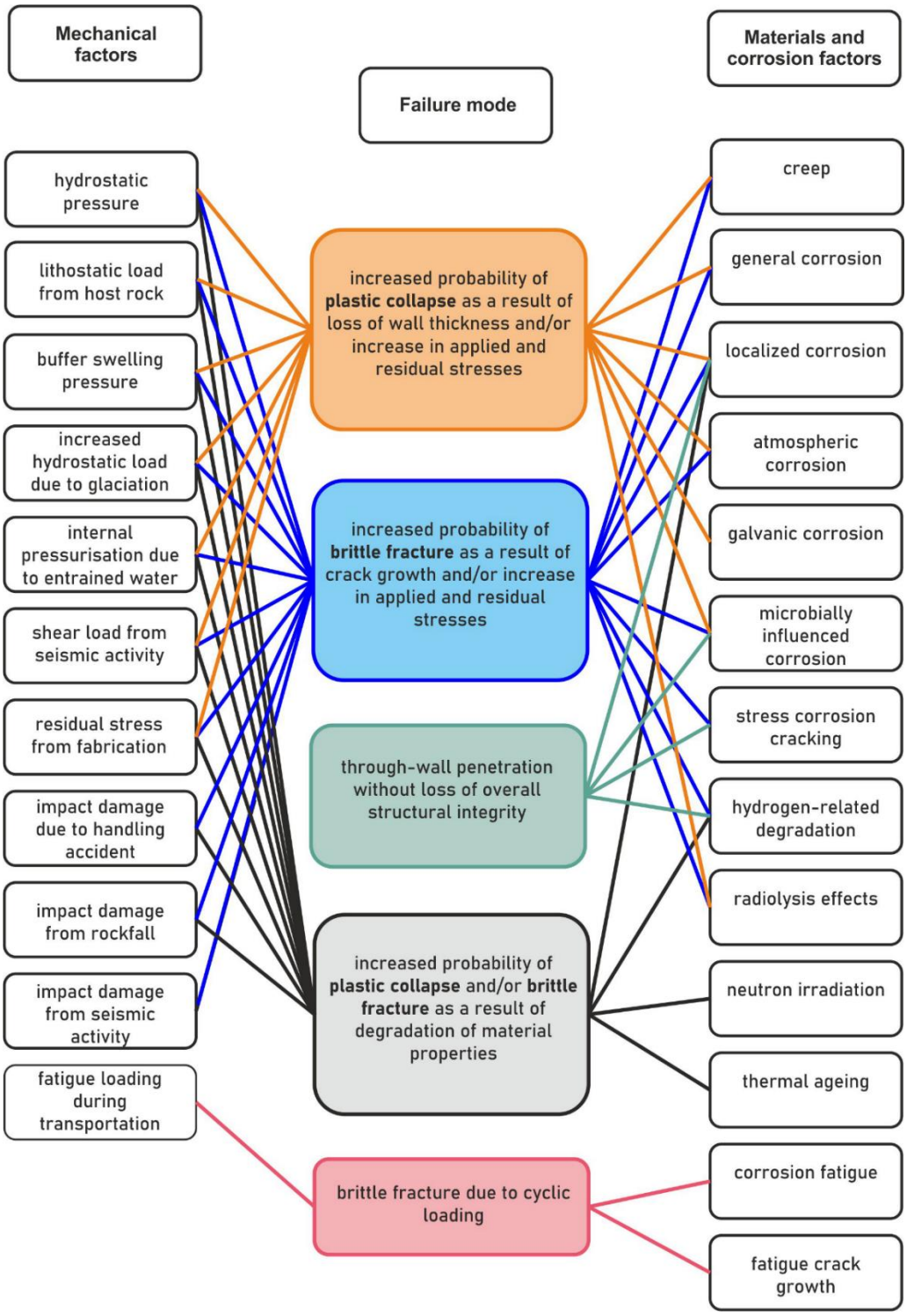

Figure 21: Schematic illustration of the mechanical and material-related factors leading to container failure and their relationship to various failure modes (adapted from King et al. 2016)

6.3.1.9 Prediction of canister lifetimes and implications for PA

At present, the most comprehensive predictions of canister lifetime have been performed for the KBS-3 concept and estimates have been made for the maximum corrosion loss that may be caused by each mechanism over a period of 10^6 years. Several processes give corrosion depths less than 200 µm, and no processes give corrosion depths larger than a few mm. If the estimated contributions from each process are added together, the total loss estimated over 10^6 years is less than 5 mm (SKB, 2010b) (SKB, 2021).

For scenarios involving erosion of the buffer by groundwater flow, the maximum predicted corrosion rates are greater than for any other mechanism considered. However, extremely high rates of corrosion are only estimated when the least favourable conditions are assumed (i.e., maximum flow rate and maximum sulphide concentration). When a statistical analysis is performed that considers the range of possible flow rates and the range of possible sulphide concentrations, the likelihood of a canister failing within 10^6 years can be estimated based on the number of canisters being stored. Application of this methodology estimates that between 0 and 2 canisters would fail within 10^6 once uncertainties are taken into account (SKB, 2010b).

For the Canadian system, a corrosion allowance of 1.27 mm over 10^6 years was described by Kwong (2011) and was based on several assumptions that have since been shown to be highly conservative (Keech et al., 2020). In particular, the corrosion allowance is dominated by sulphide corrosion due to an assumed sulphide concentration of 3 ppm (Kwong, 2011), which has subsequently been shown to be considerably higher than what is expected in Canadian deep subsurface water (Keech et al., 2020).

Erreur ! Source du renvoi introuvable.6 summarises the approaches taken for dealing with the corrosion of copper in performance assessments by various WMOs, according to the various possible corrosion mechanisms for copper.

Confidence in the predictions of longevity of containers can be increased by reference to results from (i) in situ corrosion experiments, where the environmental conditions are close to those expected in the real repository, with the exception of the external radiation dose rates, and the temperature, and (ii) comparison with natural and archaeological analogues (IAEA, 1989, 2005). Natural analogues include geological deposits, for example of native copper deposits (Milodowski, 2000, 2002), which have been found to exist for millions of years, and archaeological artefacts, such as a bronze cannon (King, 1995) and an iron-copper helmet (Smart et al., 2004).

Table 6: Comparison of approaches currently taken to account for different types of corrosion in performance assessments for copper canisters by international waste management organisations (blank cells reflect an absence of information within the public domain).

Mode of corrosion	Canada	Finland	Sweden	Switzerland	United Kingdom
Oxidic general corrosion	Mass balance within corrosion allowance				
Radiolysis-induced corrosion	Excluded or Mass Balance within Corrosion allowance				
Sulphide-induced anaerobic corrosion	Mass transport controlled – key factor driving corrosion allowance				
MIC before buffer saturation		Exclude by reasoned argument			
SCC	Exclude by reasoned argument				
Pitting	Fixed corrosion allowance to account for surface roughening		Fixed corrosion allowance to account for surface roughening		

6.3.2 PA models for steel containers

6.3.2.1 Introduction

Carbon steel has been proposed as a canister material for SF and HLW in several national disposal concepts including the UK (RWM 2016), Belgium (Kursten et al., 2017), France (Andra, 2005), Japan (JNC, 2000) and Switzerland (Patel, et al., 2012). Different WMOs specify different alloys for the canister material but in general, low-strength, low-carbon alloys are favoured. Carbon steel is a desirable canister material as its corrosion mechanisms are well characterized and predictable, based on decades of research, which enables canisters to be designed with suitable corrosion allowances (RWM, 2016). Moreover, due to the extensive use of carbon steel as an engineering material it can be readily sourced and fabricated, and it is considerably cheaper than many alternative canister materials such as copper, nickel alloys, and titanium.

Carbon steel has been considered for use with both bentonite and cementitious buffers as well as crushed rock (RWM, 2016). The high pH environment afforded by a cementitious buffer material supports the formation of a stable passivating magnetite film, which reduces the corrosion rate. However, under repository conditions, anaerobic corrosion of steel (even when passivated) leads to the formation of hydrogen gas, which has the potential to destabilize the surrounding buffer material. There is also concern that the interaction of ferrous ions released by corrosion could adversely alter the characteristics of the surrounding bentonite buffer.

In Switzerland, steel canisters for the disposal of SF and HLW emplaced within a bentonite buffer have a regulatory lifetime requirement of 1,000 years, with the expectation that 10,000 year lifetimes may be readily achieved (Nagra, 2002) and this is the design lifetime. Similarly, complete containment provided by the Belgian Supercontainer concept is expected to endure for at least 5,000 years (for conditions defined within the design reference scenario) although, considerably longer lifetimes are anticipated if long-term corrosion behaviour is governed by the uniform anaerobic corrosion rate (Weetjens et al. 2012). In the Czech concept, the double walled steel canister comprising an inner stainless steel layer surrounded by an outer carbon steel layer is designed to last for a minimum of 10,000 years (Pospiskova et al., 2017), whereas the Japanese concept, which has an inner stainless steel HLW cask surrounded by an outer carbon steel layer (termed an overpack) focuses on a 1,000 year lifetime specification, but it is expected to last considerably longer (NUMO, 2021).

6.3.2.2 Atmospheric corrosion

The atmospheric corrosion behaviour of steel canisters in air is dependent on the relative humidity; below ~60% RH, the corrosion rate can be considered to be extremely low (Nagra 2002). The presence of hygroscopic salt deposits (e.g., NaCl and $CaCl_2$) on the canister surface can influence the relative humidity at which corrosion can occur, depending on the chemical composition of the contaminating salt (Schindleholtz et al. 2014). However, due to the elevated temperature within the buffer close to the container surface, the canister is expected to remain dry even when the outer layers of bentonite begin to saturate (Nagra, 2002). Consequently, in the initial dry period, which is estimated to persist for a few decades, the extent of corrosion is expected to be less than 100 µm (Nagra, 2002) and has been accounted for in an Opalinus clay repository by applying a corrosion allowance of <1 mm (Johnson and King, 2008). This value is in broad agreement with atmospheric corrosion rates reported in RWM (2016), which shows that the atmospheric corrosion of embedded iron in subterranean environments is of the order of a few µm yr^{-1}. It is anticipated that the atmospheric corrosion of iron will generally form iron (hydr)oxides and this is not expected to directly undermine the integrity of the containers significantly in environments of limited corrosivity. However, there is uncertainty regarding the impact that the formation of a layer of rust could have on the corrosion performance a steel container during the long-term post-closure phase (RWM, 2016).

6.3.2.3 General corrosion

Following depletion of oxygen within the repository and a shift to more reducing conditions, the long-term corrosion of emplaced steel canisters is expected to occur as uniform general corrosion under anoxic conditions. In this environment, a corrosion rate of ~1 µm yr^{-1} is anticipated for corrosion occurring in a bentonite buffer (Smart et al. 2011), but there are indications that the rates are even lower if long enough experiments are performed (Diomidis et al., 2023). These rates are within the range reported for natural analogues, which exhibit corrosion rates as low as 0.1 µm yr^{-1} for conditions that are not aerated (Miller et al., 1994). For the Czech concept, uniform anoxic corrosion of the outer carbon steel canister when emplaced in Czech bentonite is assumed to occur at a rate of 5 µm yr^{-1}, based on average corrosion rates determined by mass loss over a 4-month period. However, use of these rates to make lifetime predictions is known to be conservative, as in the same study, comparison of the total corrosion loss of specimens after 2 and 4 months' exposure, implied that the instantaneous corrosion rate after 2 months had reduced to less than 1 µm yr^{-1} (Pospiskova et al., 2017).

For concepts involving a cementitious buffer, such as the Belgian Supercontainer concept, the high pH (>13) cement porewater, that is anticipated to form upon hydration of the buffer, ensures that the steel will passivate by forming a stable magnetite surface film. The passive corrosion rate under these conditions can fall below 0.1 µm yr^{-1} (Weetjens et al. 2012).

In the Japanese disposal concept, the corrosion rate of carbon steel in a bentonite buffer is considered in a range of rock types and groundwater chemistries of varying chloride and carbonate concentration. Based on laboratory testing it was found that corrosion rates dropped after 1 year of exposure and remained linear for several years at rates less than 2 µm yr^{-1}. Based on these observations, an anaerobic general corrosion rate of 2 mm over the 1,000--year design life can be assumed. However, due to the possibility of uneven corrosion, a 6 mm corrosion allowance is applied, based on an assumed pitting factor of 3 (NUMO, 2021).

6.3.2.4 Localized corrosion

Classical pitting corrosion of emplaced steel canisters is only considered to be feasible in the early oxic period. The extent of inhomogeneity in the corrosion of carbon steel was evaluated from the results of long-term field burial tests (JNC, 2000). From these tests, it has been highlighted (Johnson and King 2003) that the pitting was initially characterized by high empirical pitting factors of ~100; however, once general corrosion had reached a depth of ~0.3 mm, pitting factors reduced to ~10. Consequently, a corrosion allowance of 10 mm has been estimated for pitting in the oxic phase of the Swiss disposal concept (Johnson and King, 2003).

The presence of a passivating magnetite film introduces the risk of localized corrosion if breakdown of the film occurs, particularly in a high pH environment, such as a hydrated cementitious buffer. The propensity for pitting was examined using electrochemical measurements for conditions relevant to the Belgian disposal concept (Kursten et al., 2017) and demonstrated that the pitting potential had a strong dependence on chloride concentration (between 0.01M and 1M), with the pitting potential shifted in the active direction at higher chloride concentrations. A similar effect was observed at elevated temperatures, where increasing the temperature from 25°C to 85°C caused a shift in the pitting potential in the active direction. In the most aggressive conditions considered (1M chloride, 85°C), and taking account of statistical variations in the pitting potential, the lowest potential at which pitting was observed was ~+200 mV vs. the corrosion potential.

In the Japanese concept, pitting corrosion during the long-term anoxic phase is excluded due to the combination of near-neutral bentonite pore-water pH, a carbonate concentration of less than 0.5 mol/L

and the absence of strong oxidizing species. However, the non-uniformity of general corrosion is treated with a pitting factor of 3, which considerably increases the level of conservatism in the design. Moreover, treatment of the expected pitting corrosion during the oxic phase by use of a combined mass balance and extreme value statistical analysis approach is also conservative, leading to an allowance of up to 12 mm (NUMO, 2021).

6.3.2.5 Radiation-assisted corrosion

As with the corrosion of copper, radiolysis can lead to the formation of oxidants such as nitric acid, during the unsaturated phase and H_2O_2 during the saturated phase, that can lead to an acceleration of the corrosion rate during the period in which the waste form is still sufficiently radioactive. However, since the corrosion rate of carbon steel is greater than that of copper in repository conditions, due to the spontaneous corrosion of steel in anoxic porewater, the additional oxidation of steel by radiolysis products is small in comparison to the general corrosion loss by water oxidation.

In a series of year-long corrosion tests, Andra investigated the influence of gamma irradiation on the corrosion rate of carbon steel in humid air to simulate conditions arising in the unsaturated phase of a repository. Compared to unirradiated conditions, a gamma dose rate of 80 Gy hr^{-1} was found to increase the corrosion rate, whereas no effect was observed for dose rates of 20 Gy hr^{-1}; hence no influence of radiation is expected at the overpack surface, as the design limits the external surface dose rate to less than 10 Gy hr^{-1} (Crusset et al., 2017).

Gutierrez et al. (2018) consider the influence of radiolysis on corrosion of steel canisters for HLW and SF to be negligible in the saturated phase, owing to the thickness of the canister walls (14 cm), which provide sufficient radiation shielding to attenuate the initial surface gamma dose to ~0.2 Gy hr^{1}, which is significantly below the critical value expected to enhance corrosion (Marsh and Taylor, 1988). Corrosion testing in support of the Czech concept, considers surface dose rates around ten times greater, at around 0.3 Gy hr^{-1} (Pospiskova, et al., 2017), but these are still assumed to be too low to significantly accelerate the corrosion process. Similarly, acceleration of corrosion by gamma radiation is eliminated in the Japanese concept by the use of an 80 mm shielding allowance, which is expected to attenuate the surface dose rate to significantly below the threshold of ~3 Gy hr^{-1}, which is considered to influence corrosion under relevant conditions (NUMO, 2021). Under conditions relevant to the Belgian Supercontainer concept (i.e., young cement water containing thiosulphate, sulphide and chloride at 25 °C and 80 °C), dose rates of up to 25 Gy hr^{-1} had no significant effect on the anaerobic corrosion rate of carbon steel, with rates as low as 0.03 µm yr^{-1} measured by hydrogen gas evolution (Kursten et al., 2017).

6.3.2.6 Microbiologically influenced corrosion

As with copper-bentonite systems, the high bentonite density is expected to reduce microbial activity to the extent where sulphate reduction is negligible. Equally, within a cementitious buffer the high pH of the porewater is also expected to restrict microbiological activity to negligibly low levels such that sulphate reduction is only considered in the far-field (Kursten et al., 2017; Nagra, 2002; NUMO, 2021). Consequently, for an intact buffer, the influence of MIC is only attributable to sulphate reduction in the far-field, leading to a sulphate flux through the buffer to the canister surface. This process is the same as that for a copper-based system, since the flux is determined largely by the microbial activity and the properties of the buffer material (e.g., pH, thickness etc.).

Since the anaerobic corrosion rate of carbon steel is greater than that of copper in repository conditions, steel corrosion losses due to a sulphide flux tend to be less significant compared to general anaerobic corrosion arising from water reduction. As an example, in an Opalinus clay environment, Nagra (Nagra,

2002) consider the extent of corrosion that could occur due to a sulphide flux to the container surface, due to microbiological sulphate reduction from outside the buffer, to lead to ~0.02 mm of corrosion loss over a period of 10^3 years, whereas, the estimated anaerobic corrosion rate due to water reduction over this period is 1 mm (Johnson and King, 2003).

6.3.2.7 Environmentally assisted cracking

SCC at a weld has been evaluated and deemed unlikely based on a range of reported studies (JNC, 2000). Nagra (Nagra, 2002) also consider SCC of welded steel containers to be unlikely owing to the anticipated pH of the bentonite porewater (~7.3), which is outside the range at which SCC of steel in HCO_3^-/CO_3^{2-} occurs (i.e., around pH 10-11 or around pH 6) (Johnson and King 2003). Furthermore, if a crack was able to initiate, its growth is expected to stifle in a repository environment, owing to the absence of cyclic loading (Nagra, 2002).

Cracking of carbon steel by SCC and hydrogen embrittlement is excluded by reasoned argument in the Japanese concept. This is achieved by consideration of the chemical environment, the material properties (e.g., strength of steel) and the expected stress levels. In particular, the use of heat treatments, both on the bulk material and for welds, is expected to largely eliminate tensile residual stresses or reduce them to levels where they are insignificant from an environmental-assisted cracking perspective (NUMO, 2021).

The susceptibility of both plain and welded carbon steel to SCC in high pH (13.6) porewater was investigated for conditions relevant to the Belgian Supercontainer concept. Slow strain rate testing was performed at 140°C in the presence of sulphide concentrations up to 15.6 mM. During testing, the fracture properties of plain carbon steel in the test solution were comparable to that in argon, indicating no susceptibility to SCC. In comparison, welded specimens exhibited a slight reduction in ductility but not to the extent that would constitute a susceptibility to SCC and this was supported by fractographic analysis of the fracture surfaces, which exhibited ductile fracture features. Hence it was concluded that carbon steel is immune to SCC in the conditions tested (Kursten et al., 2017).

The risk of hydrogen embrittlement of carbon steel containers was reviewed in the context of the Swiss concept by Turnbull (2009). This assessment concluded that the risk of hydrogen embrittlement and cracking of the carbon steel canisters was minimal.

6.3.2.8 Weld corrosion

In the Japanese concept, the risk of weld corrosion is accounted for by allowing an additional 3 mm corrosion allowance for welded regions, to account for the possibility of undetected welding defects of up to 3 mm in depth. Preferential weld corrosion is also considered and is mitigated by the use of Ni doping of the weld material.

6.3.2.9 Prediction of canister lifetimes and implications for PA

Steel canisters are designed with conservative lifetimes of 1,000 to 10,000 years, which is considerably shorter than for copper canisters owing to continuous corrosion during anoxic conditions of the order of <0.1 µm yr^{-1} for cementitious alkaline conditions or 1-2 µm yr^{-1} for carbon steel in bentonite (Nagra 2002, Kursten et al. 2017, NUMO 2021). However, due to the level of conservativism adopted, it is expected that actual canister lifetimes will far exceed the design life. For example, in the Japanese concept, the overpack is expected to last in excess of 17,000 years, which is far beyond the design life.

Erreur ! Source du renvoi introuvable.7 summarises the approaches taken for dealing with the corrosion of iron-based canisters in PAs by various WMOs, according to the various possible corrosion mechanisms for steel.

Table 7: Comparison of approaches currently taken to account for various different types of corrosion in performance assessments for iron-based canisters by international waste management organisations (blank cells reflect an absence of information within the public domain).

Mode of corrosion	France	Belgium	Switzerland	Japan	United Kingdom	Czech republic
Anaerobic general corrosion	Empirical corrosion rate		Empirical corrosion rate and pitting factor		Empirical corrosion rate	
Radiolysis-induced corrosion	Limit dose rate to 10 Gy hr^{-1}.	No effect for dose rate of 25 Gy hr^{-1}.	Design requirement (<1 Gy hr^{-1})	Limit dose rate to 3 Gy hr^{-1}		
Localised corrosion		Reasoned argument based on passivity of surface film	Depth-dependent pitting factor	Mass balance and extreme value statistical analysis		
SCC	Specify resistant material	Exclude by reasoned argument				
MIC			Corrosion allowance based on mass transport	Excluded by reasoned argument – negligible rate		

Summary and Conclusions

ConCorD (Container Corrosion under Disposal conditions) is one of the work packages of the European Joint Programme on Radioactive Waste Management (EURAD). Its main aims are:

- to assess the corrosion mechanisms of traditional container materials (i.e. carbon steel and copper) in complex disposal scenarios where the corroding environment is under the influence of irradiation, temporal changes of the near-field environment, or microbial activity,
- to assess the potential of novel materials for optimisation of the container performance, and
- to integrate experimental evidence on container degradation into the prediction of container corrosion and lifetime assessment.

The state of the art on these research targets has been summarised as a basis for the development of the ConCorD research activities.

External γ-radiation fields for HLW/SF containers are modest with a maximum of a few Gy hr^{-1} or lower, although the total accumulated dose over the lifetime of the container can be several MGy. Past work on the effects radiation-induced corrosion indicates that the maximum additional wall loss due to radiation is of the order of a few tens of μm, although it is unclear whether predictions of the corrosion allowance should be based on the dose rate or the total dose. Furthermore, relatively few studies of the effects of radiation in representative systems, including the presence of compacted buffer material and of unsaturated (atmospheric) conditions, have been conducted.

For the first few thousand years following emplacement, the container will be exposed to an evolving near-field environment. In addition to the time-dependent decay of the external radiation field, the container will also be subject to a thermal transient, the evolution of redox conditions as the initially trapped atmospheric O_2 is consumed, and a saturation transient which affects both the availability of H_2O to support corrosion as well as the external load applied to the container. In turn, the buffer porewater composition and the extent of microbial activity will also change over time. Although the effects of some of these time-dependent environmental conditions have been studied, the work in ConCorD seeks to examine the combined effects of the early transient behaviour.

Near-field microbial activity can produce metabolic by-products, such as sulphide, that can lead to corrosion of the container. Although it has been known for some time that microbial activity is suppressed in compacted bentonite buffer material, the underlying physiological cause is uncertain. The activity of anaerobes, such as sulphate-reducing bacteria, may also be suppressed by the presence of residual oxygen “trapped” in the bentonite. Temperature and irradiation may affect the viability and survivability of various microbial species.

Of the various candidate container materials, most attention has been paid to the performance of copper and steel. ConCorD shed light on a set of conditions for alternative copper grades under repository conditions, showing promising results for high conductivity phosphorous copper (HCP-Cu) and set future studies on thresholds related either to the chemical environment, mechanical loading, or material state of the final disposal canister. However, there is a wide range of other materials, both metallic and non-metallic, that exhibit certain advantages and disadvantages as container materials. Ceramics have been considered in several international programmes, and work within ConCorD determines the long-standing issue of joining such materials at sufficiently low temperatures so that the waste inside the container is not thermally damaged. Both, ceramic and metallic coatings, may offer a cost-effective solution as a corrosion barrier. With the exception of copper coatings, however, the development of coated container solutions is relatively immature. The optimisation of existing container designs is also

an area of ongoing study, such as the investigation of commercial grades of phosphorus-containing copper as an alternative to the custom grade currently specified for the KBS-3 container.

The outcomes of research in the different areas discussed above, and other areas, are ultimately incorporated into the safety case and, specifically, used to support container lifetime predictions. Such information may be used directly in the development and validation of predictive models, either process models focused on specific corrosion processes or performance assessment models aimed at predicting the container performance under repository conditions. A range of process and performance assessment models have been developed for both copper and carbon steel containers. Alternatively, the research outcomes may be used more generally as part of the safety case documentation to demonstrate a sound mechanistic understanding of the corrosion processes to which the container will, and will not, be subject. An important component of the ConCorD project is the implementation of the results of the different experimental activities to improve the overall modelling and lifetime prediction of HLW/SF containers.

References

Abrahamsen, L., T. Arnold, H. Brinkmann, N. Leys, M. Merroun, K. Mijnendonckx, Moll, H., Polvika, P., Ševců, A., Small, J. Vikman, M., Wouters, K., 2015. A Review of Anthropogenic Organic Wastes and Their Degradation Behaviour, Deliverable 1.1, MIND, European Commission.

Adams, J., Cowgill, M., Moskowitz, P., Rokhvarger, A.E., 2000, Effect of radiation on spinel ceramics for permanent containers for nuclear waste transportation and storage. BNL Report BNL-67518, Brookhaven National Laboratory, Upton NY.

Ahmad, Z., 2006. Principles of Corrosion Engineering and Corrosion Control. Butterworth-Heinemann, p. 672

Ahn, T.M., Soo, P. 1995. Corrosion of Low-Carbon Cast Steel in Concentrated Synthetic Groundwater at 80 to 150°C. Waste Management 15: 471–76.

Alkhimov, A.P., Kosarev, V.F., Klinkov, S.V., Sova, A.A., 2012a. Effect of a conical separation region on cold gas-dynamic spraying. Journal of Applied Mechanics and Technical Physics 53: 948-953.

Alkhimov, A.P., Kosarev, V.F., Klinkov, S.V., Sova, A.A., Trubacheev, G.V. 2012b. Conical separation zone formation at impingement of supersonic jet on obstacle under cold spraying. Thermophysics and Aeromechanics 19: 225-232.

Amendola R, Acharjee A. Microbiologically Influenced Corrosion of Copper and Its Alloys in Anaerobic Aqueous Environments: A Review. Front Microbiol. 2022 Apr 4;13:806688. doi: 10.3389/fmicb.2022.806688.

Andersson, C.-G., et al. 2004. SKB TR-04-23 - Status report, canister fabrication. SKB, p. 96.

Andra 2005. Dossier 2005 Argile - Phenomenological evolution of a geological repository.

Appelo, C. A. J. 2013. A review of porosity and diffusion in bentonite. Working Report 2013-29, Posiva Oy, Finland.

Arcos, D., Cuevas, J., Fernández, A.M., Herbert, H.-J., Hernan, P., Van Loon, L. Martin, P.L., Savage, D., Smart, N., Villar, M.V. 2008. Key Processes affecting the Chemical Evolution of the Engineered Barrier System. Conference proceedings Euradwaste'08. 7th European Commission conference on the management and disposal of radioactive waste.

Arcos, D., Hernán, P., de la Cruz, B., Herbert, H.-J., Savage, D., Smart, N.R., Villar, M.V., Van Loon L.R. 2005. NF-PRO: Understanding and physical and numerical modelling of the key processes in the nearfield and their coupling for different host rocks and repository strategies, EDZ development and evolution. RTDC-2 Synthesis report, EC integrated project NF-PRO Deliverable D-No:2.6.4.

Aurubis, 2022. Finland Oy - Download Center, datasheets 2022, available/ link: Download Center - Aurubis Finland Oy).

Bagnoud, A., et al. 2016. A minimalistic microbial food web in an excavated deep subsurface clay rock. FEMS microbiology ecology 92: fiv138. https://doi.org/10.1093/femsec/fiv138

Bamoulid, L., et al. 2008. An efficient protection of stainless steel against corrosion: Combination of a conversion layer and titanium dioxide deposit. Surf. Coat. Technol. 202: 5020-5026.

Baroux, C., Martin, C. 2016. Summary Report of the preliminary feasibility study for ceramic HLW overpacks. Andra Report CG.RP.ASCM.13.0023.

Bataillon, C., Bouchon F., Chainais-Hillairet C., Fuhrmann J., Hoarau E., Touzani R. (2012): Numerical methods for the simulation of a corrosion model with moving oxide layer. Journal of Computational Physics, 231(18): 6213-6231.

Bataillon, C., F. Bouchon, C. Chainais-Hillairet, C. Desgranges, E. Hoarau, F. Martin, M. Tupin, J. Talandier (2010): Corrosion modelling of iron based alloy in nuclear waste repository. Electrochimica Acta, 55(15), 4451-4467.

Beese-Vasbender, P.F., Nayak, S., Erbe, A., Stratmann, M., Mayrhofer, K.J.J. 2015. Electrochemical characterization of direct electron uptake in electrical microbially influenced corrosion of iron by the lithoautotrophic SRB Desulfopila corrodens strain IS4. Electrochim. Acta 167: 321-329.

Belous, V.A. et al. 2013. Development of ion-plasma technology of deposition of the nanostructure bactericidal coatings on orthopaedic implants and fixative devices. Production of pilot samples for verification of their use in clinic. Science and Innovation 9: 46-60. ISSN 1815-2066.

Belous, V.A., Lunyov, V.M., Kuprin, A.S., Bortnitskaya, M.A. 2018. Structure and properties of TiOx and TiNxOy coatings formed in vacuum arc plasma fluxes. Probl. At. Sci. Technol. 118: 297-299.

Ben Lagha, S., Crusset, D., Mabille, I., Tran, M., Bernard, M.C., Sutter, E. 2007. Corrosion of iron: A study for radioactive waste canisters. J. Nucl. Mater. 362: 485-492.

Bengtsson, A., Blom, A., Hallbeck, B., Heed, C., Johansson, L., Stalén, J., Pedersen, K., 2017a. Microbial sulphide-producing activity in water saturated MX-80, Asha and Calcigel bentonite at wet densities from 1 500 to 2000 kg m−3. SKB TR-16-09, SKB, Sweden.

Bengtsson, A., Blom, A., Taborowski, T., Schippers, A., Edlund, J., Kalinowski, B., Pedersen, K., 2017b. FEBEX-DP: Microbiological Report. NAB 16-015, Nagra, Switzerland.

Bengtsson, A., Pedersen, K. 2017. Microbial sulphide-producing activity in water saturated Wyoming MX-80, Asha and Calcigel bentonites at wet densities from 1500 to 2000 kgm^{-3}. Appl. Clay Sci. 137: 203-212.

Bessho et al. 2015. Corrosion of copper in water and colloid formation under intense radiation field. J. Radioanal. Nucl. Chem. 303: 1117-1121.

Bevas C., Hesketh J., Rance A., Stevenson L.-A., Uthayakumaran S., Pateman B., Padovani C., Šachlová Š., Kašpar V., Dobrev D., Götz D., Kolomá K., Večerník P. 2024. Elucidation of the effect of radiation on the corrosion of canister materials. Final version as of 02/02/2024 of deliverable D15.7 of the HORIZON 2020 project EURAD. EC Grant agreement no: 847593.

Bienek, H., Finkbeiner, R., Wick, W. 1984. Container closure means for storage of radioactive material. US Patent 4,437,578, March 1984.

Bildstein O., Lartigue J., Pointeau I., Cochepin B., Munier I., Michau N. (2012): Chemical evolution in the near field of HLW cells: interactions between glass, steel and clay-stone in deep geological conditions. 5th ANDRA International Meeting, 22–25 Oct 2012, Montpellier, France

Bildstein, O., Trotignon, L., Perronnet, M., Jullien, M. 2006. Modelling iron–clay interactions in deep geological disposal conditions. Phys. Chem. Earth 31: 618–625.

Birgersson, M., Karnland, O. 2009. Ion equilibrium between montmorillonite interlayer space and an external solution – Consequences for diffusional transport. Geochim. Cosmochim. Acta 73: 1908–1923.

Björkbacka, A., Hosseinpour, S., Johnson, M., Leygraf, C., Jonsson, M. 2013. Radiation induced corrosion of copper for spent nuclear fuel storage. Radiat. Phys. Chem. 92: 80-86.

Björkbacka, Å., Hosseinpour, S., Leygraf, C., Jonsson, M. 2012. Radiation Induced Corrosion of Copper in Anoxic Aqueous Solution. Electrochem. Solid-State Lett. 15: C5-C6.

Björkbacka, Å., Johnson, C.M., Leygraf, C., Jonsson, M. 2016. Role of the oxide layer in radiation-induced corrosion of copper in anoxic water. J. Phys. Chem. C 120: 11450-11455.

Björkbacka, A., Johnson, C.M., Leygraf, C., Jonsson, M. 2017. Radiation induced corrosion of copper in humid air and argon atmospheres. J. Electrochem. Soc. 164: C201-C206.

Björkbacka, A., Yang, M., Gasparrini, C., Leygraf, C., Jonsson, M. 2015. Kinetics and mechanisms of reactions between H_2O_2 and copper and copper oxides. Dalton Trans. 44: 16045-16051

Boyle, C.H., Meguid, S.A., 2015. Mechanical performance of integrally bonded copper coatings for the long-term disposal of used nuclear fuel. Nucl. Eng. Des. 293: 403-412.

Bradbury, M.H., Baeyens, B., 2002. Porewater chemistry in compacted re-saturated MX-80 bentonite: physico-chemical characterisation and geochemical modelling. PSI Bericht 02–10, Villigen PSI and NTB 01–08, Nagra, Wettingen, Switzerland.Braithwaite, J.W., Magnani, N.J.,Munford, J.W. 1980. Titanium alloy corrosion in nuclear waste environments. NACE CONF-800305, p. SAND-79-2023C.

Brandberg, F., Skagius, K. 1991. Porosity, sorption, and diffusivity data compiled for the SKB 91 study. TR 91-16, SKB, Sweden.

Brehm, W.F. 1990. Corrosion of Ferrous Materials in a Basaltic Environment, in Workshop on corrosion of nuclear fuel waste containers, AECL-10121, 227-233.

Brennenstuhl, A.M., McBride, A., Ramamurthy, S., Davidson, R. 2002. The effects of microstructural and environmental factors on underdeposit corrosion of oxygen-free phosphorous-doped copper. Report 06819-REP-01200-10079-R00, Ontario Power Generation, Nuclear Waste Management.

Bresle, S.Å., Arrhenius, B. 1983. Studies in pitting corrosion on archaeological bronzes. Copper. SKB TR 83-05. Svensk Kärnbränslehantering AB.

Briggs, S., Lilja, C., King, F. 2020. Probabilistic model for pitting of copper canisters. Mater. Corros. 72: 308-316.

Briggs, S., McKelvie, J., Keech, P., Sleep, B., Krol, M. 2017. Transient modelling of sulphide diffusion under conditions typical of a deep geological repository. Corros. Eng. Sci. Technol. 52: 200-203.

Brown, A.R., Boothman, C., Pimblott, S.M., Lloyd, J.R. 2015. The Impact of Gamma Radiation on Sediment Microbial Processes. Appl. Environ. Microbiol. 81: 4014-4025.

Burzan, N., 2021. Growth and viability of microorganisms in bentonite and their potential activity in deep geological repository environments, PhD Thesis, École Polytechnique Fédérale de Lausanne EPFL, Lausanne.

Burzan, N., Lima, R.M., Frutschi, M., Janowczyk, A., Reddy, B., Rance, A., Diomidis, N., Bernier-Latmani R. (2022). Growth and persistence of an aerobic microbial community in Wyoming bentonite MX-80 despite anoxic in situ conditions. Frontiers in Microbiology 13 Article 858324, doi: 10.3389/fmicb.2022.858324

Burzan, N., Murad Lima, R., Frutschi, M., Janowczyk, A., Reddy, B., Rance, A., Diomidis, N., Bernier-Latmani, R. 2022. Growth and persistence of an aerobic microbial community in Wyoming bentonite MX-80 despite anoxic in situ conditions. Frontiers in Microbiology 13: 1–12. https://doi.org/10.3389/fmicb.2022.858324.

Carlson, L., Karnland, O., Olsson, S., Rance, A., Smart, N. 2006. Experimental studies on the interactions between anaerobically corroding iron and bentonite. Posiva Working Report 2006-06. Posiva.

Carlsson, T., Muurinen, A. 2008. A Practical and Theoretical Basis for Performing Redox-measurements in compacted Bentonite _ A Literature Survey. Posiva Working Report 2008-51. Posiva, Eurajoki, Finland.

Cedeno-Vente, M.L. et al. 2021. Application of a transmission line model to evaluate the influence of structural defects on the corrosion behavior of arc-PVD CrN coatings. Ceram. Int. 47: 20885-20899.

Černá, K., Bartak, D.S., 2019. State of art – attachment I to the Work report 2019, Project Limiting Factors for survivability and proliferation of microorganisms significant for corrosion of deep geological repository barrier systems (BioBen) Project number: TAČR TK02010169.

Černá, K., Černoušek, T., Polívka, P., Ševců, A., Steinová, J. 2019. MIND Deliverable 2.15: Survival of microorganisms in bentonite subjected to different levels of irradiation and pressure.

Červinka, R. Klajmon, M., Zeman, J., Vencelides, Z. 2018. The geochemical evolution of DGR/preparation of geochemical model-geochemical calculations and reactive transport modelling, Technical report 271/2018/ENG, SURAO, ÚJV Řež, a. s. Prague.

Červinka, R., Vašíček, R., a kolektiv 2018. Kompletní charakterizace bentonitu. BCV 2017, SÚRAO TZ 419/2019.

Chainais-Hillairet, C. and Gallouët, T.O. (2016). Study of a pseudo-stationary state for a corrosion model: existence and numerical approximation. Nonlinear Analysis: Real World Applications, 31, pp.38-56.

Chainais-Hillairet, C., Colin, P.-L., Lacroix-Violet, I. (2015): Convergence of a finite volume scheme for a corrosion model. Int. J. Finite, 12: 1-27.

Chaparro C., Finck,, Metz V., Geckeis, H (2021) Reactive Transport Modelling of the Long-Term Interaction between Carbon Steel and MX-80 Bentonite at 25 °C. Minerals, 11

Chapon, V., Piette, L., Vesvres, M.-H., Coppin, F., Marrec, C.L., Christen, R., Theodorakopoulos, N., Février, L., Levchuk, S., Martin-Garin, A., Berthomieu, C., Sergeant, C. 2012. Microbial diversity in contaminated soils along the T22 trench of the Chernobyl experimental platform. Appl. Geochem. 27: 1375-1383.

Chatterjee, M. et al. 2021. Proteomic study of Desulfovibrio ferrophilus IS5 reveals overexpressed extracellular multi-heme cytochrome associated with severe microbiologically influenced corrosion. Sci. Rep. 11: 15458.

Chen, J., Qin, Z., Shoesmith, D.W. 2010. Kinetics of corrosion film growth on copper in neutral chloride solutions containing small concentrations of sulfide. J. Electrochem. Soc. 157: C338-C345.

Cheptsov V.S., Vorobyova, E.A., Gorlenko, M.V., Manucharova, N.A., Pavlov, A.K., Lomasov, V.N. 2018. Effect of gamma radiation on viability of a soil microbial community under conditions of Mars. Paleontol. J. 52: 1217-1223.

Christensen, Th.H., Bjerg, P.L., Banwart, S.A., Jakobsen, R., Heron, G., Albrechtsen, H.-J. 2000. Characterization of redox conditions in groundwater contaminant plumes. Journal of Contaminant Hydrology 45, Iss. 3–4, 165-241.

Clark, D.E., Sutton, W.H. 1996. Microwave Processing of Materials. Ann. Rev. Mater. Sci. 26: 299-331.

Cloet, V., Pekala, M., Smith, P., Wersin, P., Diomidis, N. 2017. An evaluation of sulphide fluxes in the nearfield of a HLW repository. Technical Report 17-04, Nagra, Switzerland

COMSOL, 2020. COMSOL Multiphysics® v. 5.6. COMSOL AB, Sweden.

Costello, J.A. 1974. Cathodic depolarization by sulfate-reducing bacteria. S. Afr. J. Sci. 70: 202-204.

Couture, R.A. 1985. Steam rapidly reduces the swelling capacity of bentonite. Nature 318: 50-52.

Crusset, D., Deydier,V., Necib, S., Gras, J.-M., Combrade, P., Féron, D., Burger, E. 2017. Corrosion of Carbon Steel Components in the French High-Level Waste Programme: Evolution of Disposal Concept and Selection of Materials. Corros. Eng. Sci. Technol. 52: 17–24. doi: 10.1080/1478422X.2017.1344416.

Čuba, V., Silber, R., Múčka, V., Pospíšil, M., Neufuss, S., Bárta, J., Vokál, A. 2011. Radiolytic Formation of Ferrous and Ferric Ions in Carbon Steel – Deaerated Water System. Radiat. Phys. Chem. 80: 440–45. doi: 10.1016/j.radphyschem.2010.09.012.

Cuevas, J., Villar, M., Fernández, A., Gomez, P., Martín, P. 1997. Pore waters extracted from compacted bentonite subjected to simultaneous heating and hydration. Appl. Geochem. 12: 473-481.

Curti, E. (2011): Comparison of bentonite pore water calculations carried out with conventional and novel models. PSI Internal Report AN-44-11-18. Paul Scherrer Institute, Villigen, Switzerland.

Dadachova, E., Casadevall, A. 2008. Ionizing radiation: how fungi cope, adapt, and exploit with the help of melanin. Curr. Opin. Microbiol. 11: 525-531.

Daly, M.J. 2009. A new perspective on radiation resistance based on *Deinococcus radiodurans*. Nat. Rev. Microbiol. 7: 237-245.

Daly, M.J. et al. 2007. Protein Oxidation Implicated as the Primary Determinant of Bacterial Radioresistance. PLOS Biology 5: e92.

Dante, J.F., Kelly, R.G. 1993. The Evolution of the Adsorbed Solution Layer during Atmospheric Corrosion and Its Effects on the Corrosion Rate of Copper. J. Electrochem. Soc. 140: 1890.

Daub, K., Van Nieuwenhove, R., Nordin, H. 2015. Investigation of the impact of coatings on corrosion and hydrogen uptake of Zircaloy-4. J. Nucl. Mater. 467: 260-270.

Daub, K., Zhang, X., Noël, J.J., Wren, J.C. 2010. Effects of γ-Radiation versus H_2O_2 on Carbon Steel Corrosion. Electrochim. Acta 55: 2767–2776. doi: 10.1016/j.electacta.2009.12.028.

Daub, K., Zhang, X., Noël, J.J., Wren, J.C. 2019. Gamma Radiation-Induced Carbon Steel Corrosion. ECS Trans. 33:15–24. doi: 10.1149/1.3557748.

Daub, K., Zhang, X., Noël, J.J., Wren, J.C.. 2011. Gamma-Radiation-Induced Corrosion of Carbon Steel in Neutral and Mildly Basic Water at 150°C. Corros. Sci. 53: 11–16. doi: 10.1016/j.corsci.2010.09.048.

de Chialvo, M.R., Salvarezza, R.C., Vasquez, M.D., Arvia, A.J. 1985. Kinetics of passivation and pitting corrosion of polycrystalline copper in borate buffer solutions containing sodium chloride. Electrochim. Acta 30: 1501-1511.

De Combarieu, G., Barboux, P., Minet, Y. 2007. Iron corrosion in Callovo-Oxfordian argilite: From experiments to thermodynamic/kinetic modelling. – Physics and Chemistry of the Earth, 32, 346–358.

De Windt L., Miron G.D., Fabian M., Goethals, J., Wittebroodt C. 2020. First results on the thermodynamic databases and reactive transport models for steel-cement interfaces at high temperature. Final version of deliverable D2.8 of the HORIZON 2020 project EURAD. EC Grant agreement no: 847593.

Debruyn, W. 1988. Corrosion of Container Materials under Clay Repository Conditions. Proceedings of a workshop on corrosion of nuclear fuel waste containers 148: 148–162.

Deck, C.P., Khalifa, H.E., Shapovalov, K.S. 2018. SiC-SiC Composite Cladding Development for Accident Tolerant Fuel. Trans. Am. Nucl. Soc. 118: 1305-1308.

Deissmann G., Ait Mouheb, N., Martin, C., Turrero, M.J., Torres, E., Kursten, B., Weetjens, E., Jacques, D., Cuevas, J., Samper, J., Montenegro, L., Leivo, M., Somervuori, M., Carpen, L. 2021. Experiments and numerical model studies on interfaces. Final version as of 12.05.2021 of deliverable D2.5 of the HORIZON 2020 project EURAD. EC Grant agreement no: 847593.

Delage, P. (2010). A microstructure approach to the sensitivity and compressibility of some Eastern Canada sensitive clays. Géotechnique 60, No. 5, 353–68,https://doi.org/10.1680/geot.2010.60.5.353.

Diler, E. et al. 2021. Potential influence of microorganisms on the corrosion of carbon steel in the French high- and intermediate-level long-lived radioactive waste disposal context. Mater. Corros. 72: 218-234.

Diomidis N., Johnson, L.H. 2014. Materials options and corrosion-related considerations in the design of spent fuel and high-level waste disposal canisters for a deep geological repository in Opalinus clay. JOM. 66:461–470.

Diomidis, N., Cloet, V., Leupin, O., Marschall, P., Poller, A., Stein, M., 2016. Production, consumption and transport of gases in deep geological repositories according to the Swiss disposal concept. Nagra Technical Report NTB 16-03. Nagra, Wettingen, Switzerland.

Diomidis, N., Guillemot, T., King, F. 2023. Definition of reference corrosion rates for performance and safety assessments. Nagra Working Report NAB 23-22. Nagra, Wettingen, Switzerland.

Drogowska, M., Brossard, L., Ménard, H. 1992. Copper dissolution in $NaHCO_3$ and $NaHCO_3$ + NaCl aqueous solutions at pH 8. J. Electrochem. Soc. 139: 39-47.

Duro, L., Bruno, J., Grivé, M., Montoya, V., Kienzler, B., Altmaier, M., Buckau, G. 2014. Redox processes in the safety case of deep geological repositories of radioactive wastes. Contribution of the European RECOSY Collaborative Project. Appl. Geochem. 49: 206-217.

Ekeroth, E., Roth, O., Jonsson, M. 2006. The relative impact of radiolysis products in radiation induced oxidative dissolution of UO_2. J. Nucl. Mater. 355: 38-46.

El Hajj, H., Abdelouas, A., El Mendili, Y., Karakurt, G., Grambow, B., Martin, C. 2013. Corrosion of carbon steel under sequential aerobic-anaerobic environmental conditions. Corros. Sci. 76: 432-440.

El Mendili, Y., Abdelouas, A., Karakurt, G., Ait Chaou, A., Essehli, R., Bardeau, J.-F., Grenèche, J.-M., 2015. The effect of temperature on carbon steel corrosion under geological conditions. Appl. Geochem. 52: 76-85.

Enning, D. et al. 2012. Marine sulfate-reducing bacteria cause serious corrosion of iron under electroconductive biogenic mineral crust. Environ. Microbiol. 14: 1772-1787.

Enning, D., Garrelfs, J. 2014. Corrosion of Iron by Sulphate-Reducing Bacteria: New Views of an Old Problem. Appl. Environ. Microbiol. 80: 1226-1236.

Esbelin, J., Santos, T., Hébraud, M. 2018. Desiccation: An environmental and food industry stress that bacteria commonly face. Food Microbiol. 69: 82-88.

Escobar, I S, E Silva, C Silva, and A Ubal. 1999. Study of the effect of sulphide ions on the corrosion resistance of copper for use in containers for high-level waste. Proceedings of 4th International Conference Copper 99 – Cobre 99. Vol. I. Warrendale, PA. Minerals, Metals, and Materials Society: 371–386.

Fernández, A.M, Baeyens, B., Bradbury, M. and Rivas, P. 2004. Analysis of the porewater chemical composition of a Spanish compacted bentonite used in an engineered barrier. Phys. Chem. Earth 29: 105-119.

Fernández, A.M. 2019. Gas and water sampling from the FEBEX in situ test. Nagra Working Reports. NAB 16-13, 155 pp. NAGRA Technical Report.

Fernández, A.M. 2019. Geochemical outcomes of the dismantling of the engineered barrier emplacement (EB) experiment at Mont Terri (Switzerland). Informes Técnicos CIEMAT. 1469, 133. CIEMAT, 22/12/2019. ISSN 1135-9420.

Fernández, A.M., Marco, J.F., Nieto, P., León, F.J., Robredo, L.M., Clavero, M.A., Cardona, A., Fernández, S., Svensson, D., Sellin, P. 2022. Characterization of Bentonites from the in situ ABM5

Heater Experiment at Äspö Hard Rock Laboratory, Sweden. Minerals 12: 471. https://doi.org/10.3390/min12040471.

Fernandez, A.M., Rivas, P. 2005. Porewater chemistry of saturated FEBEX bentonite compacted at different densities. Advances in Understanding Engineered Barriers. Alonso & Ledesma (eds). Taylor and Francis Group, London. Pp. 505- 514, ISBN 04-1536-544-9.

Fernández, A.M., Villar, M.V. 2010. Geochemical behaviour of a bentonite barrier: results up to 8 years of thermo-hydraulic treatment in the laboratory. Appl. Geochem. 25: 809-824.

Fernández, A.M.; Sánchez-Ledesma, D.M.; Melón, A.; Robredo, L.M.; Rey, J.J.; Labajo, M.; Clavero, M.A.; Fernández, S.; González, A.E. 2018. Thermo-hydro-chemical (THC) behaviour of a Spanish Bentonite after dismantling Heater#1 and Heater#2 of the FEBEX in situ test at the Grimsel Test Site. Nagra Working Reports. NAB 16-25, 583 pp. NAGRA, 2018.

Fernandez, R., Jodoin, B. 2018. Cold Spray Aluminum–Alumina Cermet Coatings: Effect of Alumina Content, J. Therm. Spray Technol., 27, 603-623.

Féron, D., Crusset, D. 2014. Microbial induced corrosion in French concept of nuclear waste underground disposal. Corros. Eng. Sci. Technol. 49: 540-547.

Finsterle, S., Muller, R.A., Baltzer, R., Payer, P., Rector, J.W. 2019. Thermal Evolution near Heat-Generating Nuclear Waste Canisters Disposed in Horizontal Drillholes. Energies 12: 596.

Fredrickson, J.K. et al. 1997. Pore-size constraints on the activity and survival of subsurface bacteria in a late cretaceous shale-sandstone sequence, northwestern New Mexico. Geomicrobiol. J. 14: 183-202.

Gens, A.; Sánchez, M.; Guimarães, L.; Alonso, A.A.; Loret, A.; Olivella, S.; Villar, M.V.; Huertas, F.A. 2009. Full-scale in situ heating test for high-level nuclear waste disposal: Observations, analysis and interpretation. Géotechnique 59: 377–399.

Gérard, F., Clement, A. and Fritz, B., 1998. Numerical validation of a Eulerian hydrochemical code using a 1D multisolute mass transport system involving heterogeneous kinetically controlled reactions. Journal of Contaminant Hydrology, 30(3-4), pp.201-216.

Gimmi, T., Alt-Epping, P. 2018. Simulating Donnan equilibria based on the Nernst-Planck equation. Geochim. Cosmochim. Acta 232: 1–13.

Giroud, N. 2014. FEBEX - Assessment of Redox Conditions in Phase 2 before Dismantling. Technical Report NAB 14-55, Nagra, Switzerland.

Giroud, N., Tomonaga, Y., Wersin, P., Briggs, S., King, F., Vogt, T., Diomidis, N. 2018. On the fate of oxygen in a spent fuel emplacement drift in Opalinus Clay. Applied Geochemistry 97, 270-278.

Grandia, F., Domènech, C., Arcos, D., Duro, L. 2006. Assessment of the oxygen consumption in the backfill. Geochemical modelling in a saturated backfill. SKB Report, R-06-106 SKB Stockholm.

Gray, W. J. 1987. Effects of Radiation on the Oxidation Potential of Salt Brine. MRS Proceedings 112: 405. doi: 10.1557/PROC-112-405.

Greffe, V.R.G., Michiels, J. 2020. Desiccation-induced cell damage in bacteria and the relevance for inoculant production. Appl. Microbiol. Biot. 104: 3757-3770.

Grousset, S., et al. 2020. Biocorrosion detection by sulphur isotopic fractionation measurements. Corros. Sci. 165: 108386.

Guinan, M.W. 2001. Radiation effects in spent nuclear fuel canisters. SKB-TR-01-32.

Gutierrez, M.M., Caruso, S., Diomidis, N. (2018). Effects of materials and design on the criticality and shielding assessment of canister concepts for the disposal of spent nuclear fuel. App. Radiat. Isot. 139: 201-208.

Hadi, J., Wersin, P., Serneels, V., Greneche, J.M. 2019. Eighteen years of steel-bentonite interaction in the FEBEX "in situ" test at the Grimsel Test Site in Switzerland. Clays Clay Miner. 67: 111–131.

Hall, D.S., Behazin, M., Binns, W.J., & Keech, P.G. 2021. An evaluation of corrosion processes affecting copper-coated nuclear waste containers in a deep geological repository. Progress in Materials Science, 118, 100766. https://doi.org/10.1016/j.pmatsci.2020.100766

Hall, D.S., et al. 2021. An evaluation of corrosion processes affecting copper-coated nuclear waste containers in a deep geological repository. Prog. Mater. Sci. 118: 100766.

Hallberg, R.O., Engvall, A.G., Wadston, T. 1984. Corrosion of copper lightning conductor plates. Br. Corros. J. 19: 85-88.

Hammond, G., Lichtner, P., Mills, R. 2014. Evaluating the performance of parallel subsurface simulators: An illustrative example with PFLOTRAN. Water Resour. Res. 50: 208–228.

Hasal, M., Michalec, Z., Blaheta, R. (2019). *Provedení předběžného výpočtu tlaku na UOS*. Final report. – MS SÚRAO, TZ 388/2019, Praha (CZ).

Havlova V., Kiczka M., Mendoza Miranda A., Klajmon M., Wersin P., Pekala M. Jenni A., Hadi J., Samper J., Montenegro L., Mon A., Fabian M, Osan J., A. Dauzeres, D. Jacques (2020): Modelling of the steel-clay interface – approaches, first results and model refinements. Final version as of 28 08 2020 of deliverable D2.6 of the HORIZON 2020 project EURAD. EC Grant agreement no: 847593

Haynes, H.M., Pearce, C.I., Boothman, C., Lloyd, J.R. 2018. Response of bentonite microbial communities to stresses relevant to geodisposal of radioactive waste. Chem. Geol. 501: 58-67.

Hoch, A.R., Smart, N.R., Wilson, J.D., Reddy, B. 2010. A Survey of Reactive Metal Corrosion Data for Use in the SMOGG Gas Generation Model. Serco Report SA/ENV-0895, issue 2.

Holdsworth, S.R., 2013. Ceramic Material Solutions for Nuclear Waste Disposal Canisters. NAGRA working report NAB12-45.

Holdsworth, S.R., Graule, T., Mazza, R. 2014. Feasibility evaluation study of candidate canister solutions for the disposal of spent nuclear fuel and high-level waste-A status review. NAGRA working report NAB14-90.

Holdsworth, S.R., King, F., Diomidis, N. 2018. Alternative coating Materials as Corrosion Barriers for SF and HLW Disposal Canisters. NAGRA report NAB18-19.

Hua F., Mon K., Pasupathi P., Gordon G. Shoesmith D. (2005). A Review of Corrosion of Titanium Grade 7 and Other Titanium Alloys in Nuclear Waste Repository Environments. CORROSION 61 (10): 987–1003.

Huertas, F. et al. 2005. Full-Scale Engineered Barriers Experiment for a Deep Geological Repository for High-Level Waste in Crystalline Host Rock – Phase II. Euratom EUR 21922.

Hunter, F., Bate, F., Heath, T., Hoch, A. 2007. Geochemical Investigation of Iron Transport into Bentonite as Steel Corrodes. SKB Report TR-07-09.

Hutchison, E.A., Miller, D.A., Angert, E.R., Eichenberger, P., Driks, A. 2014. Sporulation in Bacteria: Beyond the Standard Model. Microbiol. Spectr. 2: doi: 10.1128/microbiolspec.TBS-0013-2012.

IAEA (1989), Natural Analogues in Performance Assessments for the Disposal of Long Lived Radioactive Wastes, IAEA Technical Reports Series No. 304.

IAEA (2005), Anthropogenic analogues for geological disposal of high level and long lived waste, Final report of a coordinated research project 1999–2004), IAEA report IAEA-TECDOC-1481.

Ibrahim, B., Zagidulin, D., Behazin, M., Ramamurthy, S., Wren, J.C., Shoesmith, D.W. 2018. The corrosion of copper in irradiated and unirradiated humid air. Corros. Sci. 141: 53-62.

Idiart, A., Coene, E. 2019. Modelling diffusion through compacted bentonite in the BHA vault. R-19-10, SKB, Sweden.

Idiart, A., Coene, E., Bagaria F., Román-Ross G., Birgersson, M. 2019. Reactive transport modelling considering transport in interlayer water. New model, sensitivity analyses and results from the Integrated Sulphide Project inter-model comparison exercise. TR-18-07, SKB, Sweden.

Itälä, A. 2009. Chemical Evolution of Bentonite Buffer in a Final Repository of Spent Nuclear Fuel During the Thermal Phase. VTT Publications 721: 78.

Jacobs, S., Edwards, O. 2000. Sulphide scale catalysis of copper corrosion. Water Res. 34: 2798-2808.

Jakupi, P. et al. 2015. Characterization of commercially cold sprayed copper coatings and determination of the effects of impacting copper powder velocities. J. Nucl. Mater. 466: 1-11.

Jalique, D.R. et al. 2016. Culturability and diversity of microorganisms recovered from an eight-years old highly compacted, saturated MX-80 Wyoming bentonite plug. Appl. Clay Sci. 126: 245-250.

Jenni, A., Wersin, P., Thoene, T., Baeyens, Ferrari, A., Gimmi, T., Mäder , U., Marschall, P. 2019. Bentonite backfill performance in a high-level waste repository: A geochemical perspective. Nagra Technical Report 19-03.

Jia, R., Unsal, T., Xu, D.K., Lekbach, Y., Gu, T.Y. 2019. Microbiologically influenced corrosion and current mitigation strategies: A state of the art review. Int. Biodeterior. Biodegrad. 137: 42-58.

JNC 2000. H12: Project to establish the scientific and technical basis for HLW disposal in Japan, Supporting report 2 - Repository Design and Engineering Technology. Technical report JNC TN1410 2000-003. Japan Nuclear Cycle Development Institute, Ibaraki, Japan.

Johansson, A.J., Lilja, C., Sjögren, L., Gordon, A., Hallbeck, L., Johansson, L. 2017. Insights from post-test examination of three packages from the MiniCan test series of copper-cast iron canisters for geological disposal of spent nuclear fuel: impact of the presence and density of bentonite clay. Corros. Eng. Sci. Technol. 52: 54-60.

Johnson, L.H., King, F. 2003. Canister Options for the Disposal of Spent Fuel. Technical report 02-11, National Cooperative for the Disposal of Radioactive Waste, Wettingen, Switzerland.

Johnson, L.H., King, F. 2008. The effect of the evolution of environmental conditions on the corrosion evolutionary path in a repository for spent fuel and high-level waste in Opalinus Clay. J. Nucl. Mater. 379: 9–15.

Johnson, L.H., LeNeveu, D.M., King, F., Shoesmith, D.W., Kolar, M., Oscarson, D.W., Sunder, S., Onofrei, C., Crosthwaite, J.L. 1996. The disposal of Canada's nuclear fuel waste: a study of postclosure safety of in-room emplacement of used CANDU fuel in copper containers in permeable plutonic rock. Volume 2: vault model. Report AECL-11494-2, COG-96-552-2, Atomic Energy of Canada.

Jolivet, E., L'Haridon, S., Corre, E., Forterre, P., Prieur, D. 2003. Thermococcus gammatolerans sp. nov., a hyperthermophilic archaeon from a deep-sea hydrothermal vent that resists ionizing radiation. Int. J. Syst. Evol. Microbiol. 53: 847-851.

Jonsson, M., Emilsson, G., & Emilsson, L. (2018). Mechanical Design Analysis for the Canister: Posiva SKB Report 04.

Jung, K.-W., Lim, S., Bahn, Y.-S. 2017. Microbial radiation-resistance mechanisms. J. Microbiol. 55: 499-507.

Kalfayan, G. 2019. PhD-Thesis. Procédé d''assemblage par chauffage micro-ondes à température modérée d''un matériau céramique alumino-silicaté pour conteneur de déchets radioactifs. École nationale supérieure des Mines de Saint-Etienne.

Kania, A., Szindler, M.M., Szindler, M. 2021. Structure and corrosion behavior of TiO2 thin films deposited by ALD on a biomedical magnesium alloy. Coatings 11: 70-84.

Karnland,O., Olsson,S., Dueck, A., Birgersson,M., Nilsson,U., Hernan-Håkansson, T., Pedersen,K., Nilsson,S., Eriksen,T., Rosborg, B. 2009. Long term test of buffer material at the Äspö Hard Rock Laboratory, LOT project. Final report on the A2 test parcel. SKB Technical Report TR-09-29, Svensk Kärnbränslehantering AB.

Kašpar, V., Šachlová, Š., Hofmanová, E., Komárková, B., Havlová, V., Aparicio, C., Černá, K., Bartak, D., Hlaváčková, V., 2021. Geochemical, geotechnical, and microbiological changes in Mg/Ca bentonite after thermal loading at 150 °C. Minerals 11: 965. https://doi.org/10.3390/min11090965

Kaufhold, S., Baille, W., Schanz, T., Dohrmann, R. 2015. About differences of swelling pressure — dry density relations of compacted bentonites. Appl. Clay Sci. 107: 52-61.

Kawana, A., Ichimura, H., Iwata, Y., Ono, S. 1996. Development of PVD ceramic coatings for valve seats. Surf. Coat. Technol. 86-87: 212-117.

Keech, P.G. et al. 2014. Design and development of copper coatings for long term storage of used nuclear fuel. Corros. Eng. Sci. Technol. 49: 425-430.

Keech, P.G., Behazin, M., Binns, J.W., Briggs, S. 2020. An update on the copper corrosion program for the long-term management of used nuclear fuel in Canada. Mater. Corros. 72: 25-31.

Kelm, M., Bohnert, E. 2004. A kinetic model for the radiolysis of chloride brine, its sensitivity against model parameters and a comparison with experiments, Forschungszentreum Karlsruhe, FZKA 6977.

Kerber, A., Knorr, J. 2013. SiC encapsulation of high-level waste for long-term immobilization. atw 58: 8-13.

Kiczka, M., Pekala, M., Maanoja, S., Muuri, E., Wersin, P. 2021. Modelling of solute transport and microbial activity in diffusion cells simulating a bentonite barrier of a spent nuclear fuel repository. Appl. Clay Sci. 211: 106193.

King, F. 1995. A natural analogue for the long-term corrosion of copper nuclear waste containers – reanalysis of a study of a bronze cannon. Appl. Geochem. 10, 477-487.

King, F. 2005. Evolution of environmental conditions in a deep geological repository in the sedimentary rock of the Michigan Basin, Ontario. Ontario Power Generation Nuclear Waste Management Division Report 06819-REP-01300-10102-R00.

King, F. 2006. Review and gap analysis of the corrosion of copper containers under unsaturated conditions, Ontario Power Generation, Nuclear Waste Management Division Report 06819-REP-01300-10124-R00.

King, F. 2007. Overview of a carbon steel container corrosion model for a deep geological repository in sedimentary rock', Nuclear Waste Management Organization Report NWMO TR-2007-01.

King, F. 2008a. Corrosion of carbon steel under anaerobic conditions in a repository for SF and HLW in Opalinus Clay', Nagra Technical Report 08-12, Nagra, Wettingen, Switzerland.

King, F. 2008b. Mixed-Potential Modelling of the Corrosion of Copper in the Presence of Sulphide. Working Report 2007-63, Posiva Oy, Finland.

King, F. 2013a. Container materials for the storage and disposal of nuclear waste. Corrosion 69, 986e1011.

King, F. 2013b. A review of the properties of pyrite and the implications for corrosion of the copper canister. TR-13-19, SKB, Sweden.

King, F. 2014a. Durability of High Level Waste and Spent Fuel Disposal Containers-an overview of the combined effect of chemical and mechanical degradation mechanisms. Appendix B. 6-Corrosion of Nickel Alloys. AMEC Nuclear UK Limited (AMEC).

King, F. 2014b. Predicting the Lifetimes of Nuclear Waste Containers. J. Mater. 66: 526-537.

King, F. 2017. Nuclear waste canister materials: corrosion behaviour and long-term performance in geological repository systems. Chapter in: Geological Repository Systems for Safe Disposal of Spent Nuclear Fuels and Radioactive Waste. Eds. Apted, M.J., Ahn, J. Elsevier Ltd: 365-408.

King, F. 2020. Canister Materials for the Disposal of Nuclear Waste. In: Comprehensive Nuclear Materials. 2nd Edition. Elsevier.

King, F., Behazin, M. 2021. A Review of the Effect of Irradiation on the Corrosion of Copper-Coated Used Fuel Containers. Corros. Mater. Degrad. 2: 678-707.

King, F., Chen, J., Qin, Z., Shoesmith, D., Lilja, C. 2017b. Sulphide-transport control of the corrosion of copper canisters. Corros. Eng. Sci. Technol. 52: 210-216.

King, F., Hall, D.S., Keech, P.G. 2017a. Nature of the nearfield environment in a deep geological repository and the implications for the corrosion behaviour of the container. Corros. Eng. Sci. Technol. 52: 25-30.

King, F., Kolář, M. 2000. The copper container corrosion model used in AECL's second case study. 06819-REP-01200-10041-R00. Ontario Power Generation, Nuclear Waste Management Division.

King, F., Kolář, M. 2006. Consequences of microbial activity for corrosion of copper used fuel containers–analyses using the CCM-MIC. OPG 06819-REP-1300-10120-R00. Toronto, Canada: Ontario Power Generation.

King, F., Kolář, M. 2019. Copper Sulphide Model (CSM). Model improvements, sensitivity analyses, and results from the Integrated Sulphide Project inter-model comparison exercise. TR-18-08, SKB, Sweden.

King, F., Kolář, M., Keech, P.G. 2014. Simulations of long-term anaerobic corrosion of carbon steel containers in Canadian deep geological repository. Corros. Eng. Sci. Technol. 49, 455-459.

King, F., Kolář, M., Maak, P. 2008. Reactive-transport model for the prediction of the uniform corrosion behaviour of copper used fuel containers. J. Nucl. Mater. 379: 133-141.

King, F., Kolář, M., Puigdomenech, I., Pitkänen, P., Lilja, C. 2021. Modelling microbial sulphate reduction and the consequences for corrosion of copper canisters. Mater. Corros. 72: 339-347.

King, F., Kolář, M., Vähänen, M., and Lilja, C. 2011. Modelling long term corrosion behaviour of copper canisters in KBS-3 repository. Corros. Eng. Sci. Technol. 46: 217-222.

King, F., LeNeveu, D. 1992. Prediction of the lifetimes of copper nuclear waste containers. Proceedings of the Topical Meeting on Nuclear Waste Packaging, Focus '91. Las Vegas: La Grange Park: American Nuclear Society: 253-261.

King, F., Lilja, C. 2014. Localised corrosion of copper canisters. Corros. Eng. Sci. Technol. 49: 420-424.

King, F., Lilja, C., Pedersen, K., Pitkänen, P., Vähänen, M. 2010. An Update of the State-of-the-Art Report on the Corrosion of Copper Under Expected Conditions in a Deep Geologic Repository. Swedish Nuclear Fuel and Waste Management Co. Report, Technical Report TR-10-67 and Posiva Oy Report, POSIVA 2011-01.

King, F., Litke, C.D., Ryan, S.R. 1992. A Mechanistic Study of The Uniform Corrosion of Copper In Compacted Na-Montmorillonite/Sand Mixtures. Corros. Sci. 33: 1979-1995.

King, F., Padovani, C. 2011. Review of the corrosion performance of selected canister materials for disposal of UK HLW and/or spent fuel. Corros. Eng. Sci. Technol. 46: 82-90.

King, F., Sanderson, D., Watson, S. 2016. Durability of High-Level Waste and Spent Fuel Disposal Containers – an overview of the combined effect of chemical and mechanical degradation mechanisms. AMEC Report 17697/TR/03.

Knorr, J., Lippmann, W., Reinecke, A-M., Wolf, R., Kerber, A. and Wolter, A. 2008. SiC encapsulation of (V)HTR components and waste by laser beam joining of ceramics. Nucl. Eng. Des. 238: 3129-3135.

Koivuluoto, H., Vuoristo, P. 2010. Structural analysis of cold-sprayed nickel-based metallic and metallic ceramic coatings. J. Therm. Spray Technol. 19: 975-989.

Kojima, Y., Hioki, T., Tsujikawa, S. 1995. Simulations of the state of carbon steel n years after disposal with n years of corrosion product on its surface in a bentonite environment. Materials Research Society Symposium Proceedings 353: 711-718.

Konovalova, V. 2021. The Effect of Temperature on the Corrosion Rate of Iron-Carbon Alloys. Materials Today: Proceedings 38: 1326–29. doi: 10.1016/j.matpr.2020.08.094.

Kotelnikova, S., Pedersen, K. 1998. Distribution and activity of methanogens and homoacetogens in deep granitic aquifers at Aspo Hard Rock Laboratory, Sweden. FEMS Microbiology Ecology 26. Issue 2, 121-134. DOI 10.1016/S0168-6496(98)00028-2.

Kottemann, M., Kish, A., Iloanusi, C., Bjork, S., DiRuggiero, J. 2005. Physiological responses of the halophilic archaeon Halobacterium sp. strain NRC1 to desiccation and gamma irradiation. Extremophiles 9: 219-227.

Kumpalainen, S., Kiviranta, L., Korkeakoski, P. 2016. Long-term effects of an iron heater and Äspö groundwater on smectite clays: Chemical and hydromechanical results from the in situ alternative buffer material (ABM) test package 2. Clay Miner. 51: 129–144.

Kursten B., MacDonald, D.D., Smart, N.R., Gaggiano, R. 2017. Corrosion Issues of Carbon Steel Radioactive Waste Packages Exposed to Cementitious Materials with Respect to the Belgian Supercontainer Concept. Corros. Eng. Sci. Technol. 52: 11-16.

Kursten, B., Smailos, E., Azkarate, I., Werme, L., Smart, N.R., Santarini, G. 2003. COBECOMA State-of-the-Art Document on the Corrosion Behaviour of Container Materials. EUROPEAN COMMISSION 5th EURATOM FRAMEWORK PROGRAMME 1998-2002.

Kwong, G.M. 2011. Status of Corrosion Studies for Copper Used Fuel Containers Under Low Salinity Conditions. NWMO TR-2011-14. Nuclear Waste Management Organization.

Landolt, D., Davenport A., Payer A., Shoesmith D. 2009. A review of materials and corrosion issues regarding canisters for disposal of spent fuel and high-level waste in Opalinus clay. NAGRA Technical Report 09-02.

Lapuerta, S., Bérerd, N., Moncoffre, N., Millard-Pinard, N., Jaffrézic, H., Crusset, D., Féron. D. 2008. The Influence of Relative Humidity on Iron Corrosion under Proton Irradiation. J. Nucl. Mater. 375: 80–85. doi: 10.1016/j.jnucmat.2007.10.011.

Lapuerta, S., Moncoffre, N., Millard-Pinard, N., H. Jaffrézic, H., Bérerd, Crusset, D. 2006. Role of proton irradiation and relative air humidity. J. Nucl. Mater. 352: 174-181.

Larker, H. 1980. Method of containing spent nuclear fuel or high-level nuclear fuel waste. Patent US4209420, United States.

Lee, M.S, et al. 2011. Application of Cold Spray Technique to the underground disposal copper canister and its corrosion properties, Nucl. Eng. Technol. 43: 557-566.

Lee, S., Staehle, R.W. 1997. Adsorption of water on copper, nickel and iron. Corrosion 53: 33-42.

Lee, Y.T.R., Ashrafizadeh, H., Fisher, G., McDonald, A. 2017. Effect of type of reinforcing particles on the deposition efficiency and wear resistance of low-pressure cold-sprayed metal matrix composite coatings. Surf. Coat. Technol. 324: 190-200.

Legoux, J.G. 2014. Development of cold spray coating for nuclear waste storage container application, EUCOSS 2014, Paris, May 26th.

Li, M., Zinkle, S. 2012. Physical and Mechanical Properties of Copper and Copper Alloys. In: Konings R.J.M., (ed.) Comprehensive Nuclear Materials, volume 4, pp. 667-690 Amsterdam: Elsevier.

Liang, D. et al. 2021. Extracellular electron exchange capabilities of Desulfovibrio ferrophilus and Desulfopila corrodens. Environ. Sci. Tech. 55: 16195-16203.

Litke, C.D., Ryan, S.R., King, F. 1992. TA mechanistic study of the uniform corrosion of copper in compacted clay-sand soil. AECL-10397, COG-91-304, Atomic Energy of Canada Ltd.

Little, B.J., Hinks, J., Blackwood, D.J. 2020. Microbially influenced corrosion: Towards an interdisciplinary perspective on mechanisms. Int. Biodeterior. Biodegrad. 154: 105062.

Liu, C., Wang, J., Zhang, Z., Han, E-H. 2017. Studies on Corrosion Behaviour of Low Carbon Steel Canister with and without γ-Irradiation in China's HLW Disposal Repository. Corros. Eng. Sci. Technol. 52: 136–40. doi: 10.1080/1478422X.2017.1348762.

Lobach, K., Kupriiyanova, Y., Kolodiy, I., Sayenko, S., Shkuropatenko, V., Voyevodin, V., Zykova, A., Bykov, A., Chunyayev, O., Tovazhnyanskyy, L. 2018. Optimisation of Properties of Silicon Carbide Ceramics with the Use of Different Additives. Funct. Mater. 25: 496-504.

Lobach, K.V. et al. 2020. Corrosion stability of SiC-based ceramics in hydrothermal conditions. Mater. Sci. 55: 672-682.

Lopez-Fernandez, M., Cherkouk, A., Vilchez-Vargas, R., Jauregui, R., Pieper, D., Boon, N., Sanchez-Castro, I., Merroun, M.L. 2015. Bacterial Diversity in Bentonites, Engineered Barrier for Deep Geological Disposal of Radioactive Wastes. Microb. Ecol. 70: 922–935.

Lousada, C. M., Soroka, I. L., Yagodzinsky, Y. et al. 2016. Gamma radiation induces hydrogen absorption by copper in water. Scientific Reports 6, no. 1.

Lu, C., Samper, J., Fritz, B., Clement, A., and Montenegro, L., (2011) Interactions of corrosion products and bentonite: An Extended multicomponent reactive transport model. Physics and Chemistry of the Earth, 36, 1661

Lundgren, K. 2004. Final disposal of fuel - electron radiation outside copper canister. Technical Report SKB-TR-04-06. Swedish Nuclear Fuel and Waste Management Co., Stockholm, Sweden.

Lv, M.Y., Du, M. 2018. A review: microbiologically influenced corrosion and the effect of cathodic polarization on typical bacteria. Rev. Environ. Sci. Biotechnol. 17: 431-446.

Maak, P., King, F. 2006. A Model for Predicting Stress Corrosion Cracking of Copper Containers in A Deep Geologic Repository. MRS Online proceedings Library 932: 291.

Maanoja, S. et al. 2020. Compacted bentonite as a source of substrates for sulfate-reducing microorganisms in a simulated excavation-damaged zone of a spent nuclear fuel repository. Appl. Clay Sci. 196, 105746.

Maanoja, S. et al. 2021. The effect of compaction and microbial activity on the quantity and release rate of water-soluble organic matter from bentonites. Appl. Clay Sci. 211: 106192.

Malmström, M., Banwart, S., Duro, L., Wersin, P., & Bruno, J. (1995). Biotite and chlorite weathering at 25 degrees C: the dependence of pH and (bi)carbonate on weathering kinetics, dissolution stoichiometry, and solubility; and the relation to redox conditions in granitic aquifers-. SKB Technical Report 95-0.1, Stockholm, Sweden.

Mand J, Park HS, Okoro C, Lomans BP, Smith S, Chiejina L and Voordouw G (2016) Microbial Methane Production Associated with Carbon Steel Corrosion in a Nigerian Oil Field. *Front. Microbiol.* 6:1538. doi: 10.3389/fmicb.2015.01538

Marion (2014) Modélisation électrochimique de la vitesse de corrosion généralisée du fer en milieu poreux. Contribution à un modèle prédictif de la durabilité des aciers non alliés en conditions de stockage géologique [PhD Thesis]. Université de Bourgogne;2014.

Marsh, G.P., Taylor, K.J. 1988. An Assessment of Carbon Steel Containers for Radioactive Waste Disposal. Corros. Sci. 28: 289–320. doi: 10.1016/0010-938X(88)90111-4.

Marshall, M.H.M., McKelvie, J.R., Simpson, A.J., Simpson, M.J. 2015. Characterization of natural organic matter in bentonite clays for potential use in deep geological repositories for used nuclear fuel. Appl. Geochem. 54: 43-53.

Marty, N.C.M., Fritz, B., Clément, A., Michau, N. 2010. Modelling the long-term alteration of the engineered bentonite barrier in an underground radioactive waste repository. Appl. Clay Sci. 47: 82–90.

Masurat, P., Eriksson, S., Pedersen, K. 2010. Microbial sulphide production in compacted Wyoming bentonite MX-80 under in situ conditions relevant to a repository for high-level radioactive waste. Appl. Clay Sci. 47: 58-64.

Matschiavelli, N. et al. 2019. The Year-Long Development of Microorganisms in Uncompacted Bavarian Bentonite Slurries at 30 and 60 °C. Environ. Sci. Tech. 53: 10514-10524.

Matts, O. et al. 2019. Influence of Cold Spray Nozzle Displacement Strategy on Microstructure and Mechanical Properties of Cu/SiC Composites Coating. Key Eng. Mater. 813: 110-115.

Mattson, E. 1980. Aluminium oxide as the encapsulation material for unreprocessed nuclear fuel waste-evaluation from the viewpoint of corrosion, Swedish Corrosion Institute, Final Report KBS 80-15.

McNamara, N.P., Black, H.I.J., Beresford, N.A., Parekh, N.R. 2003. Effects of acute gamma irradiation on chemical, physical and biological properties of soils. Appl. Soil Ecol. 24: 117-132.

Mendoza, A. 2017. Gas generation and migration in clay media as a result of anaerobic steel corrosion. Technical report No. 187/2017. SURAO, Prague.

Mijnendonckx, K., Van Gompel, A., Coninx, I., Bleyen, N., Leys, N., 2015. Radiation and microbial degradation of bitumen, Deliverable 1.3, MIND, European Commission.

Miller, W., Alexander, R., Chapman, N., McKinley, M., Smellie, J. 1994. Natural analogue studies in the geological disposal of radioactive wastes. Nagra Technical Report NTB-93-03. Wettingen, Sweden.

Milodowski, A.E., Styles, M.T., Hards, V.L. (2000), A natural analogue for copper waste canisters: The copper-uranium mineralised concretions in the Permian mudrocks of south Devon, SKB Report TR-00-11.

Milodowski, A.E., Styles, M.T., Horstwood, M.S.A., Kemp, S.J. (2002), Alteration of uraniferous and native copper concretions in the Permian mudrocks of south Devon, United Kingdom. A natural analogue study of the corrosion of copper canisters and radiolysis effects in a repository for spent nuclear fuel, SKB Report TR-02-09.

Milošev, I., Navinšek, B. 1993. Corrosion properties of selected Cr-based hard and protective coatings. Surf. Coat. Technol. 60: 545-548.

Milošev, I., Strehblow, H.H., Navinšek, B. 1997. Comparison of TiN, ZrN and CrN hard nitride coatings: electrochemical and thermal oxidation. Thin Solid Films 303: 246-254.

Minhas, B., Dino, S., Zuo, Y., Qian, H., Zhao, X. 2021. Improvement of Corrosion Resistance of TiO2 Layers in Strong Acidic Solutions by Anodizing and Thermal Oxidation Treatment. Materials 14: 1188-13.

Mironenko, N.V., Alekhina, I.A., Zhdanova, N.N., Bulat, S.A. 2000. Intraspecific variation in gamma-radiation resistance and genomic structure in the filamentous fungus Alternaria alternata: A case study of strains inhabiting Chernobyl reactor no. 4. Ecotoxicology and Environmental Safety 45: 177-187.

Mohajerani, M., Delage, P., Sulem, J., Monfared, M., Tang, A.M., Gatmiri, B. 2012. A laboratory investigation of thermally induced pore pressures in the Callovo-Oxfordian claystone International Journal of Rock Mechanics and Mining Sciences, 52: 112-121.

Mohamed-Said, M., Vuillemin, B., Oltra, R., Marion, A., Trenty, L. & Crusset, D. (2017): Predictive modelling of the corrosion rate of carbon steel focusing on the effect of the precipitation of corrosion products. Corrosion Engineering, Science and Technology 52/sup1, 178-185.

Mon, A., Samper, J., Montenegro, L., Naves, A., Fernández, J. (2017): Reactive transport model of compacted bentonite, concrete and corrosion products in a HLW repository in clay. Journal of Contaminant Hydrology, 197: 1-16.

Montes-H, G., Marty, N., Fritz, B., Clement, A., and Michau, N., (2005) Modelling of long-term diffusion-reaction in a bentonite barrier for radioactive waste confinement. Applied Clay Science 30: 181–198.

Morco, R. P. 2020. Gamma-Radiolysis Kinetics and Its Role in The Overall Dynamics of Materials Degradation. Doctoral dissertation, The University of Western Ontario (Canada).

Müller, H.R., Garitte, B., Vogt, T., Köhler, S., Sakaki, T., Weber, H., Spillman, T., Hertrich, M., Becker, J.K., Giroud, N., Cloet, V., Diomidis, N., Vietor, T., 2017. Implementation of the full-scale emplacement (FE) experiment at the Mont Terri rock laboratory. Swiss J. Geosci. 110: 287-306.

Muyzer, G., Stams, A.J. 2008. The ecology and biotechnology of sulphate-reducing bacteria. Nat. Rev. Microbiol. 6: 441-454.

N.R. Smart, A.P. Rance, P. Fennell, L. Werme (2003), Expansion Due To Anaerobic Corrosion of Steel and Cast Iron: Experimental and Natural Analogue Studies, Presented at International Workshop on Prediction of Long Term Corrosion Behaviour in Nuclear Waste Systems, Cadarache, November 2001, in 'Prediction of Long Term Corrosion Behaviour in Nuclear Waste Systems' (D. Feron and D.D. Macdonald, eds), EFC Publication No 36, published by Institute of Materials, Minerals and Mining, pg. 280.

N.R. Smart, R. Adams, L.O. Werme (2003), Analogues for the Corrosion-induced Expansion of Iron in HLW Containers, presented at MRS 2003 Kalmar, Sweden, June 15-18, 2003, Materials Research Society Symposium Proceedings Volume 807, Scientific Basis for Nuclear Waste Management XXVII, V.M. Oversby and L.O. Werme (eds.), p. 879-884, 2004.

Nagra. 2002. Demonstration of disposal feasibility for spent fuel, vitrified high-level waste and long-lived intermediate-level waste (Entsorgungsnachweis). Nagra Technical Report Number 02-05.

Nardi, A., Idiart, A., Trinchero, P., de Vries, L. M., Molinero, J., 2014. Interface COMSOL-PHREEQC (iCP), an efficient numerical framework for the solution of coupled multiphysics and geochemistry. Comput. Geosci. 69: 10–21.

Necib, S., Diomidis, N., Keech, P., Nakayama, M. 2017. Corrosion of carbon steel in clay environments relevant to radioactive waste geological disposals, Mont Terri rock laboratory (Switzerland). Swiss J. Geosci. 110: 329-342.

Necib, S., Linard, Y., Crusset, D., Michau, N., Daumas, S., Burger, E., Romaine, A., Schlegel, M.L. 2016. Corrosion at the carbon steel-clay borehole water and gas interfaces at 85°C under anoxic and acidic transient conditions. Corros. Sci. 111: 242-258.

Nelson, J.L., Westerman, R.E., Gerber, F.S. 1983. Irradiation-Corrosion Evaluation of Metals for Nuclear Waste Package Applications in Grande Ronde Basalt Groundwater. MRS Proceedings 26: 121. doi: 10.1557/PROC-26-121.

Ngo et al. (2014): Ngo, V.V., Delalande, M., Clément, A., Michau, N., Fritz, B., 2014. Coupled transport reaction modelling of the long-term interaction between iron, bentonite and Callovo-Oxfordian claystone in radioactive waste confinement systems. Applied Clay Science 101, 430-443.

Nguyen, T.S., Selvadurai, A.P.S., Armand, G. 2005. Modelling the FEBEX THM experiment using a state surface approach. Int. J. Rock Mech. Min. Sci. 42: 639–651.

NUMO. 2021. The NUMO Pre-siting SDM-based Safety Case, NUMO-TR-21-01. Nuclear Waste Management Organization of Japan.

NWMO 2016. Implementing Adaptive Phased Management 2016 to 2020. Nuclear Waste Management Organization Report.

Ochs, M., Talerico, C. 2004. SR-Can. Data and uncertainty assessment. Migration parameters for the bentonite buffer in the KBS-3 concept. SKB TR-04-18, SKB, Sweden.

Ogawa, K., et al. 2008. Characterization of low pressure cold-sprayed aluminium coatings, J. Therm. Spray Technol. 17: 728-735.

Ogwu MC, Kerfahi D, Song H, Dong K, Seo H, Lim S, Srinivasan S, Kim MK, Waldman B, Adams JM. Changes in soil taxonomic and functional diversity resulting from gamma irradiation. Sci Rep. 2019 May 27;9(1):7894. doi: 10.1038/s41598-019-44441-7. PMID: 31133738; PMCID: PMC6536540.

Ojovan, M.I., Lee, W.E., Kalmykov, S.N. 2019. Nuclear Waste Disposal in An Introduction to Nuclear Waste Immobilisation, pp. 415–432. Elsevier, Amsterdam.

Otte, J.M., Blackwell, N., Soos, V., Rughöft, S., Maisch, M., Kappler, A., Kleindienst, S., Schmidt, C. 2018. Sterilization impacts on marine sediment - Are we able to inactivate microorganisms in environmental samples? EMS Microbiol. Ecol. 94: fiy189. https://doi.org/10.1093/femsec/fiy189

Padovani, C., King, F., Lilja, C., Féron, D., Necib, S., Crusset, D., Deydier, V., Diomidis, N., Gaggiano, R., Ahn, T., Keech, P.G., Macdonald, D.D., Asano, H., Smart, N., Hall, D.S., Hänninen, H., Engelberg, D., Noël, J.J., Shoesmith, D.W. 2017. The Corrosion Behaviour of Candidate Container Materials for the Disposal of High-Level Waste and Spent Fuel – a Summary of the State of the Art and Opportunities for Synergies in Future R&D. Corr. Eng. Sci. Tech. 52: 227–31. doi: 10.1080/1478422X.2017.1356973.

Padovani, C., Pletser, D., Jurkschat, K., Armstrong, D., Dugdale, S., Brunt, D., Faulkner, R., Was, G., Johansson A.J. 2019. Assessment of microstructural changes in copper due to gamma radiation damage. Report number: SKB TR-19-12.

Parkhurst, D.L., Appelo, C.A.J. 2013. Description of input and examples for PHREEQC version 3 – A computer program for speciation, batch-reaction, one-dimensional transport, and inverse geochemical calculations. Techniques and Methods 6–A43, U.S. Geological Survey, Denver, Colorado.

Pastina, B., LaVerne, J.A. 2001. Effect of molecular hydrogen on hydrogen peroxide in water radiolysis. The Journal of Physical Chemistry A, 105: 9316-9322.

Patel, R., Punshon, C., Nicolas, J., Bastid, P., Zhou, R., Schneider, C., Bagshaw, N., Howse, D., King, F. 2012. Canister design concepts for disposal of spent fuel and high level waste, Nagra Technical Report, NTB 12-06.

Payer, J.H., Finsterle, S., Apps, J.A., Muller, R.H. 2019. Corrosion Performance of Engineered Barrier System in Deep Horizontal Drillholes. Energies 12: 1491.

Pedersen, K. 2010. Analysis of copper corrosion in compacted bentonite clay as a function of clay density and growth conditions for sulfate-reducing bacteria. J. Appl. Microbiol. 108: 1094-1104.

Pedersen, K. 2017. MIND deliverable 2.4: Bacterial activity in compacted bentonites. https://mind15.eu/deliverables/

Pedersen, K., Motamedi, M., Karnland, O., Sandén, T. 2000. Mixing and sulphate-reducing activity of bacteria in swelling, compacted bentonite clay under high-level radioactive waste repository conditions. J. Appl. Microbiol. 89: 1038-1047.

Pękala, M., Alt-Epping, P., Wersin, P. (2019). 3D and 1D Dual-Porosity Reactive Transport Simulations - Model Improvements, Sensitivity Analyses, and Results from the Integrated Sulfide Project Inter-Model Comparison Exercise. Posiva Working Report 2018-31.

Pekala, M., Smith, P., Wersin, P., Diomidis, N., & Cloet, V. (2020). Comparison of models to evaluate microbial sulphide generation and transport in the near field of a SF/HLW repository in Opalinus Clay. Journal of contaminant hydrology, 228, 103561.

Pekala, M., Wersin, P., Cloet, V., & Diomidis, N. (2019). Reactive transport calculations to evaluate sulphide fluxes in the near-field of a SF/HLW repository in the Opalinus Clay. Applied geochemistry, 100, 169-180.

Peña J, Torres E, Turrero MJ, Escribano A, Martín PL (2008): Kinetic modelling of the attenuation of carbon steel canister corrosion due to diffusive transport through corrosion product layers. Corrosion Science, 50(8): 2197-2204.

Phillips, R.W., Wiegel, J., Berry, C.J., Fliermans, C., Peacock, A.D., White, D.C., Shimkets, L.J. 2002. Kineococcus radiotolerans sp. nov., a radiationresistant, Gram-positive bacterium. Int. J. Syst. Evol. Microbiol. 52: 933-938.

Pignatelli, I., Bourdelle, F., Bartier, D., Mosser-Ruck, R., Truche, L., Mugnaioli, E., Michau, N. 2014. Iron-clay interactions: Detailed study of the mineralogical transformation of claystone with emphasis on the formation of iron-rich T-O phyllosilicates in a step-by-step cooling experiment from 90 °C to 40 °C. Chem. Geol. 387: 1-11.

Pignatelli, I., Mugnaioli, E., Hybler, J., Mosser-Ruck, R., Cathelineau, M., Michau, N. 2013. A multi-technique characterization of cronstedtite synthesized by iron-clay interaction in a step-by-step cooling procedure. Clays and Clay Miner. 61: 277-289.

Pinnel, M.R., Tompkins, H.G., Heath, D.E. 1979. Oxidation of copper in controlled clean air and standard laboratory air at 50°C to 150°C. Appl. Surf. Sci. 2: 558-577.

Poller, A., Mayer, G., Darcis, M., Smith, P. 2016. Modelling of gas generation in deep geological repositories after closure. Nagra Technical Report NTB 16-04. Nagra, Wettingen, Switzerland.

Posiva. 2007. Expected evolution of a spent nuclear fuel repository at Olkiluoto. Posiva Report 2006-05.

Posiva. 2013. Safety Case for the Disposal of Spent Nuclear Fuel at Olkiluoto - Models and Data for the Repository System 2012. Eurajoki: Posiva Oy.

Posiva. 2021a. Canister evolution. Posiva Oy Working Report, WR-2021-06.

Posiva. 2021b. Sulfide fluxes and concentrations in the spent nuclear fuel repository at Olkiluoto – 2021 update. Posiva Oy Working Report, WR-2021-07.

Pospiskova, L., Dobrev, D., Kouril, M., Stoulil, J., Novikova, D., Kotnour, P., Matal, O. 2017. Czech national programme and disposal canister concept. Corros. Eng. Sci. Technol. 52: 6-10.

Puigdomenech, I., Ambrosi, J.-P., Eisenlohr, L., Lartigue, J.-E., Banwart, S.A., Bateman, K., Milodowski, A.E., West, J.M., Griffault, L., Gustafsson, E., Hama, K., Yoshida, H., Kotelnikova, S., Pedersen, K., Michaud, V., Trotignon, L., Rivas Perez, J., Tullborg, E.-L., 2001. O2 depletion in granitic media — the REX project. Svensk Kärnbränslehantering AB. Report no. TR-01-05.

Puigdomenech, I., Taxén, C., 2000. Thermodynamic data for copper. Implications for the corrosion of copper canister under repository conditions. Technical Report TR-00-13. Svensk Kärnbränslehantering AB, Stockholm, Sweden.

Pusch, R., Karnland, O., Lajudie, A., Decarreau, A. 1992. MX 80 Clay Exposed to High Temperatures and Gamma Radiation. SKB Technical Report 93–03(93–03).

Qin, Z., Daljeet, R., Ai, M., Farhangi, N., Noël, J.J., Ramamurthy, S., Shoesmith, D., King, F., Keech, P. 2017. The active/passive conditions for copper corrosion under nuclear waste repository environment. Corros. Eng. Sci. Technol. 52: 45-49.

Raikko, H., Sandström, R., Rydén, H., & Johansson, M. (2010). Design analysis report for the canister. SKB TR-10-28, SKB Report, Stockholm.

Raiko H., Salo J.-K. (1999). Design report of the disposal canister for twelve fuel assemblies. Posiva 99-18.

Rajala, P. et al. 2015. Microbially induced corrosion of carbon steel in deep groundwater environment. Front. Microbiol. 6: 647.

Rebata-Landa, V., Santamarina, J.C. 2006. Mechanical limits to microbial activity in deep sediments. Geochem. Geophys. Geosystems 7, doi:10.1029/2006GC001355.

Refait, P., Grolleau, A.-M., Jeannin, M., Francois, E., Sabot, R. 2016. Localized corrosion of carbon steel in marine media: Galvanic coupling and heterogeneity of the corrosion product layer. Corros. Sci. 111: 583-595.

Riba, O. C. (2020). Spent fuel alteration model integrating processes of different time-scales. MRS Advances, 159-166

Riba, O., Coene, E., Silva, O., & Duro, L. 2021. Development of a reactive transport model of spent fuel dissolution under near field environmental conditions. Deliverable D5.5, DISCO project, grant agreement 755443, Horizon 2020 Framework Programme, European Commission.

Rockhvarger, A.E., Khizh, A.B. 1998. Large size, thick-walled ceramic containers. NUCON SYSTEMS INC, Patent WO9844834.

Rockhvarger, A.E., Khizh, A.B. 1999. Process for the preparation of thick-walled ceramic products. ROKON SYSTEMS INC., Patent US5911941A.

Rockhvarger, A.E., Khizh, A.B. 2000. Processus and apparatus for joining thick-walled ceramic parts. Patent US6054700.

Romaine, A., Jeannin, M., Sabot, R., Necib, S., Refait, P. 2015. Corrosion processes of carbon steel in argillite: Galvanic effects associated with the heterogeneity of the corrosion product layer. Electrochim. Acta 182: 1019-1028.

Romanoff, M. 1989. Underground corrosion. Houston: NACE International.

Roy, S.K., Sircar, S.C. 1981. A critical appraisal of the logarithmic rate law in thin-film formation during oxidation of copper and its alloys. Oxidation of Metals 15: 9-20.

Rutqvist, J., Tsang,C-F. 2008. Review of SKB´s Work on Coupled THM Processes Within SR-Can: external review contribution in support of SKI´s and SSI´s review of SR-Can. SKI Report 2008:08.

RWM 2016. Geological Disposal-Waste Evolution Status Report, NDA Report DSSC/451/01. Radioactive Waste Management.

Saheb, M., Marsal, F., Matthiesen, H., Neff, D., Dillmann, P., Pellegrini, D. 2011. Fluctuation of redox conditions in radioactive waste disposal cell: characterisation of corrosion layers formed on archaeological analogues. Corros. Eng. Sci. Technol. 46: 199-204.

Samper, J., Lu, C., and Montenegro, L., (2008) Reactive transport model of interactions of corrosion products and bentonite. Physics and Chemistry of the Earth 33: S306–S316.

Samper, J., Naves, A., Montenegro, L., Mon., A. (2016): Reactive transport modelling of the long-term interactions of corrosion products and compacted bentonite in a HLW repository in granite: Uncertainties and relevance for performance assessment, Applied Geochemistry, 67: 42-51.

Sánchez, M., Gens, A., Olivella, S. 2012. THM analysis of a large-scale heating test incorporating material fabric changes. Int. J. Numer. Anal. Meth. Geomech. 36: 391–421.

Savage, D. (2012): Prospects for Coupled Modelling. STUK-TR 13. Radiation and Nuclear Safety Authority, Helskinki, Finland.

Savage, D., Watson, C., Benbow, S., and Wilson, J., (2010) Modelling iron-bentonite interactions. Applied Clay Science 47: 91–98

Schanz, T. 2016. Transient boundary conditions in the frame of THM processes at nuclear waste repositories. E-UNSAT 2016. E3S Web of Conferences 9, 03001.

Schindleholtz, E., Risteen, B.E., Kelly, R.G. 2014. Effect of relative humidity on corrosion of carbon steel under sea salt aerosol proxies I. NaCl. J. Electrochem. Soc. 161: C450-C459.

Schlegel, M.L., Necib, S., Daumas, S., Blanc, C., Foy, E., Trcera, N., Romaine, A. 2016. Microstructural characterization of carbon steel corrosion in clay borehole water under anoxic and transient acidic conditions. Corros. Sci. 109: 126-144.

Schlegel, M.L., Necib, S., Daumas, S., Labat, M., Blanc, C., Foy, E., Linard, Y. 2018. Corrosion at the carbon steel-clay borehole water interface under anoxic alkaline and fluctuating temperature conditions. Corros. Sci. 136: 70-90.

Schutz, R.W. 1996. Ruthenium enhanced titanium alloys: Minor ruthenium additions produce cost effective corrosion resistant commercial titanium alloys. Platinum Metals Review 40: 54–61.

Scully, J.R., Edwards, M. 2013. Review of the NWMO Copper Corrosion Allowance. Toronto: NWMO TR-2013-04.

Senior, N.A., Newman, R C., Artymowicz, D., Binns, W.J., Keech, P.G., Hall, D.S. (2019) Communication—A Method to Measure Extremely Low Corrosion Rates of Copper Metal in Anoxic Aqueous Media. Journal of The Electrochemical Society, 166 (11) C3015-C3017 DOI: 10.1149/2.0031911jes.

Sharma A. et. al. 2017. Across the tree of life, radiation resistance is governed by antioxidant Mn2+, gauged by paramagnetic resonance. PNAS 114, E9253-E9260. https://doi.org/10.1073/pnas.1713608114

Sherar, B.W.A., Keech, P.G., Shoesmith, D.W. 2011. Carbon steel corrosion under anaerobic-aerobic cycling conditions in near-neutral pH saline solutions – Part 1: Long term corrosion behaviour. Corros. Sci. 53: 3636-3642.

Shoesmith, D.W. 2006. Assessing the corrosion performance of high-level nuclear waste containers. Corrosion 62: 703-722.

Shoesmith, D.W., King, F. 1999. The effects of gamma radiation on the corrosion of candidate materials for the fabrication of nuclear waste packages. AECL-11999, Atomic Energy of Canada Limited.

Shrestha, R. et al. 2021. Anaerobic microbial corrosion of carbon steel under conditions relevant for deep geological repository of nuclear waste. Sci. Total Environ. 800: 149539.

Shuryak, I. et al. 2017. Microbial cells can cooperate to resist high level chronic ionizing radiation. PloS one 12: e0189261. https://doi.org/10.1371/journal.pone.0189261

SKB 2006a. Buffer and backfill process report for the safety assessment SR-Can. SKB Technical Report TR-06-18: 201.

SKB 2006b. Long-term safety for KBS-3 repositories at Forsmark and Laxemar - a first evaluation. Main report of the SR-Can project, SKB Technical Report TR-06-09. Swedish Nuclear Fuel and Waste Management Company, Stockholm, Sweden.

SKB 2010a. Fuel and canister process report for the safety assessment SR-Site. Updated 2015-06. SKB Technical Report TR-10-46, Stockholm: SKB.

SKB 2010b. Corrosion calculations report for the Safety Assessment SR-site. SKB Technical report TR-10-66, SKB.

SKB 2010c. Design, production and initial state of the buffer. Stockholm: Svensk Kärnbränslehantering AB.

SKB 2011. Long-term safety for the final repository for spent nuclear fuel at Forsmark, Main report of the SR-Site project, Volume 2. Svensk Kärnbränslehantering AB, Stockholm.

SKB 2019. Supplementary information on canister integrity issues. SKB TR-19-15.

SKB 2021. Post-closure safety for the final repository for spent nuclear fuel at Forsmark. SKB Technical Report, TR-21-01. SKB.

Smailos, E., Schwarzkopf, W., Koester, R., Fiehn, B., Halm, G. 1991. Corrosion Testing of Selected Packaging Materials for Disposal of High-Level Waste Glass in Rock-Salt Formations. Report EUR-13672. Commission of the European Communities, Luxembourg.

Smart N., Rance A.P., Carlson L., Werme L.O. (2006): Further Studies of the Anaerobic Corrosion of Steel in Bentonite. In: P.V. Isheghem, (Ed.), Scientific Basis for Nuclear Waste Management XXIX.

Smart, N R, Rance, A P and Fennell P A H. (2005). Galvanic corrosion of copper-cast iron couples. SKB technical report TR-05-06.

Smart, N. R., Rance, A. P., 2005. Effect of radiation on anaerobic corrosion of iron (No. SKB-TR--05-05). Swedish Nuclear Fuel and Waste Management Co.

Smart, N., Rance, A., Reddy, B., Lydmark, S., Pedersen, K., Lilja, C. 2011. Further studies of in situ corrosion testing of miniature copper-cast iron nuclear waste containers. Corr. Eng. Sci. Tech. 46: 142-147.

Smart, N. R., Reddy, B., Rance, A. P., Nixon, D. J., Frutschi, M., Bernier-Latmani, R. & Diomidis, N. 2017. The anaerobic corrosion of carbon steel in compacted bentonite exposed to natural Opalinus Clay porewater containing native microbial populations. Corros. Eng. Sci. Technol. 52: 101-112.

Smart, N.R., Blackwood, D.J., Werme, L.O. 2001a. The anaerobic corrosion of carbon steel and cast iron in artificial groundwaters, SKB Technical Report TR-99-06. Swedish Nuclear Fuel and Waste Management Co., Stockholm.

Smart, N.R., Blackwood, D.J., Werme, L. 2001b. The anaerobic corrosion of carbon steel and cast iron in artificial groundwaters. Technical Report SKB-TR-01-22, Swedish Nuclear Fuel and Waste Management Co., Stockholm, Sweden.

Smart, N.R., Blackwood, D.J., Werme, L. 2002a. Anaerobic corrosion of carbon steel and cast iron in artificial groundwaters: Part 2 – Gas generation. Corrosion 58: 627-637.

Smart, N.R., Blackwood, D.J., Werme, L. 2002b. Anaerobic corrosion of carbon steel and cast iron in artificial groundwaters: Part 1 – Electrochemical aspects. Corrosion 58: 547-559.

Smart, N.R., Fennell, P.A.H., Rance, A.P. (2006). Expansion Due to the Anaerobic Corrosion of Iron, SKB Report TR-06-41.

Smart, N.R., Hoch, A.R. 2010. A Survey of Steel and Zircaloy Corrosion Data for Use in the SMOGG Gas Generation Model. Serco Assurance Report SA/ENV 0841 issue 3.

Smart, N.R., Rance, A.P., Werme, L.O. 2008. The Effect of Radiation on the Anaerobic Corrosion of Steel. J. Nucl. Mater. 379: 97-104. doi: 10.1016/j.jnucmat.2008.06.007.

Smith, J.M., Qin, Z., Wren, J.C., Shoesmith, D.W. 2006. The influence of peroxidation on the corrosion of copper nuclear waste canister in aqueous anoxic sulphide solutions. MRS Online Proceedings Library 985: 811.

Soroka, I., Chae, N., Jonsson, M. 2021. On the mechanism of γ-radiation-induced corrosion of copper in water. Corros. Sci. 182: 109279.

Sova, A., Doubenskaia, M., Grigoriev, S., Okunkova, A., Smurov, I. 2013. Parameters of the Gas-Powder Supersonic Jet in Cold Spraying Using a Mask. J. Therm. Spray Technol. 22: 551-556.

Sova, A., Klinkov, S., Kosarev, V., Ryashin, N., Smurov, I. 2013. Preliminary study on deposition of aluminium and copper powders by cold spray micronozzle using helium. Surf. Coat. Technol. 220: 98-101.

Sova, A., Okunkova, A., Grigoryev, S., Smurov, I. 2013. Velocity of the particles accelerated by a cold spray micronozzle: Experimental measurements and numerical simulation. J. Therm. Spray Technol. 22: 75-80.

Stroes-Gascoyne, S. 2010. Microbial occurrence in bentonite-based buffer, backfill and sealing materials from large-scale experiments at AECL's Underground Research Laboratory. Appl. Clay Sci. 47: 36-42.

Stroes-Gascoyne, S., Hamon, C.J., Dixon, D.A., Kohle, C.L., Maak, P. 2007. The Effects of Dry Density and Porewater Salinity on the Physical and Microbiological Characteristics of Compacted 100%

Bentonite. MRS Online Proceedings Library, 985: 1302. https://doi.org/10.1557/PROC-985-0985-NN13-02.

Stroes-Gascoyne, S., Hamon, C.J., Maak, P. 2011. Limits to the use of highly compacted bentonite as a deterrent for microbiologically influenced corrosion in a nuclear fuel waste repository. Phys. Chem. Earth, Parts A/B/C 36: 1630-1638.

Stroes-Gascoyne, S., Hamon, C.J., Maak, P., Russell, S. 2010. The effects of the physical properties of highly compacted smectitic clay (bentonite) on the culturability of indigenous microorganisms. Appl. Clay Sci. 47: 155-162.

Stroes-Gascoyne, S., Hamon, C.J., Vilks, P., Gierszewski, P. 2002. Microbial, redox, and organic characteristics of compacted clay-based buffer after 6.5 years of burial at AECL''s Underground Research Laboratory. Appl. Geochem. 17: 1287-1303.

Stroes-Gascoyne, S., Lucht, L.M., Borsa, J., Delaney, T.L., Haveman, S.A., Hamon, C.J. 1995. Radiation Resistance of the Natural Microbial Population in Buffer Materials. MRS Online Proceedings Library Archive 353: 345–352. https://doi.org/10.1557/PROC-353-345.

Stroes-Gascoyne, S., West, J.M., 1997. Microbial studies in the Canadian nuclear fuel waste management program. FEMS Microbiology Reviews 20: 573–590. https://doi.org/10.1111/j.1574-6976.1997.tb00339.x

Sudharshan Phani, P., Vishnukanthan, V., Sundararajan, G. 2007. Effect of heat treatment on properties of cold sprayed nanocrystalline copper alumina coatings. Acta Mater. 55: 4741-4751.

Svemar, C., Johannesson, L-E., Grahm, Svensson, D. 2016. Opening and retrieval of outer section of Prototype Repository at Äspö Hard Rock Laboratory. Svensk Kärnbränslehantering AB, Stockholm.

Svensson, D., Sandén, T., Olsson, S., Dueck, A., Eriksson, S., Jägerwall, S., Hansen, S. 2011. Alternative buffer material Status of the ongoing laboratory investigation of reference materials and test package 1. SKB TR-11-06: 146. Svensk Kärnbränslehantering AB: Stockholm, Sweden.

Swanton, S.W., Baston, G.M.N., Smart, N.R. 2015. Rates of steel corrosion and carbon-14 release from irradiated steels – state of the art review (D.2.1): 160. Carbon-14 Source Term (CAST Project).

Takase, H. 2004. Discussion on PA model development for bentonite barriers affected by chemical interaction with concrete: do we have enough evidence to support bentonite stability?. In: International Workshop on Bentonite-Cement Interaction in Repository Environments, Tokyo, Japan, NUMO-TR 04-05, A3-172 – A3-177; Posiva Report 2004-25: 192.

Taniguchi, N. 2003. Effect of magnetite as a corrosion product on the corrosion of carbon steel overpack. In: Prediction of Long-Term Corrosion Behaviour in Nuclear Waste Systems. European Federation of Corrosion Publication No. 36 :424– 438.

Taxén, C. 2003. Atmospheric corrosion of copper 450 metres underground. Results from three years exposure in the Äspö HRL. MRS Online Proceedings Library volume 807: 612–617.

Tay, B.K., Zhao, Z.W., Chua, D.H.C. 2006. Review of metal oxide films deposited by filtered cathodic vacuum arc technique. Mater. Sci. Eng.:R.:Rep. 52: 1-48.

Terlain, A., Desgranges, C., Gauvain, D., Feron, D., Galtayries, A., Marcus, P. 2001. Oxidation of materials for nuclear waste containers under long term conditions, Corrosion/2001, Paper 01119. NACE International, 2001: Houston, TX.

Theodorakopoulos, N., Février, L., Barakat, M., Ortet, P., Christen, R., Piette, L., Levchuk, S., Beaugelin-Seiller, K., Sergeant, C., Berthomieu, C., Chapon, V. 2017. Soil prokaryotic communities in Chernobyl waste disposal trench T22 are modulated by organic matter and radionuclide contamination. EMS Microbiol. Ecol. 93: fix079. https://doi.org/10.1093/femsec/fix079.

Tournassat, C., Steefel, C.I., Bourg, I.C., Bergaya, F. 2015. Natural and Engineered Clay Barriers. Develop. Clay Sci. 6: 432.

Triantou, K.I., Pantelis, D.I., Guipont, V., Jeandin, M. 2015. Microstructure and tribological behaviorbehaviour of copper and composite copper+alumina cold sprayed coatings for various alumina contents. Wear 336-337: 96-107.

Trinchero, P., Molinero, J., Román-Ross, G., Berglund, S., Selroos, J.O. 2014. FASTREACT–An efficient numerical framework for the solution of reactive transport problems. Appl. Geochem. 49: 159-167.

Truche, L., Berger, G., Destrigneville, C., Guillaume, D., Giffaut E. 2010. Kinetics of pyrite to pyrrhotite reduction by hydrogen in calcite buffered solutions between 90 and 180 °C: Implications for nuclear waste storage. Geochim. Cosmochim. Acta 74: 2894-2914.

Truche, L., Berger, G., Destrigneville, C., Pages, A., Guillaume, D., Giffaut E., Jacquot, E. 2009. Experimental reduction of aqueous sulphate by hydrogen under hydrothermal conditions: Implication for the nuclear waste storage. Geochim. Cosmochim. Acta 73: 4824-4835.

Truche, L., Jodin-Caumon, M.C., Lerouge, C., Berger, G., Mosser-Ruck, R., Giffaut, E., Michau, N., 2013. Sulphide mineral reactions in clay-rich rock induced by high hydrogen pressure. Application to disturbed or natural settings up to 250°C and 30bar. Chem. Geol. 351, 217–228.

Turnbull, A., 2009. A Review of the Possible Effects of Hydrogen on Lifetime of Carbon Steel Nuclear Waste Canisters. Technical Report 09-04, Nagra, Wettingen, Switzerland.

Vachon, M.A. et al. 2021. Fifteen shades of clay: distinct microbial community profiles obtained from bentonite samples by cultivation and direct nucleic acid extraction. Sci. Rep. 11: 22349.

Van Gerwen, S.J.C., Rombouts, F M., Van´t Riet, K., Zwietering, M.H. 1999. A Data analysis of the irradiation parameter D10 for bacteria and spores under various conditions. J. Food Prot. 62: 1024-1032.

Van Loon, L., Soler, J.M., and M.H. Bradbury (2003) Diffusion of HTO, 36Cl− and 125I− in Opalinus Clay samples from Mont Terri: Effect of confining pressure. J. Contam. Hydrol. 61: 73-83.

Van Loon, L.R., Glaus, M.A., Müller, W. 2007. Anion exclusion effects in compacted bentonites: towards a better understanding of anion diffusion. Appl. Geochem. 22: 2536–2552.

Vandenborre, J., Crumière, F., Blain, G., Essehli, R., Humbert, B., Fattahi, M. 2013. Alpha Localized Radiolysis and Corrosion Mechanisms at the Iron/Water Interface: Role of Molecular Species. J. Nucl. Mater. 433:124–31. doi: 10.1016/j.jnucmat.2012.09.034.

Venzlaff, H. et al. 2013. Accelerated cathodic reaction in microbial corrosion of iron due to direct electron uptake by sulfate-reducing bacteria. Corros. Sci. 66: 88-96.

Villar, M. V., & Gómez-Espina, R. (2009). Report on Thermo-Hydro-Mechanical Laboratory Tests Performed by CIEMAT on Febex Bentonite 2004-2008. CIEMAT Technical Report 1178., Madrid, Spain.

Villar, M.V., Armand, G., Conil, N., de Lesquen, Ch., Herold, Ph., Simo, E., Mayor, J.C., Dizier, A., Li, X., Chen, G., Leupin, O., Niskanen, M., Bailey, M., Thompson, S., Svensson, D., Sellin, P., Hausmannova, L. 2020. D7.1 HITEC. Initial State-of-the-Art on THM behaviour of i) Buffer clay materials and of ii) Host clay materials. Deliverable D7.1 HITEC. EURAD Project, Horizon 2020 No 847593: 214.

Villar, M.V., Fernández, A.M., Romero, E, Dueck, A., Cuevas, J., Plötze, M., Kaufhold, S., Dohrmann, R., Iglesias, R., Sakaki, T., Voltolini, M., Zheng, L., Kawamoto, K., Kober, F., 2017. FEBEX-DP: Post-mortem THM/THC Report. Analysis of Results. Nagra Working Report NAB 16-017: 147.

Villar, M.V., Lloret, A. 2008. Influence of dry density and water content on the swelling of a compacted bentonite. Appl. Clay Sci. 39: 38-49.

Wada, Yoichi, Tachibana, Masahiko, Watanabe, Atsushi, Ishida, Kazushige, Ota, Nobuyuki, Shigenaka, Naoto, Inagaki, Hiromitsu, & Noda, Hiroshi (2016). Effects of seawater components on radiolysis of water at elevated temperature and subsequent integrity of fuel materials. Journal of Nuclear Science and Technology (Tokyo), 53(6), 809-820.

Wang L., Fan S., Sun H., Ji B., Zheng B., Deng J.,Zhang L., Cheng L. (2020). Pressure-less joining of SiC_f/SiC composites by Y_2O_3–Al_2O_3–SiO_2 glass: Microstructure and properties, Ceramics International 46, 27046–27056, DOI: 10.1016/j.ceramint.2020.07.181

Wang, Y., Normand, B., Mary, N., Yu, M., Liao, H. 2014. Microstructure and corrosion behaviour of cold sprayed SiCp/Al 5056 composite coatings. Surf. Coat. Technol. 251: 264-275.

Weetjens, E., Marivoet, J., Govaerts, J. 2012. Conceptual model description of the reference case, External Report SCK•CEN-ER-215. Niras / Ondraf.

Wersin P. (2003): Goechemical modelling of bentonite porewater in high-level waste repositories. J. Contam. Hydrol. 61, 405-422.

Wersin P., Curti E., Appelo C.A.J. 2004. Modelling bentonite–water interactions at high solid/liquid ratios: swelling and diffuse double layer effects. – Appl. Clay Sci. 26, 249-257.

Wersin, P., Alt-Epping, P., Pekala, M., Pitkänen, P., & Snellman, M. (2017). Modelling sulfide fluxes and Cu canister corrosion rates in the engineered barrier system of a spent fuel repository. Procedia earth and planetary science, 17, 722-725.

Wersin, P., Alt-Epping, P., Pitkänen, P., Román-Ross, G. 2014. Sulphide Fluxes and Concentrations in the Spent Nuclear Fuel Repository at Olkiluoto. Posiva 2014-01, Posiva Oy, Finland.

Wersin, P., Birgersson, M., Olsson, S., Karnland, O., and Snellman, M. (2008) Impact of corrosion-derived iron on the bentonite buffer within the KBS-3H disposal concept: the Olkiluoto site as case study, SKB Report R-08-34, Swedish Nuclear Fuel and Waste Management Company, Stockholm, Sweden.

Wersin, P., Birgersson, M., Olsson, S., Karnland, O., Snellman, M. 2008. Impact of corrosion-derived iron on the bentonite buffer within the KBS-3H disposal concept. The Olkiluoto site as case study. – SKB report R-08-34. Svensk Kärnbränslehantering AB.

Wersin, P., Hadi, J., Jenni, A., Svensson, D., Grenèche, J.-M., Sellin, P., Leupin, O.X. 2021. Interaction of Corroding Iron with Eight Bentonites in the Alternative Buffer Materials Field Experiment (ABM2). Minerals 11: 907.

Wersin, P., Spahiu, K., Bruno, J. 1994. Time evolution of dissolved oxygen and redox conditions in a HLW repository. TR 94-02, SKB, Sweden.

Westerman, R.E., Nelson, J.L., Pitman, S.G., Kuhn, W.L., Basham, S.J., Moak, D.P. 1983. Evaluation of Iron-Base Materials for Waste Package Containers in a Salt Repository. MRS Proceedings 26: 427. doi: 10.1557/PROC-26-427.

Westerman, R.E., Pitman, S.G., Nelson, J.L. 1982. General Corrosion, Irradiation-Corrosion and Environmental-Mechanical Evaluation of Nuclear-Waste-Package Structural-Barrier Materials. Progress report PNL-4364, Office of Nuclear Waste Isolation, Pacific Northwest Laboratory, Washington.

Wieland, E., Hummel, W. 2015. Formation and stability of 14C-cointaining organic compounds in alkaline iron-water systems: preliminary assessment based on a literature survey and thermodynamic modelling. Mineral. Mag. 79: 1275-1286.

Wilfinger, K. 1994. Ceramic Package Fabrication for YMP Nuclear Waste Disposal. Lawrence Livermore National Laboratory, Report UCRL-ID-118660, California, US.

Williams, A.G.B., Scherer, M.M. 2004. Spectroscopic evidence for Fe(II)-Fe(III) electron transfer at the iron oxide-water interface. Environ. Sci. Technol. 38: 4782-4790.

Wilson et al. (2015): Wilson, J., Benbow, S., Sasamoto, H., Savage, D., Watson, C., 2015. Thermodynamic and fully-coupled reactive transport models of a steel–bentonite interface. Applied Geochemistry 61, 10-28

Wilson J., Cressey G., Cressey B., Cuadros J., Ragnarsdottir K.V., Savage D., Shibata M. (2006a): The effect of iron on montmorillonite stability. (II) Experimental investigation. Geochimica et Cosmochimica Acta, 70: 323–336.

Wilson, J., Savage, D., Bond, A., Watson, S., Pusch, R., Bennett, D. 2011. Bentonite. A Review of key properties, processes and issues for consideration in the UK context. Quintesa report QRS-1378ZG-1 : 137.

Wilson, J., Savage, D., Cuadros, J., Shibata, M., Ragnarsdottir, K.V. (2006b): The effect of iron on montmorillonite stability. (I) Background and thermodynamic considerations. Geochim. Cosmochim. Acta, 70: 306–322.

Winsley, R.J., Smart, N.R., Rance, A.P., Fennell, P.A.H., Reddy, B., Kursten, B. 2011. Further Studies on the Effect of Irradiation on the Corrosion of Carbon Steel in Alkaline Media. Corros. Eng. Sci. Technol. 46:111–16. doi: 10.1179/1743278210Y.0000000010.

Wolfaardt, G.M., Korber, D.R. 2012. Nearfield microbiological considerations relevant to a deep geological repository for used nuclear fuel - State of science review. Toronto: Nuclear Waste Management Organization.

Wötting, G., Martin, W. 2007. Large sized, complex shaped sintered silicon carbide components with excellent mechanical properties. Proceedings of the 10th ECerS Conference, Baden-Baden: 1067-1070.

Xiong, Y. et al. 2021. Lead/lead-alloy as a corrosion-resistant outer layer packaging material for high level nuclear waste disposal. Nucl. Eng. Des. 380: 111294.

Yang, Q., Toijer, E., Olsson, P. 2019. Analysis of radiation damage in the KBS-3 canister materials. SKB TR-19-14, Svensk Kärnbränslehantering AB.

Yin, S. et al. 2017. Advanced diamond-reinforced metal matrix composites via cold spray: properties and deposition mechanism. Compos. B. Eng. 113: 44-54.

Yunker, W. H., Glass, R. S., 1986. Long-term corrosion behavior of copper-base materials in a gamma irradiated environment. In: Bates J K, Seefeldt W B (eds). Scientific basis for nuclear waste management X: symposium held in Boston, Massachusetts, USA, 1–4 December 1986. Pittsburgh, PA: Materials Research Society. (Materials Research Society Symposium Proceedings 84), pp 579–590.

Yunker, W.H. 1990. Corrosion behavior of copper-base materials in a gamma-irradiated environment. Report WHC-EP-0188, Westinghouse Hanford Company, Richland, Washington.

Zhang, H., Datta, A.K. 2003. Microwave Power Absorption in Single - and Multiple - Item Foods. Food Bioprod. Process. 81: 257–265.

Zheng, L., Rutqvist, J., Birkholzer, J.T., Liu, H.H. 2015. On the impact of temperatures up to 200°C in clay repositories with bentonite engineer barrier systems: A study with coupled thermal, hydrological, chemical, and mechanical modeling. Eng. Geol. 197: 278–295.

Zheng, L., Xu, H., Ruqvist, J.; Reagan, M.; Birkholzer, J.; Villar, M.V.; Fernández, A.M. 2020. The hydration of bentonite buffer material revealed by modeling analysis of a long-term in situ test. Appl. Clay Sci. 185: 105360.

Zheng, L.; Samper, J.; Montenegro, L.; Fernández, A.M. 2011. A coupled THMC model of a heating and hydration laboratory experiment in unsaturated compacted FEBEX bentonite. J. Hydrol. 386: 80–94.

Zhou, H. (2012). Titanium and Titanium alloy Coatings for Corrosion Protection. Proceedings of the 12th World Conference on Titanium, 3 1906-1910.

Zhujing Y., Changqing L., Li Y. Weitao W. (1991) Corrosion performance of ion-plated titanium and yttrium modified TiN coatings, Surface and Coatings Technology, 46: 307-315

Zymelka, D. 2013. PhD Thesis. Suivi par méthode optique du frittage micro-ondes d''oxydes céramiques. École Nationale Supérieure des Mines de Saint-Etienne.